Study and Development of near-Infrared Reflective and Absorptive Materials for Energy Saving Application

by

Yu Xing Cui, M.Sc.

A thesis submitted to the Faculty of Graduate and Postdoctoral Affairs in partial fulfillment of the requirements for the degree of

Doctor of Philosophy

in

Chemistry

Carleton University
Ottawa, Ontario

Library and Archives Canada

Published Heritage Branch

395 Wellington Street
Ottawa ON K1A 0N4
Canada

Bibliothèque et Archives Canada

Direction du Patrimoine de l'édition

395, rue Wellington
Ottawa ON K1A 0N4
Canada

Your file Votre référence
ISBN: 978-0-494-87749-4

Our file Notre référence
ISBN: 978-0-494-87749-4

Abstract

Near-Infrared (NIR) materials find applications in the field of energy saving. Both NIR reflective and absorptive materials can be used as energy saving materials with different working principles. The reflective materials can reflect the NIR light preventing it from being transmitted. Silver thin films are the best option as reflective films based on its reflectivity and cost. On the other hand, NIR absorptive materials can effectively convert the absorbed NIR light from sunlight to heat or electric energy.

The first part of this research explored methods of preparing silver thin films that could be processed at low cost. The second part involved the design, synthesis and characterization of nickel coordination polymers as NIR absorptive materials.

In part 1, different solution based methods of preparing silver thin films were studied. A silver nanoparticles solution was used to make thin film by a spray-pyrolysis process. Another method involved the surface activation with a fluoro-compound or silver nanoparticles followed by electroless silver plating on different substrates. Both methods could be processed at low cost. The obtained silver films showed NIR reflection of 50~90% with transmission of 15-28% in the visible region.

In part 2, two Nickel coordination polymers were explored. Tetraamino compounds were used as bridging ligands to increase the scope of electronic delocalization and metal-ligand orbital overlap which would reduce the energy gap to the NIR region. As a result, both polymers showed broad NIR absorption with maximum of 835 and 880 nm, respectively. In addition, the polymer showed NIR halochromism. This ground study pointed out both Ni coordination polymers as NIR absorptive materials with NIR halochromism.

Acknowledgements

It would not be possible to write this thesis without the help and support of the people around me. To only some of them it is possible to give particular mention here.

First of all, I would like to express my deep gratitude to my supervisor, Dr. Zhi Yuan (Wayne) Wang for his support, warm encouragement and thoughtful guidance along the Ph.D. study.

The members of Wang have contributed immensely to my personal and professional time at Carleton. The friendship has been invaluable on both academic and personal level. I also want to thank Dr. Jane Gao for her kind advice, encouragement and assistance.

To Jim Logan, Tony O'Neil, Keith Bourque, and Jianqun Wang, I would like to say thank you all for support of the instrumental techniques.

I also appreciate Dr. Anatoli Ianoul and Dr. Shan Zu for the help and discussion of AFM scan.

Last but not least, I want to thank my family for all their love and encouragement. To my parents who raised me and have supported me in all my pursuits, to my brother and sister who have been supportive, to my parents-in-law who have been helpful, to my daughter, Michelle, whose smile is always a positive encouragement, and most of all to my loving, supportive, encouraging wife, Meng whose faithful support in the past.

Table of Contents

List of Figures

List of Schemes

List of Tables

List of Abbreviations

NIR	near-Infrared
ρ	reflectance
α	absorbance
τ	transmittance
PVD	physical vapor deposition
CVD	chemical vapor deposition
D-A	donor-acceptor
HOMO	highest occupied molecular orbital
LUMO	lowest unoccupied molecular orbital
MLCT	metal to ligand charge transfer
LMCT	ligand to metal charge transfer
LLCT	ligand to ligand charge transfer
ε	molar extinction coefficient
NLO	non-linear optical
MOF	metal-organic framework
MEMS	microelectromechanical system
OLED	organic light emission diode
EP	electroless plating
AgNPs	silver nanoparticle solution
GIXRD	Grazing Incidence X-Ray Diffraction
SPR	surface plasmon resonance
PFO	1H,1H,H,2H-perfluorooctyltriethoxysilane
OTES	octyltriethoxysilane
APTES	aminopropyltriethoxysilane
θ	contact angle
Ra	roughness
PVP	poly(vinyl pyrrolidone)
PMMA	poly(methyl methacrylate)
SEM	Scanning electron microscope
EDX	Energy-dispersive X-ray spectroscopy
BTA	1,2,4,5-benzenetetraamine
BHPBTA	1,5-N,N'-bis(4-heptylphenyl)-1,2,4,5-benzenetetraamine
BDBPBTA	N,N'-bis(3,5-di-tert-butylphenyl)-1,2-benzenediamine
W/O	water in oil
O/W	oil in water
ATR	attenuated total reflection
TGA	thermogravimetric analysis
ASTM	American Society for Testing and Materials
AAS	Atomic absorption spectroscopy

Chapter 1 Introduction

Energy saving materials are of interest in recent years as the global energy demand grows. According to the report of "World Energy Outlook" by the International Energy Agency, world energy demand could grow 55 percent by 2030, and potentially double by 2050.[1] The energy supply stresses are inevitable. Additionally, there are other issues, such as climate change, energy crisis, and economic benefits that stress the importance of energy saving.

Climate change: It is believed that green house emission, which stems from the over consumption of fossil energy, relates to climate change. Researchers estimated that climate change contributes to 150,000 deaths and 5 million illnesses each year according to the report from the World Health Organization.[2] Heat waves, shortage of fresh water, food crisis, and rising sea levels are all the consequence of climate change. In addition, environment pollution also threatens the subsistence of human beings.

Finite resources and energy crisis: Since the industrial revolution, fossil fuels have been overused and over-relied on for many years. Continuously increased demand of energy and finite resources has thrown us into a deep energy crisis. The proved world oil reserves as of Jan. 1st, 2010, as reported by U.S. Energy Information Administration in International Energy Outlook 2010, were estimated at 1,354 billion barrels.[3] The daily oil consumption of global economy is 80 million barrels. Accordingly, energy researchers predict that oil can only last for 40 years and coal will last 200 years at most. Energy saving is apparently in need to extend the energy

supply. In addition, it leaves more time for scientists to find alternative energy sources which could completely replace fossil fuels.

Economy benefits and energy saving: Energy saving is able to bring significant economic returns. Some energy saving building materials, such as reflective roof coating and smart window materials can block solar energy from entering rooms in summer and prevent heat loss in winter by the function of near-Infrared (NIR) reflection or absorption. Therefore, heating and cooling bills will be reduced significantly. On the other hand, NIR absorptive materials can be used to convert solar radiation to heat energy. Thus the consumption of electricity or natural gas will be reduced.

Energy saving will benefit future generations from reduced green house emission and diminish environment pollution.

1.1 Solar radiation and heat transfer

In this thesis, we focus on the study of NIR reflective and absorptive materials that block transmission of NIR light from solar radiation or heat transfer.

There are three modes of heat transfer: conduction, convection and radiation. Conduction is a heat transfer process that takes place through material surfaces with different temperatures when adjacent atoms vibrate against one another, or as electrons move from one atom to another. Conduction is the most significant means of heat transfer within a solid or between solid objects in thermal contact. Convection is heat transfer process taking place in liquid or gas through diffusion and advection, the movements of fluids. Both conduction and convection are driven by temperature differences and the heat transfer requires a medium. The energy transferred is a function of temperature, geometry and thermal constants. In terms of heat blocking, conduction and convection can be reduced by using heat insulation materials with low thermal conductivity. Radiation, the third heat transfer mode, is energy emitted via electromagnetic waves. The magnitude of energy transferred by radiation is a function of temperature to the 4^{th} power, geometry and emissivity. The emissivity (ε) of a material is a relative ability of its surface to emit energy by radiation. It is the ratio of energy radiated by a material to the energy radiated by a black body at the same temperature. The true black body would have $\varepsilon = 1$ while any real object would have $\varepsilon < 1$. Radiation does not require medium to transfer energy. Sunlight is a source of radiation whose electromagnetic spectrum ranges from ultraviolet to visible and up to NIR region.

Figure 1.1 shows the solar radiation spectra based on ASTM Terrestrial

Reference Spectra. The figure shows the solar radiation spectra for direct light at both the top of earth's atmosphere and at sea level. As the sunlight passes through the atmosphere, some is absorbed by gases. The solar energy is distributed from UV (below 400 nm, 4.6%) to visible (400 – 750 nm, 43.4%) and NIR region (750 -2500 nm, 52%). The spectra are also standards adopted by photovoltaics industry to ensure consistent test conditions.

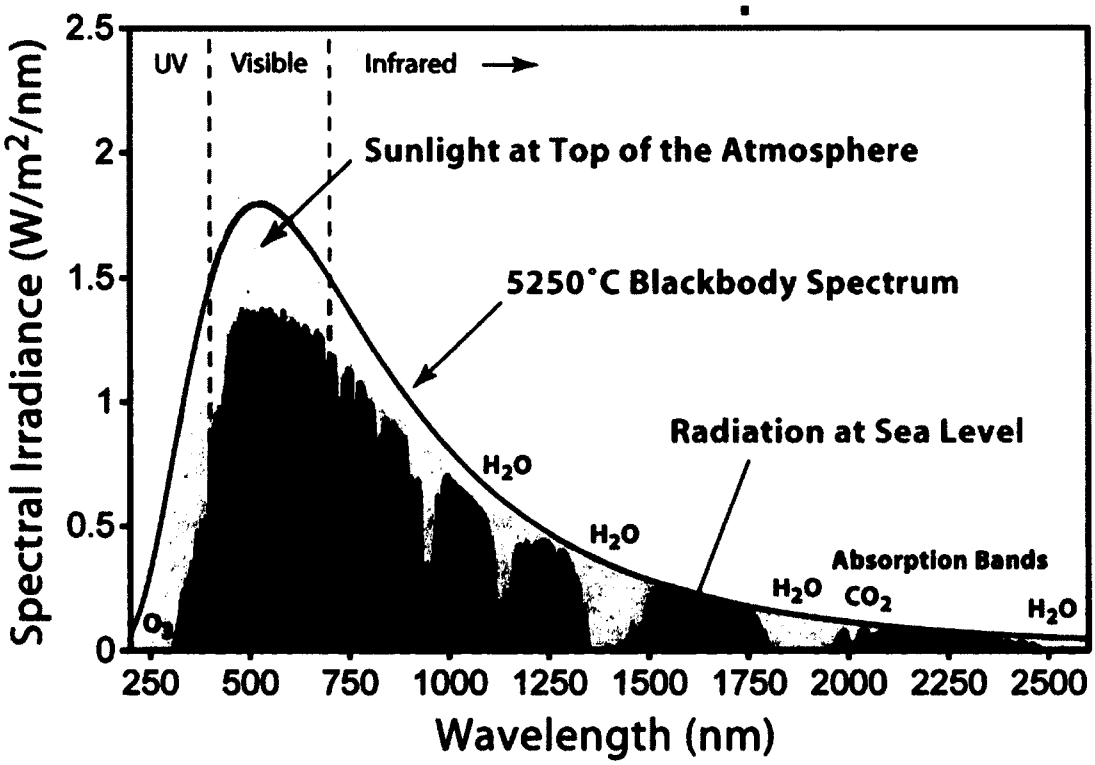

Figure 1.1. Solar radiation spectra

When light impinges an object's surface, it will be reflected, absorbed or transmitted as shown in Figure 1.2. The process of scattering, as a special form of reflection in case of non-smooth surface, is included in reflection. Light absorption results in energy increase of an object. In the case of non-luminescent materials, the absorbed light will be mainly converted to heat resulting in temperature increase.

Absorption of NIR light is the main source of heat gain of an object as NIR totals 52% of the available solar energy.

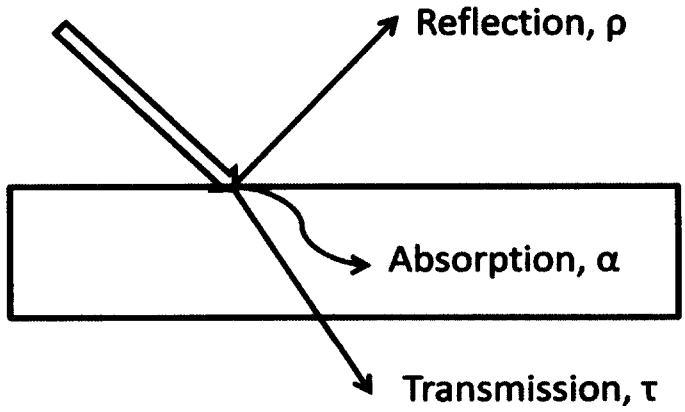

Figure 1.2. Light propagation through the interface

The sum of energy from three components equals the incident light. Equation 1.1 shows the relationship among reflectance (ρ), absorbance (α) and transmittance (τ).

$$\rho + \alpha + \tau = 1 \qquad 1.1$$

When the surface of the object is opaque, transmittance (τ) is zero. This reduces the eq. 1.1 to $\rho + \alpha = 1$. Materials with high reflectance must have low absorbance and/or transmittance.

1.2 Principles of energy saving by NIR reflective and absorptive materials

Energy saving by NIR reflective materials

Unlike other heat insulators blocking conduction and convection with low thermal conductivity, NIR reflective materials reflect the thermal radiation preventing it from being transmitted or absorbed. Thus the heat transfer by radiation is blocked. An example that depicts how NIR reflective coating, specifically low-emissive coating, prevents the transmittance of NIR is shown in Figure 1.3. When sunlight strikes on the window, visible light is transmitted with little reflection. The NIR light is mostly reflected towards the outside. In this case, the cooling load of the inside is significantly reduced without the loss of visible light. The reflective roof coating performs the same way as a low-emissive coating except for transmission of visible light.

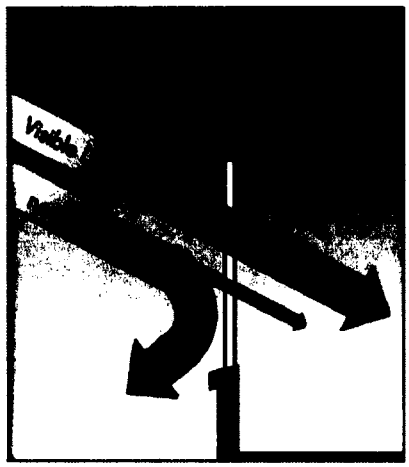

Figure 1.3. NIR reflective glass (Low-Emissive coating)

The reflectivity of a material depends on the refractive index change (equation 1.2). For example, when sunlight strikes on glass in air, the refractive index of air is

1.00 and 1.50 for glass, thus the reflectivity of the glass is 4%. Apparently, a large difference in refractive index between the two media will result in a high reflectivity of a surface.

$$R = \left(\frac{n1-n2}{n1+n2}\right)^2 \qquad (1.2)$$

Where n1, n2 are the refractive indices of the two media.

Energy saving by NIR absorptive materials

NIR absorptive materials function as an energy-saving material in two ways. The major one is to convert the NIR portion of sunlight to thermal energy or electric power.[4-6] One of the most prominent applications of NIR absorptive materials is used for solar-thermal energy conversion.[7] As aforementioned, NIR light comprises 52% of the available solar energy. Therefore, the use of NIR absorbing materials will enhance the efficiency of solar-thermal energy conversion of solar collectors, especially when the sunlight passes through clouds. In that case the majority of the available light is NIR light which can be harvested by solar collector panels. In the field of photovoltaics, current materials focus on visible light. It is believed that power conversion performance will be significantly increased by harvesting NIR as well as visible light.[8,9]

NIR absorbers can also be used as transmission plastic laser welding (Figure 1.4).[10-15] When a NIR laser beam is irradiated on the plastic, only the area that contains NIR absorptive material will absorb the laser resulting in heat and melting the plastic in the affected area. All other areas retain low temperature without any shape deformation since the plastic itself is not NIR absorptive.

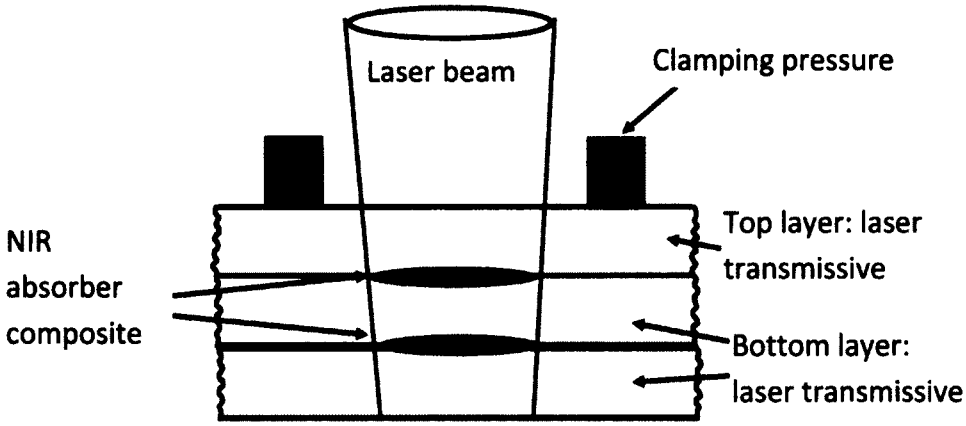

Figure 1.4. NIR absorber used for transmission laser welding

Another aspect for energy saving application is by blocking the NIR heat through absorbing and re-emitting the heat to atmosphere. Polyethylene films blended with NIR absorptive materials can also be used as greenhouse films for energy saving by reducing the heat requirement. Another application example is used as solar control window films by combining with NIR reflective materials.[16]

1.3 Review of NIR reflective materials

NIR reflective materials are divided into four categories: transition metals, inorganic or organic compounds, and natural substances.

1.3.1 Transition metals

The transitional metals are the most NIR reflective materials with different skin depth and absorption in visible region. Figure 1.5 summarizes the reflectance of gold, silver, copper, aluminum, titanium and rhodium. Aluminum reflects a wide range from UV to NIR with some absorption at 820 nm. Silver claims the highest reflectivity from 400 nm up to 10 μm. The reflective behaviors of copper and gold are similar to each other with different absorption in the visible region. Being highly NIR reflective even as thin as 10 nm in thickness, which is transparent to visible light, silver is the most employed metal in multilayer NIR reflective low-emissive coatings. The silver layer is sandwiched by metal oxides with a high refractive index to reduce the metallic glare as shown in Figure 1.6. When used as a single layer without protection, an aluminum mirror is used for wide range reflector. For example, telescope mirrors used over a broad spectral range are usually coated with aluminum.[17] Aluminum and silver are also used as IR reflective material in the form of flakes in NIR reflective coating. Although gold possesses high reflectivity and is anti-oxidizing, it is not utilized due to the cost.

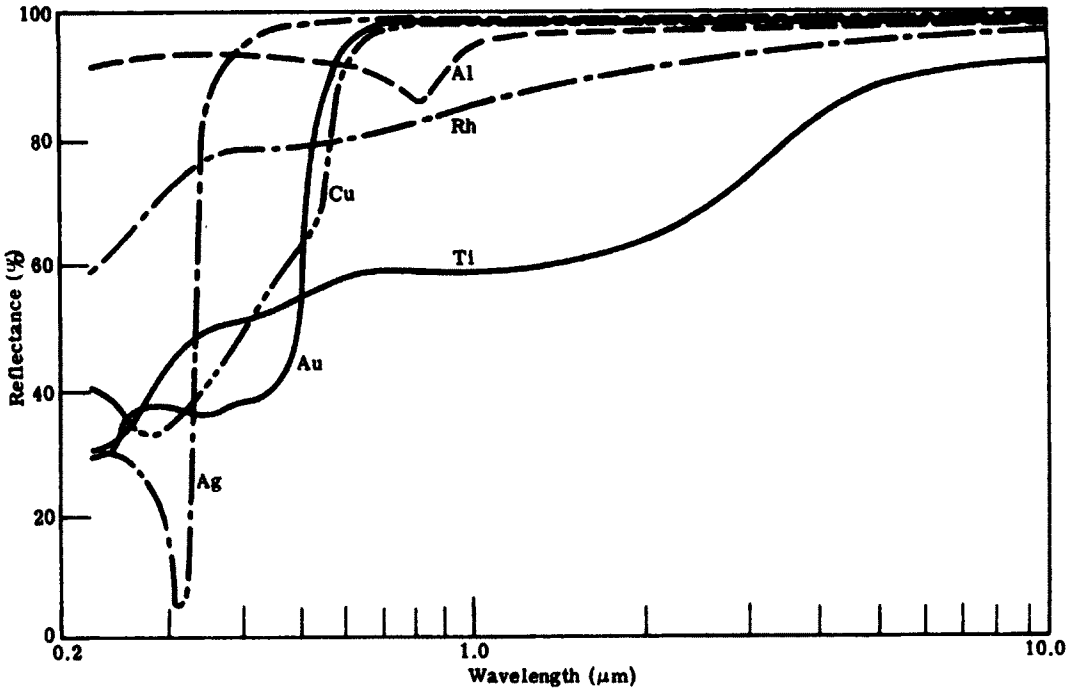

Figure 1.5. Reflectance of metals

Metal Oxides (i.e. SnO_x)
Ag
Metal Oxides (i.e. SnO_x)
Ag
Metal Oxides (i.e. SnO_x)
Substrate (Glass)

Figure 1.6. Multilayer low-E coating

Low emissivity in the NIR region is also important in radiation heat transfer problems. In order to minimize either radiant heating or heat loss by radiation, low emissivity is necessary.[18] In terms of infrared emissivity only, the best material would

be gold or silver. The published optical constants of aluminum, silver, and gold have been used to calculate the emissivity's at 6 and 10 μm in wavelength (Table 1.1).

Table 1.1. Reflectivity and calculated normal spectral emissivity at 6 and 10 μm for aluminum, gold and silver

Metal	6μm		10μm	
	n-*ik*	Emissivity	n-*ik*	Emissivity
Aluminum	10.8-*i*48.56	0.0221	26.0-*i*67.3	0.0198
Gold	4.7-*i*35.2	0.0148	11.5-*i*67.3	0.00976
Silver	4.15-*i*42.6	0.0090	10.69-*i*69.0	0.00873

Being NIR reflective materials, transition metals are used in the form of thin films or flakes. The preparation methods of thin film can be physical vapor deposition (PVD), chemical vapor deposition (CVD) or electro/electroless plating. PVD produces uniform ultra-thin silver film with good transparency in the visible region. The drawback of PVD is that the process is usually conducted in large sized equipment which requests high vacuum. It is also costly to retain the high vacuum. In the case of CVD, the availability of stable silver complex precursor is limited. Additionally, the equipment for CVD is expensive especially for large area deposition. Plating is a low cost method which is usually conducted between room temperature and 60°C. The substrate can be in any shape for plating. The challenge of both electro and electroless plating is preparing films as thin as 50 nm or less. Besides, the substrate has to be electrically conductive if electro plating is needed.

1.3. 2 NIR reflective Inorganic materials

The NIR reflective inorganic materials are mainly metal oxides and sulfides. In recent years, they are mostly used as pigments in NIR reflective coating for residential and commercial buildings. They can also be used as visual/IR camouflage since these metal oxides usually absorb some bands in the visible region. The most used metal oxides/sulfides are doped TiO_2, Fe_2O_3, CrO_3, MnO_x, and CdS. Other metals such as Ni, Sb, Fe, Mn, Zn, Cr, Bi, Sr, Y, Cu, etc are used as dopants to adjust the color of pigments. Of all those pigments, doped rutile titanates are the most popular choice due to its non-toxicity. Some commercially available IR reflective pigments with different visible colors are shown as examples in Figure 1.7.[19,20] Reflectance of selected pigments is also provided.

Klabunde and coworkers studied the NIR reflectance of metal oxides nanoparticles. They found the nanocrystalline metal oxides possess higher NIR reflectance of ~15-20% and attributed the increase of reflectance to smaller crystallite sizes coupled with smaller mean aggregate sizes.[21] Table 1.2 lists some metal oxides with the size dependence reflectance.

Most of metal oxides are used as NIR reflective painting materials in the form of fine powder. The preparation of powdery metal oxides is economically feasible on industrial scale.

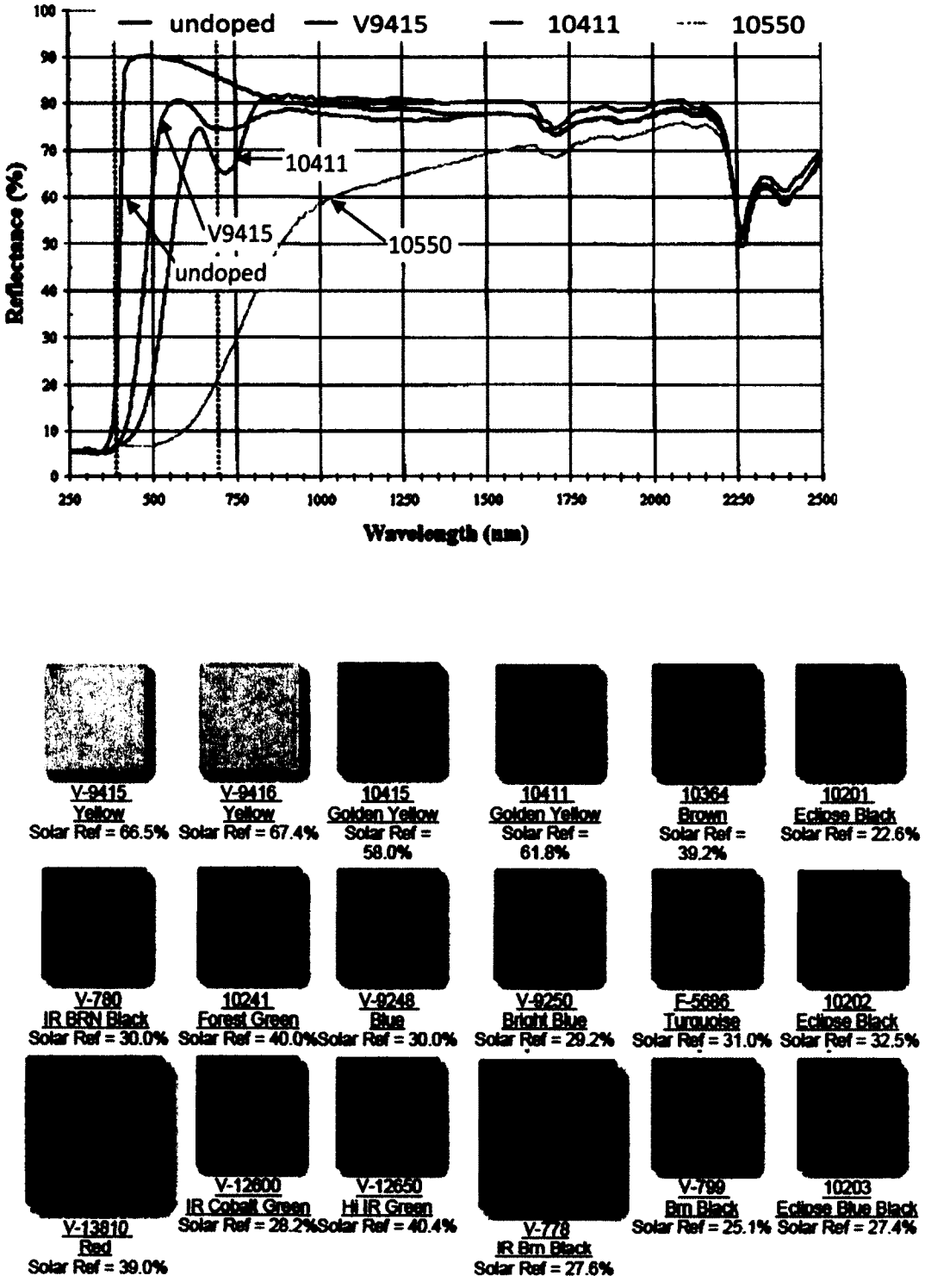

Figure 1.7. Top: Reflectance of metal oxides pigments, the reflectance was compared to commercial rutile TiO_2; Bottom: Samples of metal oxides with different colors, solar ref.: ratio of solar radiation reflected from a material to the amount shone on the material. Visible light is included . Adopted from ref.19 & 20.

Table 1.2. NIR reflectance properties of nanocrystalline metal oxides and macrocrystalline metal oxides.

Metal oxides	R% at 810 nm	Mean particle aggregate size (μm)	Average crystallite size (nm)	Surface area (m^2/g)
NC-CeO_2	110	61.6	≤ 7	≥ 50
MC-CeO_2	92	95	55	6
NC-Al_2O_3	102	1.4	amorphous	≥ 275
MC-Al_2O_3	92	2.6	70	68
NC-TiO_2	108	14.5	amorphous	≥ 500
MC-TiO_2	98	16.4	79	8
NC-MgO-I	109	4.2	8	≥ 230
NC-MgO-II	105	7.8	≤ 4	≥ 600
MC-MgO	103	2.4	23	45

NC: nanocrystalline; MC: macrocrystalline.
R% : the relative reflectivity was calculated compared to bulk materials.

Another type of inorganic NIR reflective material is doped high band gap metal oxides, such as indium tin oxide, antimony or fluorine doped tin oxide. It is believed that the band gap of these materials is large (approximately 3 eV)[19,22] enough to make them transparent to visible light. As they reflect the light with wavelength range over 1300 nm, they could be used as transparent heat mirrors.

1.3.3 NIR reflective organic materials

NIR reflective organic materials are rare. Two patents claim black pigments containing copper phthalocyanine[23] and azo pigments[24] that are of high NIR reflection. When incorporated with commercially available pearlescent mica, the reflectance of halogenated copper phthalocyanine pigment can be over 50% in the wavelength range of 1000 to 1500 nm and maintains above 35% from 1500 to 2200 nm as shown in Figure 1.8. The azo compounds depicted below (shown in Figure 1.9) can be used as textile printing agents, paints and printing inks with dark green color. The IR reflectance of the colored articles is as high as that of green plants, so they can give camouflage, which cannot be distinguished from surroundings by IR detectors, to various military equipment, devices and facilities.

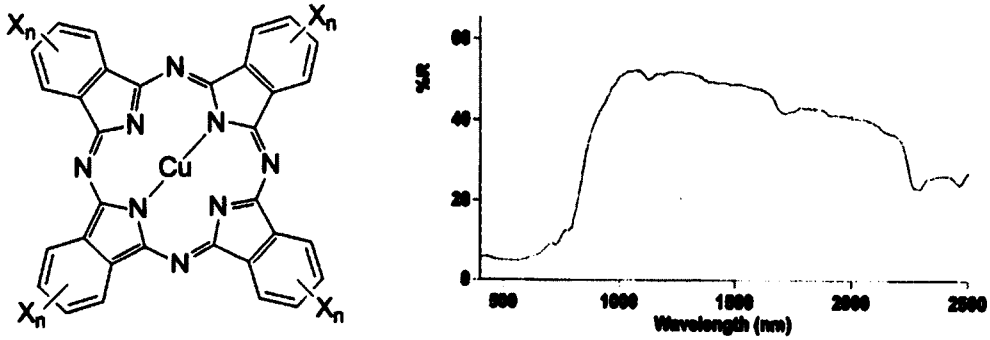

Figure 1.8. Structure and IR reflectance of Copper Phthalocyanine

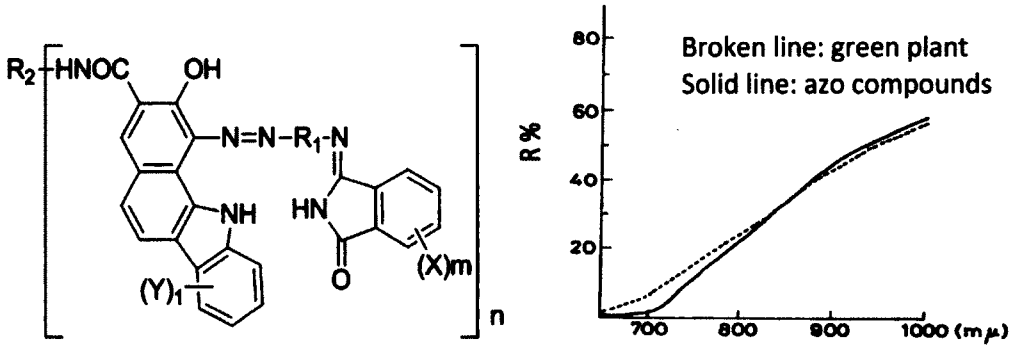

Figure 1.9. Structure and IR reflectance of azo compounds

1.3.4 Natural NIR reflective material: chlorophyll

Chlorophyll is the only known NIR reflective natural material to date. As shown in Figure 1.10, leaves can reflect both green and NIR light from sunlight. The unique reflective spectrum of different leaves can be used to identify the types of plants. In military applications, the conventional green pigments serve as camouflage in coatings since they reflect green light, but they absorb IR whereas chlorophyll reflects it.[19,25] Unfortunately, there is no chlorophyll used as camouflaging material probably due to its poor stability.

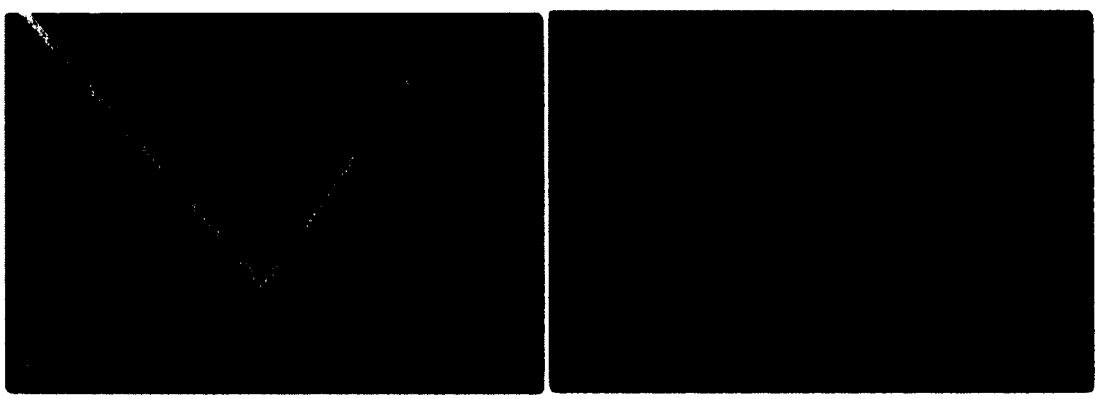

Figure 1.10. Reflection of chlorophyll

1.3.5 Evaluations of NIR reflective materials

To evaluate the performance of NIR reflective materials, there are several methods and procedures available. Heat build-up test: ASTM D 4803 is a test method predicting the heat build-up of the exterior objects in the laboratory. By testing the temperature increase of an object which is exposed to a 250 watt heat lamp until thermal equilibrium in an insulated box is reached, one can predict the heat build-up correlating to the temperature of an actual exposed exterior surface. Solar spectral reflectrometer: the result from this method is a general percentage total solar reflective value. ASTM C 1549 utilizes this method in determining the solar reflectance of substrates. Emissometer: this is an instrument used to measure the emissivity of a specimen. UV/Vis/NIR spectrometer: the instrument measures the percentage reflectance and transmittance over a wide wavelength range of UV to NIR. The measurement gives detailed characterization of unique materials utilized in IR reflecting applications. The result of reflectance or transmittance correlates to the wavelength. Depending on the type of detector and geometry of setup, specular or total reflectance can be obtained. UV/Vis/NIR is a necessary research tool when developing IR reflective materials. ASTM E 903 outlines a standard test method for determining absorbance, reflectance and transmittance of materials.

When incorporating the reflective pigments with coating matrix, some factors can affect the NIR reflective performance of the pigments.[19] First of all, the selection of pigment is of importance. Besides the reflectivity, the selection should also be based on L, a, and b values of the pigments. L, a and b are color scale parameters. The L ranges from 0 to 100. The maximum of L is 100, which represents a perfect

reflecting diffuser or white. The minimum of L is 0, which represent black. The a and b have no specific numerical limits. Positive a is red, while negative a is green. Positive b is yellow, while negative b is blue. Dispersion is another concern as pigments should be dispersed in a small media mill to obtain the required fitness of mesh size and avoiding further grinding which affects the color and also maybe the IR reflectivity partially due to thermal buildup during grinding. When blending different pigments to increase the IR reflectivity, the IR reflectivity may decrease by different absorption band in some cases. Opacity to IR requires higher thickness of film than to the visible light, so does volume concentration of pigments. Contamination may occur when blending two pigments with different IR absorption. The IR absorption dominates when blending one pigment is IR absorptive and the other one is IR reflective in the same band. Finally, the particle size is an important parameter. The highest reflectivity comes from the particles whose size is more than half the wavelength of the light to be reflected. Normally, the particle size for non-crystallines should be at least 0.35 to 0.55 μm for NIR reflection.

1.3. 6 Applications of NIR reflective materials

NIR reflective materials have been used in the military, architectural, plastic, and ink industries. Some of these applications are well established, such as camouflage, others are relatively new but growing rapidly such as automotive interiors, paint, textiles, stadium seating, and parking surfaces. The newly growing applications focus on energy saving or efficiency. For example, NIR reflective materials are employed into coatings for external walls and roofs of buildings to reduce the cooling load of air conditioners. Cooling deserves more attention than heating because the energy consuming for cooling is more than three times that of heating. Transparent NIR reflective coatings can be applied onto glass windows so that the solar heat is blocked without affecting the indoor brightness. Some NIR reflective screens made of polymer composites with NIR pigments can be used for greenhouses allowing transmission of visible light, which is needed for photosynthesis, and reflecting NIR light. Another application of NIR materials is camouflage, for example in textile printing. Most of the literature on NIR reflective materials exists as patents indicating the importance of potential and practical applications.

There is an increasing demand to develop new NIR reflective pigments and there is also ongoing research on processing NIR materials like metallic thin films which is the highest NIR reflective material with low emissivity.

1.4 Review of NIR absorptive materials

Unlike NIR reflective materials, most of NIR absorptive materials are organic compounds. A few metal oxides can absorb NIR light with electrochromic properties.

1.4.1 NIR absorptive organic materials

Origin of NIR absorption

There are numerous organic materials that are NIR absorptive. Basically, they can be classified as organic conjugated or donor-acceptor (D-A) system and metal complex. The NIR absorption of organic compounds is determined by the energy gap between highest occupied molecular orbital (HOMO) and lowest unoccupied molecular orbital (LUMO). Generally, the energy gap can be tuned by modifying the conjugation length, bond length alteration, and donating/withdrawing strength of donors and acceptor.[26,27] With the extension of conjugation length, the energy gap of π-conjugated systems can be decreased to a certain extent. Bond length alteration between double and single bonds determines the energy gap of typical π conjugated compounds. The closer the bond length of double and single bond is, the smaller the energy gap of the molecule is. In the D-A system, the donating and withdrawing strength influence both the bond characteristics between D and A units and the energy level of HOMO and LUMO after hybridization resulting in reduced energy gap.

The spectroscopic absorption of metal complexes is summarized in Table 1.3. d-d transition occurs from one of d-orbitals of the metal to another one. Since d-d transition is usually spin allowed but Laporte forbidden, the absorption from this transition is weak. Charge transfer occurs between orbitals with mainly metal

character (orbitals of metal) and orbitals with mainly ligand character (orbitals of ligand). When an electron is excited from an orbital of metal to an orbital of a ligand, metal to ligand charge transfer (MLCT) occurs. The opposite process, ligand to metal charge transfer (LMCT) occurs when an electron is excited from an orbital of ligand to an orbital of metal. As charge transfer is both spin and Laporte allowed transitions, the intensity of the absorption is as high as logε = 3~5. Figure 1.11 shows an example for molecular orbital diagram of octahedral complex and how MLCT and LMCT occur. The NIR absorption of metal complexes normally originates from charge transfer. The energy gap of the charge transfer is determined by the d orbital of metal, the oxidation state of metal, and the electron donating capability of the ligand.

Table 1.3. Intensity of electronic spectroscopy of metal complex

	Selection Rule	ε/L mol^{-1}cm^{-1}	log ε
d-d transition	Spin forbidden	< 1	0
d-d transition	Laporte forbidden	20~100	1~2
Charge transfer	Spin and Laporte allowed	>1000	3~5

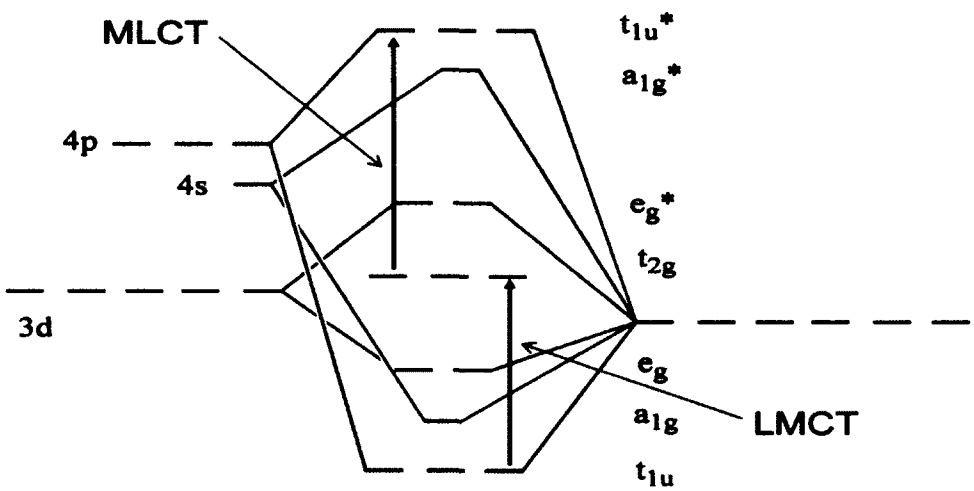

Figure 1.11. MO diagram of octahedral complex and charge transfer

Organic compounds

Organic compounds with extended π conjugation systems would absorb NIR light. Typical NIR absorptive organic compounds are polymethines including cyanines and merocyanines, conjugating compounds with donor-acceptor systems, polyenes, quinone derivatives, phthalocyanines and naphthalocyanines, and other chromophores like azo compounds. As described before, the NIR absorption was attributed to a reduced energy gap mainly by the extension of conjugation system and/or donor-acceptor system. Those compounds have been extensive reviewed.[26-28] In the following paragraph, only two types of compounds, polymethines and donor-acceptor systems, will be discussed as examples.

A. Polymethines

Polymethines represent a class of dyes whose molecules contain π conjugated system including electron-donor and acceptor groups as ending groups. The general structure of polymethines is shown as below (**1**). Polymethines can be charged species, such as cyanine, or uncharged species such as merocyanines. Cyanines are strong candidates for optical signal processing devices between 1000 and 1600 nm owing to their fast response and decay time.[29] Merocyanines are also called neutrocyanines which absorb NIR if dissolved in polar solvents.

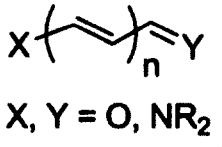

1

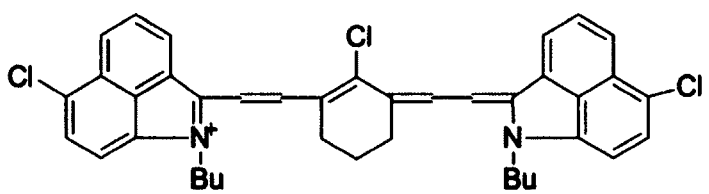

2

The absorption of polymethines covers a wide NIR region due to the contributing extension of conjugation which can make the NIR absorption red shift up 100 nm.[26,30] In general, the absorption extinction coefficient and oscillator strength increase as the chain length is extended. Annelation of heterocyclic ending group will result in red shift of absorption. However, the photo- and thermal stability decrease with the extension of conjugation length. To improve the stability, some modifications are made by introducing fused rings and halogens. NIR dye IR1050 (**2**) is an example .[31]

B. Donor-acceptor type of compounds

The energy gap of organic compounds can be tuned by using electron donors and acceptors. This is a generally accepted approach in molecular design. The HOMO/LUMO of donor and acceptor units can interact through π-conjugating system leading to narrow energy gaps if the linkage is a π spacer. If the two donor units are employed in one molecule, the D- π-A-π-D system will be constructed. Since a duo-donor system will enhance the orbital hybridization, the energy gap of the molecule will be further reduced comparing to a molecule with a single donor. For example, a new series of NIR absorption compounds were obtained by Wang and his co-workers (Figure 1.12). [32] The absorption of the compounds ranges from 600 to 1400 nm with emission of 900-1600 nm.

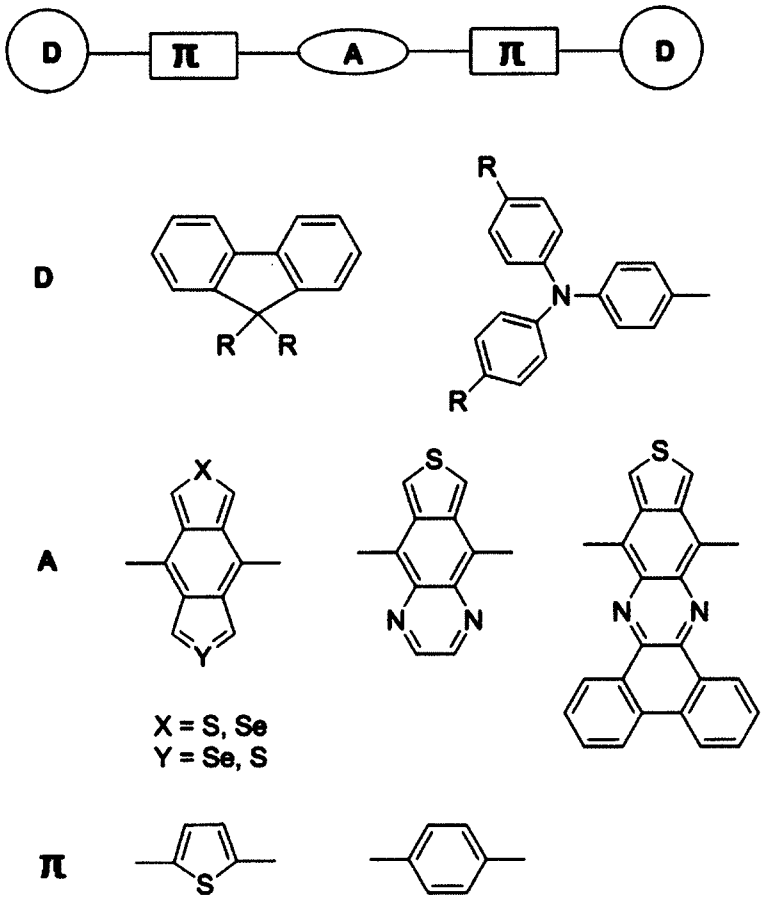

Figure 1.12. Structures of compounds with D-π-A-π-D type

On the other hand, if the donor and acceptor are linked by σ spacer, HOMO and LUMO of the molecule can be tuned independently since there is no hybridization between HOMO and LUMO.

In general, the extended π-conjugated systems have the shortcoming of an increased chemical reactivity save from some exceptions. The majority of the known organic materials are not stable under the environmental influences of light, moisture and atmospheric oxygen.

Metal complexes

The dithiolene complexes of transition metals with the general structure shown in Figure 1.13 are the first reported NIR absorptive metal complexes which show intense and broad absorption at neutral and monoanion states. Dithiolenes have aroused interest for some reasons: (a) their intense absorption in the NIR region; (b) their redox properties; (c) high thermal and photochemical stability and (d) capability of tuning the absorption wavelength by introducing substituents to the ligands.[33] One distinguishable characteristic of dithiolene complexes from pure organic NIR dyes such as cyanines is their broad band absorption and no vibrational fine structure.[34] Most complexes studied in this system are derived from Ni because of the higher delocalization within these complexes compared to the Pd and Pt analogues.[35-37]

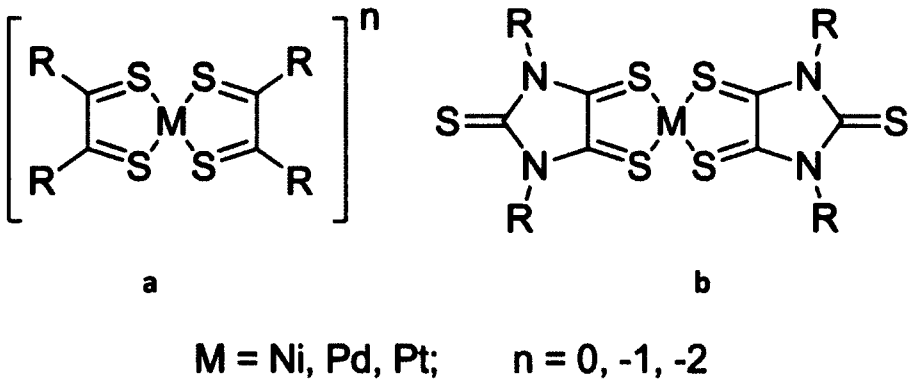

Figure 1.13. (a) General structure of dithiolene metal complexes; (b) Complexes of dialkyl-substitued imidazolidine-2,4,5-trithiones

The origin of the NIR absorption was controversial. The strong NIR absorption was assigned to π-π transition by Schrauzer and Mayweg[38] while Gray[39-41] assigned them to L(π)- π^* transition. Meanwhile, the oxidation state of Ni was considered to be

0, +2 and +4 in the neutral, monoanion and dianion species respectively, while the ligands were normal 1,2-dithiolate.[42] More recently, Weighardt argued that the Ni(II) remained in all species but the ligands involved electron transfer giving rise to dianion and radical anion.[43] The factors that influence the absorption wavelength had been studied by Mueller-Westerhoff and co-workers.[34] Basically, the ligand structure had a strong effect on the electronic spectra. The following factors must be considered to attempt a bathochromic shift the absorption: (a) coplanarity of the ligand π system and dithiolene; (b) extended π system; (c) electron donating substituents on ligand; (d) coplanarity of substituents and ligand.

Nevertheless, numerous dithiolene derivatives were synthesized and used to prepare complexes with Ni, Pd and Pt. The NIR absorption ranges from 700 to 1400 nm with molar extinction coefficients up to 80,000 M^{-1} cm^{-1} depending on the nature of ligands.[44] Particularly, the neutral complex (Figure 1.13b) that gave the highest extinction coefficient was based on a planar ligand, disubstituted imidazolidine-2,4,5-trithiones.[45] The electron donating N-substituents were coplanar with a dithiolate unit which enhanced the donation effect and resulted in an extinction coefficient of 80,000 M^{-1} cm^{-1} at ca. 1000 nm. It proved the effect of co-planarity and substituents on intensity and wavelength of absorption.

Analogues to dithiolene complexes are o-benzoquinone and o-phenylenediamine complexes which possess similar electron delocalizaion.[46] The o-phenylenediamine Ni complexes (Figure 1.14) exhibit a bathochromic shift of 60 nm compared with dithiolene complexes.[28] It was originally discovered by Feig and Furth in 1927.[47,48] And it was found that the complexes have unusually long-wavelength

absorption (λ = 780 nm, ε = 55,000 $M^{-1} \cdot cm^{-1}$). Research on electronic structures, oxidation states and spectroscopic properties of this type of complexes had been investigated since then.[48-55] The complex was confirmed as a central member of five-member series of planar complexes interrelated by reversible one-electron-transfer reactions.[48,50] The NIR absorption was assigned to $\pi - \pi^*$ transition.[53]

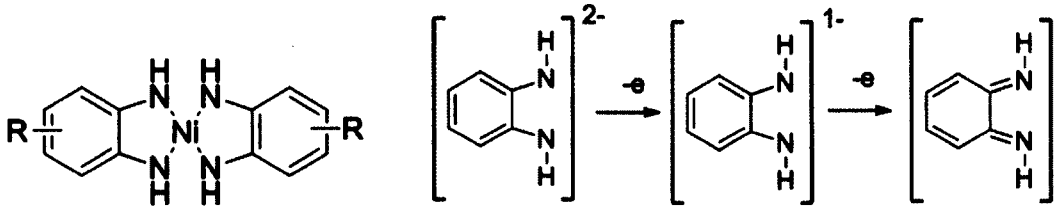

Figure 1.14. Ni[*o*-$(NH)_2C_6H_4]_2$ and oxidation state

Babler and Park found that the substituent groups on aromatic rings have a strong influence on NIR absorption and reduction/oxidation behavior of the complexes.[52,56] The substitution groups, either electron donating or withdrawing, make NIR absorption red shift up to 840 nm. But the electron withdrawing groups will reduce the extinction coefficient in NIR region. It was also found that the thermal and light stability of this type of complexes are as same as or higher than that of dithilolene complexes.with melting point of over 300 °C.[57] Other properties such as electric conductivity, optical non-linearity, and magnetism were also investigated for potential application in the fields of semiconductors,[58-60] optical data storage,[56] NLO materials and metal recognition sensors.[61,62]

Coordination polymers

Coordination polymers, which are also called "metal-organic frameworks" (MOF), "coordination framework", "metallosupramolecular network" and "hybrid material",[63] have attracted a great deal of attention in the past decade since the influential paper reporting the structure of MOF-5 (shown as below).[64]

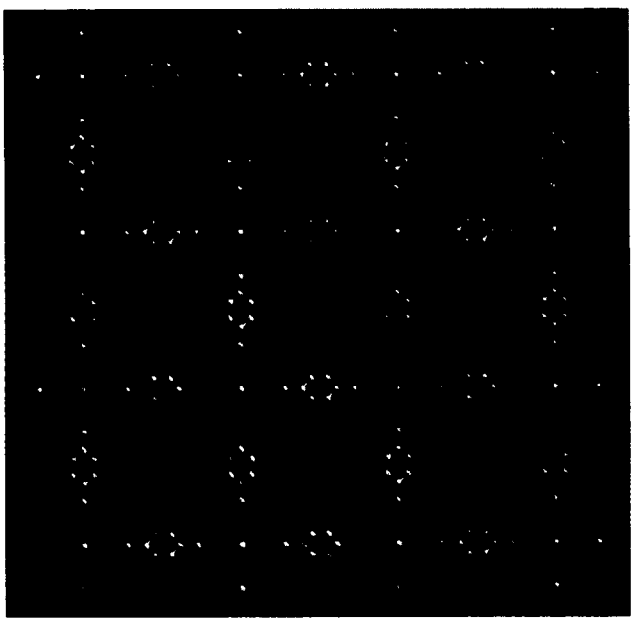

Representation of MOF-5.
Formular: $Zn_4O(BDC)_3(DMF)_8(C_6H_5Cl)$.
BDC: 1,4-benzenedicarbonate.
DMF: N,N-dimethylformamide.
C_6H_5Cl: chlorobenzene.

The intrinsic microporosity and incredible surface area of this type of materials enhanced the field of supramolecular chemistry. Basically, coordination polymer consists of metallo center spaced by organic bridging ligands. There are two types of coordination polymers, type A and B (Figure 1.15). The main difference between the two types is whether the backbone of polymer chain contains metallo center. In type A, metal ions link with organic molecules which are usually small molecules forming the backbone of the polymer. In type B, the metal ions link with the side chains of organic polymer chains. Usually type A is called metal-organic framework. As it is possible to tailor the bridging ligand to achieve specific properties, coordination

polymers are more versatile than traditional inorganic porous zeolite as porous materials.

(a) Type A:

(b) Type B:

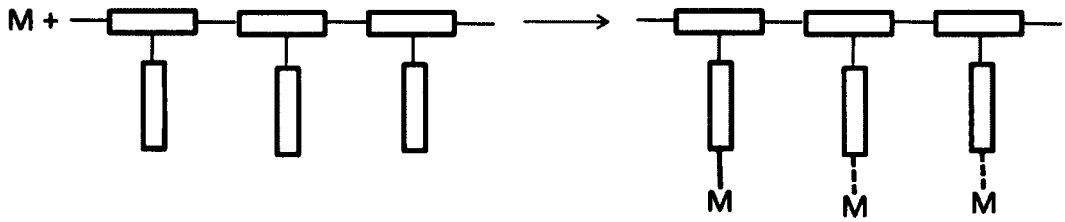

Figure 1.15. Coordination polymers (a) Metal center as backbone and (b) Metal attached to side chains of organic polymer.

Another distinct feature of coordination polymers is the low synthesis temperature (usually less than 100 °C). Moreover, the capability to construct new materials with functionalized bridging ligands leads to new properties for this type of materials. Besides the most notable porosity, other properties of coordination polymers have been investigated, such as luminosity resulting from conjugated organic linkers, charge transfer (MLCT or LMCT), high thermal stability, electronic conducting property, pH-sensitive stability.[65] These properties enable their energy-related applications which include gas storage, fuel cell, energy gas separation, CO_2 capture.[66,67] In the case of spectroscopic absorption, most coordination polymers show wide energy gaps which means their absorption fall in the region of visible light. To date, there are only two reported coordination polymers that are NIR active. Jackson and his co-workers synthesized one dimensional Ni dithiolene polymer which showed broad NIR absorption ranging from 900 to 2100 nm (Figure 1.16a).[68]

With the extension of co-planarity of metal centers and bridging ligands, the interaction between orbitals of metal and ligand is enhanced. The energy gap of the coordination polymer is reduced, thus the absorption red shifted to NIR region. Taube's group designed ruthenium polynuclear complex using pyrazine as bridging ligand. The polymer was also one dimension and the absorption was red shifted from 485 to 726 nm with the extension of chain length (Figure 1.16b).[69]

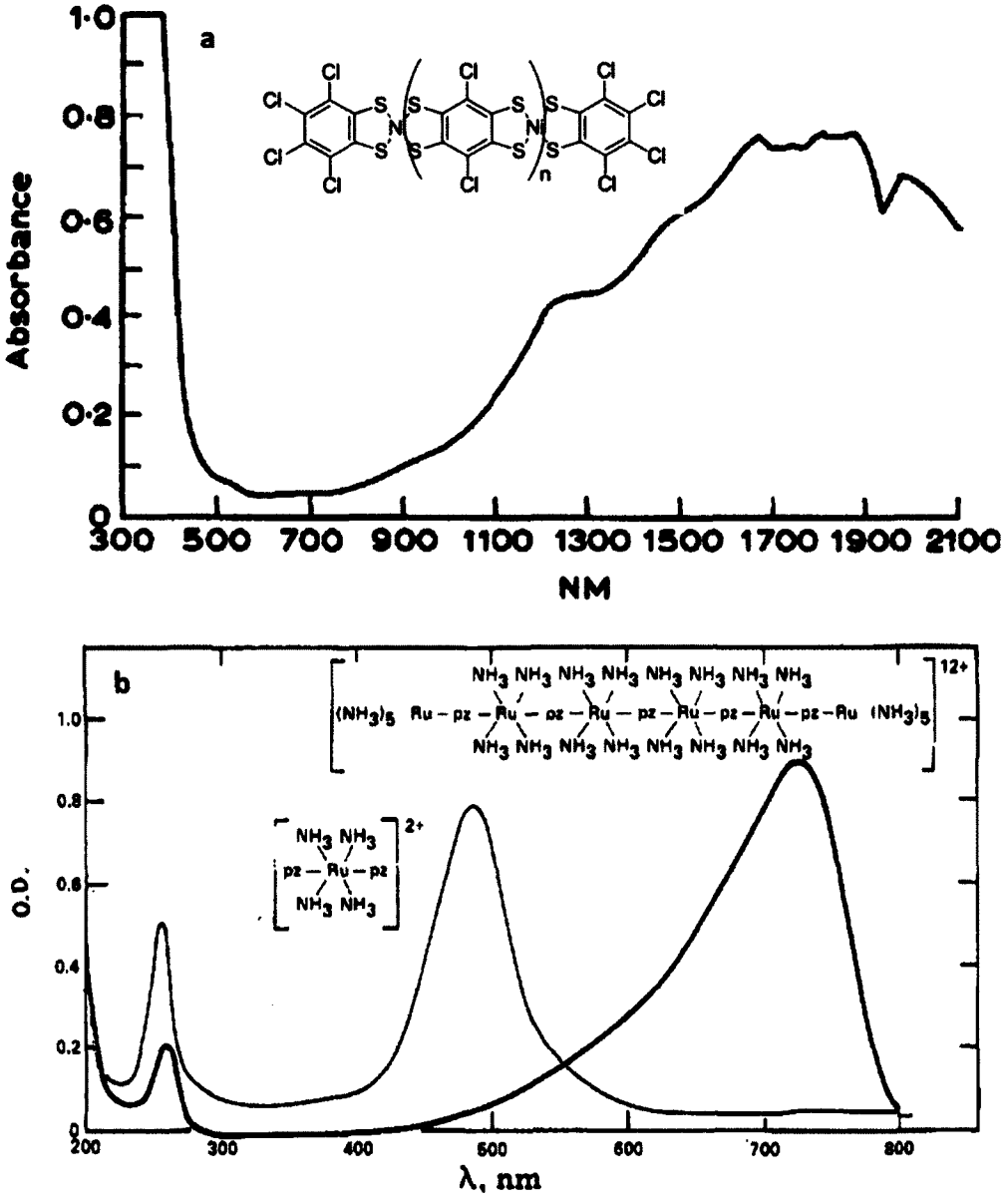

Figure 1.16. Spectroscopic absorption of (a) Ni dithiolene and (b) Ru amine coordination polymer. Adopted from the ref.68 & 69.

To design the coordination polymer, the selection of bridging ligand and metal ion is of vital importance. Typically, multicarboxylates, multiphosphonates, N-heterocyclic compounds, multicyanides, and compounds with mixed functional groups are employed as building ligands which must be able to link at least two metal sites. Figure 1.17 shows some examples of bridging ligands. As the coordination polymers are usually insoluble once formed, they must be prepared in a single step. Therefore, the ligand could either be synthesized in situ or by conventional organic synthesis prior to use.[70]

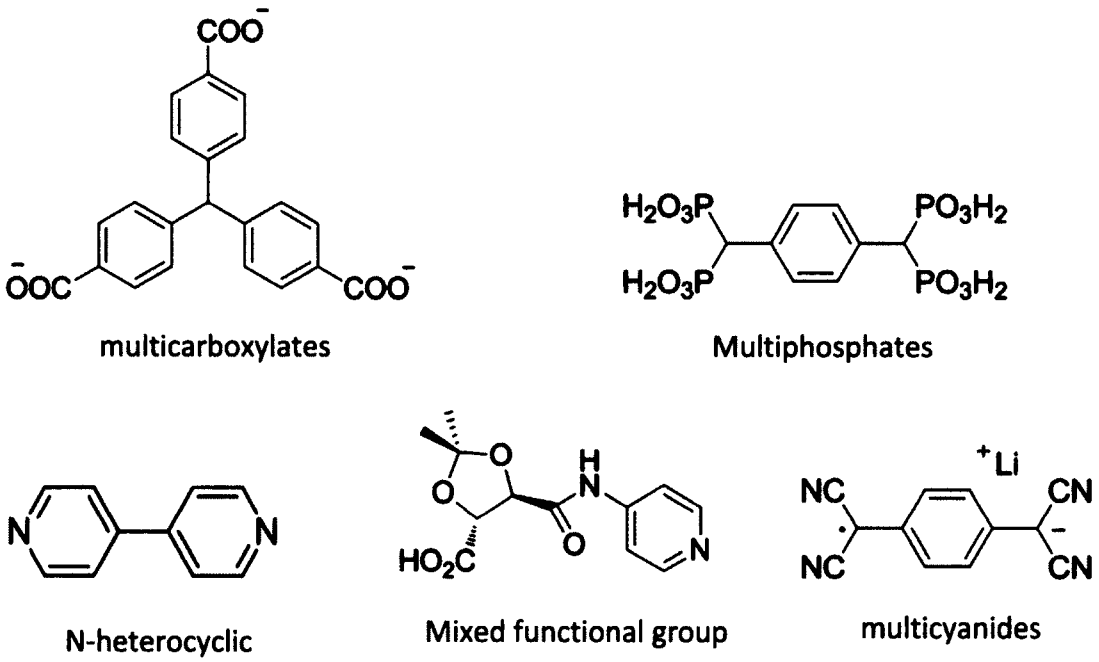

Figure 1.17. Examples of simple bridging ligands

The selection of metal ion depends on the desired geometry of coordination polymer. The metal ion can adopt geometries as linear, trigonal planar, square planar, octahedral, square pyramid, etc (Figure 1.18).

However, only dimensionality is predictable with certainty in many cases. For

example, tetrahedral metal ions linked with linear linker will generate a three dimensional four connected nets. In some cases, even the dimensionality is not predicable. For example, metal ions with coordination number of 4 and square planar geometry coordinates with linear ligands will generate two-dimensional networks or three-dimensional NbO type net.

Most study of coordination polymer mainly focuses on their porosity and magnetism, based on which the applications have been developed. The study of other properties such as electronic spectroscopy, pH-sensitivity, and electric conductivity is still in an early stage.

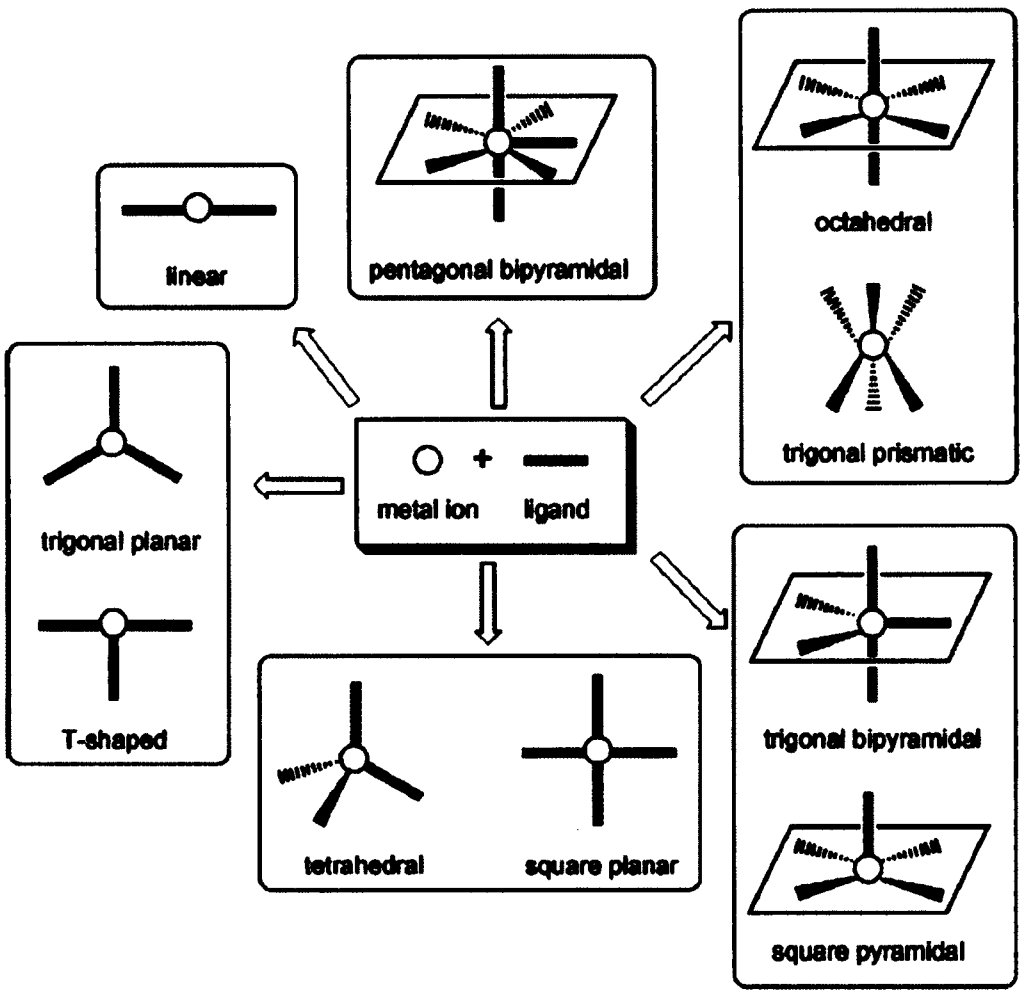

Figure 1.18. Coordination numbers and geometry of metal ions

1.4.2 NIR absorptive inorganic materials

Some transition metal compounds are NIR absorptive. The NIR absorption originated from d-d transition of metal ions. As known, d-d transition is spin-allowed but Laporte forbidden transition. Consequently, the intensity of the absorption will be weak with log $\varepsilon \sim 2$.[70] Preferably, NIR absorptive transition metals are present in the form of ions such as titanium (III), vanadium (IV), chromium (V), iron (II), nickel (II), cobalt (II) or copper (II) ion. Although the absorptivity is low, those metal ions can be used as IR cut-off optical filters[72-75], screen-printing or Intaglio inks,[76,77] for barcodes on invisible security documents, heat wave shielding[75] or even passive solar collectors and the like[78]. Iron (II) and copper (II) compounds have proven to be efficient broad-band IR absorbing exhibiting at most a slightly yellowish or bluish shade and they are the most employed inorganic IR-absorbers industrially.

Other type of IR absorptive metal oxides which express electrochromism have been well documented.[44,79] Electrochromism was discovered in the late 1960s and early 1970s.[80,81] Electrochromic materials could be used as smart windows which were first coined by Svensson and Granqvist in 1984.[80,82,83] Different shading is used to denote cathodic and anodic electrochromism. Cathodic is found in oxides of Ti, Nb, Mo, Ta, and W with tungsten being the most extensively studied. Anodic is found in oxides of Cr, Mn, Fe, Co, Ni, Rh, and Ir with nickel and iridium being the ones investigated in most detail.

Tungsten oxide is the most employed one for energy saving smart windows. Its color can switch from intense blue in the reduced form to colorless or slight blue in the bleached state. It is also NIR absorptive in broad band when reduced. The redox

reaction taking place is (eq. 1.2):

$$WO_3 + x\,(M^+ + e^-) \longrightarrow M_xW^{V}_{x}\,W^{VI}_{(1-x)}\,O_3 \qquad 1.2$$

Where M^+ is the inserted cation H^+ or Li^+ and x is the so-called ion insertion coefficient. The reversibility of color switch depends on the ion insertion coefficient which is usually less than 0.2. The reduced tungsten oxide absorbs NIR with a maximum at 980 nm.

NIR electrochromic metal oxide film can be prepared through many methods such as thermal evaporation, chemical vapor deposition, sputtering, electro deposition, and sol-gels.[44] The preparation methods will influence the morphology of the resulting film from amorphous to crystalline. Color efficiency, which is the most important criteria of selecting electrochromic materials, also relies on the preparative methods.

1.4.3 Applications of NIR absorptive materials

Generally, the application of NIR active materials is based on their properties such as invisibility to human eyes, penetration in tissues, energy conversion from light to heat or electric current. Therefore, NIR absorptive materials are broadly used in many fields such as security, camouflage, solar collection, laser optical recording system, thermal writing displays, laser printing system, infrared photography, medical or biological application.[28,84] The collecting of NIR sunlight also enhances the efficiency of using solar energy. As the absorbed NIR light can be converted to heat, those highly NIR absorptive materials can also be used for transmission laser welding based on its high molar extinction coefficient. The energy-related applications of coordination polymers, which includes fuel cells, energy gas storage, CO_2 capture, gas separation, and catalysis, have received much attention recently.[66] By harvesting NIR light, the power conversion performance of fuel cells is believed to be significantly increased.[8,9]

1.5 Rationale and objectives

NIR reflective and absorptive materials have been of interest in recent years owing to their energy related applications. In terms of reflective materials, the reflectivity varies largely with the type of materials. Among the available options, which are either inorganic or organic or natural materials, silver as transition metal is the best choice based on its reflectivity and fairly low cost. However, the preparation process of silver films is costly. Usually, the preparation methods involve high vacuum, strong magnetic field and high electric energy for melting. Therefore, the practical applications are hampered. It is believed that solution based preparation process, such as electroless plating, be conducted at low cost. Currently, electroless plated films with the thickness of over 0.5 μm can be obtained under the condition that the surface activated by Pd/Sn or silver nanoparticles. The adoption of Pd/Sn introduces impurities into the film and also leads to dark color. It is not acceptable for a product to contain impurities or dark color in some applications. The surface activation method using silver nanoparticles which are stabilized by polymers results in a high annealing temperature of 420 °C. This research project aimed at exploring new solution based methods of preparing silver thin films with low costs. Spray-pyrolysis of silver nanoparticles on substrate was proposed as a direct preparation process which can be conducted at low cost. Also, two improved surface activation methods for electroless plating were designed aiming at low annealing temperature and to be impurities free.

In the case of NIR absorptive materials, most of the strongly absorptive materials are organic based compounds. The absorptive organic materials suffer from

short term stability under the environmental influence of light, moisture and atmospheric oxygen. The research on metal coordination polymers has been of interest in the last decades owing to their energy related applications based on unique properties and extraordinary stability. Unfortunately, the NIR absorptive coordination polymers are still unexplored and only few reports were published to date. It is highly desirable to design new coordination polymers which are NIR absorptive. Tetraamino ligands are able to coordinate strongly with metal ions. The electronic delocalization and orbital overlap between metal and ligand would reduce the energy gap resulting in NIR absorption. In this thesis, two nickel coordination polymers with tetraamino bridging ligands were designed and synthesized aiming at broad absorption in the NIR region.

Accordingly, the objectives of this thesis research are:

1. To prepare silver nanoparticles solution in organic solvents as raw materials for preparing silver thin film by different methods;

2. To explore spray-pyrolysis method of preparing silver thin film and evaluate the reflection and transmission of the resulting film;

3. To explore surface activation methods for electroless silver plating by chemical redox reaction followed by evaluation of reflection and transmission;

4. To prepare tetraamino bridging ligands and Ni coordination polymer;

5. To investigate the properties of synthesized coordination polymers, NIR absorption, thermal stability, stability to chemical oxidation, and NIR halochromism.

1.6 References

(1) International Energy Agency, *World Enery Outlook,* **2010**.

(2) World Health Organization, *WHO World Health Report*, **2002**.

(3) U.S. Energy Information Administration, *2010 International Energy Outlook*, Report Number: DOE/EIA-0484(2011), **2010**.

(4) Hiramoto, M.; Kitada, K.; Iketaki, K.; Kaji, T. *Appl. Phys. Lett*, **2011**, 98(2), 023302/1-023302/3.

(5) Yue, W.; Zhao, Y.; Shao, S.; Tian, H.; Xie, Z.; Geng, Y.; Wang, F. J. *Mater. Chem.* **2009**, 19, 2199.

(6) Bürckstümmer, H.; Kronenberg, N. M.; Meerholz, K.; Würthner, F. *Org. Lett.* **2010**, *12*, 3666.

(7) Mitrea, S. A.; Hodorogea, S. M.; Duta, A.; Isac, L.; Purghel, E.; Voinea, M. *World Academy of Science, Engineering and Technology* **2008**, *47*, 360.

(8) Nazeeruddin, M. K.; Gratzel, M. In *Comprehensive coodination chemistry II: From Biology to Nanotechnology*; mcCleverty, J. A., Meyer, T. J., Eds.; Elsevier: Oxford, **2003**; Vol. 9, p 719.

(9) Shan, G.-B.; Demopoulos, G. P. *Adv. Mater.* **2010**, *22*, 4373.

(10) William M. Steen; Mazumder., J. *Laser material processing* 4th ed., **2010**.

(11) Sallavanti, R. A.; Frieder III, L. P. *US 7276136*, **2007**

(12) Gobin, A. M.; O'Neal, D. P.; Watkins, D. M.; Halas, N. J.; Drezek, R. A.; West, J. L. *Lasers Surg. Med.* **2005**, *37*, 123.

(13) Boehm, A. J.; Seeger, O. *Annu. Tech. Conf. - Soc. Plast. Eng.* **2005**, *63rd*, 2816.

(14) Boehm, A. J.; Glaser, A.; Muellen, K. *Annu. Tech. Conf. - Soc. Plast. Eng.* **2003**,

61st, 3687.

(15) Jones, I. A.; Hilton, P. A.; Sallavanti, R.; Griffiths, J. In *SPE ANTEC 2000 conference* Orlando, Florida, USA, **2000**; Vol. 1, p 1166.

(16) Hojnowski, S. L. *US 5695617509/127311*, **1998**.

(17) Song, D.-Y.; Sprague, R. W.; Macleod, H. A.; Jacobson, M. R. *Appl. Opt.* **1985**, *24*, 1164.

(18) Bennett, J. M.; Ashley, E. J. *Appl. Opt.* **1965**, *4*, 221.

(19) Bendiganavale, A. K.; Malshe, V. C. *Recent Patents on Chemical Engineering* **2008**, *1*, 67.

(20) Detrie, T.; Swiler, D. In *High performance pigments*; Faulkner, E. B., Schwartz, R. J., Eds.; Wiley - VCH: **2009**; Vol. 2nd ed., p 467.

(21) Jeevanandam, P.; Mulukutla, R. S.; Phillips, M.; Chaudhuri, S.; Erickson, L. E.; Klabunde, K. J. *J. Phys. Chem. C* **2007**, *111*, 1912.

(22) Haacke, G. *US 3998752*, **1976**

(23) Baler, F. *US 6989056 10/945515*, **2006**

(24) Horiguchi, S.; Ohira, S.; Abe, Y.; Zama, Y.; Saikatu, H. *EP 0211272*, **1987**

(25) Sliwinski, T. R.; Pipoly, T. A.; Blonski, R. P. *US 20026454848*, **2002**

(26) Qian, G.; Wang, Z. Y. *Chem. Asian J.* **2010**, *5*, 1006.

(27) Fabian, J.; Nakazumi, H.; Matsuoka, M. *Chem. Rev.* **1992**, *92*, 1197.

(28) Masaru *Infrared absorbing dyes*; Plenum Press: New York and London, **1990**.

(29) Blau, W. *Phys. Technol.* **1987**, *18*, 250.

(30) Asato, A. E.; Watanabe, D. T.; Liu, R. S. H. *Org. Lett.* **2000**, *2*, 2559.

(31) Chen, X.; Peng, X.; Cui, A.; Wang, B.; Wang, L.; Zhang, R. *J. Photochem.*

Photobiol. A **2006**, *181*, 79.

(32) Qian, G.; Dai, B.; Luo, M.; Yu, D.; Zhan, J.; Zhang, Z.; Ma, D.; Wang, Z. Y. *Chem. Mater.* **2008**, *20*, 6208.

(33) Stiefel, E. I. *Ditholene Chemistry: Synthesis, Properties, and Applications*; John Wiley & Sons, Inc.: Hoboken, New Jersey, **2004**; Vol. 52.

(34) Mueller-Westerhoff, U. T.; Vance, B.; Ihl Yoon, D. *Tetrahedron* **1991**, *47*, 909.

(35) Kuhr, M.; Bock, B.; Musso, H. *Chem. Ber.* **1976**, *109*, 1955.

(36) Nazzal, A.; Muller-Westerhoff, U. T. *Transition Met. Chem.* **1980**, *5*, 318.

(37) Bock, B.; Kuhr, M.; Musso, H. *Chem. Ber.* **1976**, *109*, 1184.

(38) Schrauzer, G. N.; Mayweg, V. P. *J. Am. Chem. Soc.* **1965**, *87*, 3585.

(39) Shupack, S. I.; Billig, E.; Clark, R. J. H.; Williams, R.; Gray, H. B. *J. Am. Chem. Soc.* **1964**, *86*, 4594.

(40) Baker-Hawkes, M. J.; Billig, E.; Gray, H. B. *J. Am. Chem. Soc.* **1966**, *88*, 4870.

(41) Williams, R.; Billig, E.; Waters, J. H.; Gray, H. B. *J. Am. Chem. Soc.* **1966**, *88*, 43.

(42) Sellmann, D.; Binder, H.; Häußinger, D.; Heinemann, F. W.; Sutter, J. *Inorg. Chim. Acta* **2000**, *300-302*, 829.

(43) Ray, K.; Weyhermüller, T.; Neese, F.; Wieghardt, K. *Inorg. Chem.* **2005**, *44*, 5345.

(44) Monk, P. M.; Mortimer, R. J.; Rosseinsky, D. R. *Electrochromism and Electrochromic Devices*; Cambridge University Press: New York, **2007**.

(45) Aragoni, M. C.; Arca, M.; Demartin, F.; Devillanova, F. A.; Garau, A.; Isaia, F.; Lelj, F.; Lippolis, V.; Verani, G. *J. Am. Chem. Soc.* **1999**, *121*, 7098.

(46) Mueller-westerhoff, U. T.; Yoon, D. I.; Plourde, K. *Mol. Cryst. Liq. Cryst.* **1990**, *183*, 291.

(47) Feigl, F.; Fiirth, M. *Monatsh.* **1927**, *48*,, 445

(48) Stiefel, E. I.; Waters, J. H.; Billig, E.; Gray, H. B. *J. Am. Chem. Soc.* **1965**, *87*, 3016.

(49) Balch, A. L.; Holm, R. H. *J. Am. Chem. Soc.* **1966**, *88*, 5201.

(50) Hall, G. S.; Soderberg, R. H. *Inorg. Chem.* **1968**, *7*, 2300.

(51) Miles, M. G.; Wilson, J. D. *Inorg. Chem.* **1975**, *14*, 2357.

(52) Bäbler, F.; von Zelewsky, A. *Helv. Chim. Acta* **1977**, *60*, 2723.

(53) Jacques, W.; Daul, C.; Van Zelewsky, A.; Goursot, A.; Penigault, E. *Chem. Phys. Lett.* **1982**, 88, 78.

(54) Lelj, F.; Rosa, A.; Ricciardi, G. P.; Casarin, M.; Cristinziano, P. L.; Morelli, G. *Chem. Phys. Lett.* **1989**, 160, 39.

(55) Kim, S. H.; Matsuoka, M.; Yomoto, M.; Tsuchiya, Y.; Kitao, T. *Dyes and Pigments* **1987**, 8, 381.

(56) Park, S.; Jun, K. *J. Ind. Eng. Chem.* **2005**, 11, 883.

(57) Vogler, A.; Kumkely, H.; Hlavatsch, J.; Merz, A. *Inorg. Chem.* **1984**, 23, 506.

(58) Noro, S.-i.; Takenobu, T.; Iwasa, Y.; Chang, H.-C.; Kitagawa, S.; Akutagawa, T.; Nakamura, T. *Adv. Mater.* **2008**, 20, 3399.

(59) Noro, S.-i.; Chang, H.-C.; Takenobu, T.; Murayama, Y.; Kanbara, T.; Aoyama, T.; Sassa, T.; Wada, T.; Tanaka, D.; Kitagawa, S.; Iwasa, Y.; Akutagawa, T.; Nakamura, T. *J. Am. Chem. Soc.* **2005**, 127, 10012.

(60) Taguchi, T.; Wada, H.; Kambayashi, T.; Noda, B.; Goto, M.; Mori, T.; Ishikawa,

K.; Takezoe, H. *Chem. Phys. Lett.* **2006**, 421, 395.

(61) Fukui, H.; Kishi, R.; Minami, T.; Nagai, H.; Takahashi, H.; Kubo, T.; Kamada, K.; Ohta, K.; Champagne, B. t.; Botek, E.; Nakano, M. J. *Phys. Chem. A* **2008**, 112, 8423.

(62) Fukui, H.; Nagai, H.; Kishi, R.; Minami, T.; Takahashi, H.; Kubo, T.; Nakano, M. *Synth. Met.* **2009**, 159, 2416.

(63) Kepert, C. J. *Porous Materials*; Wiley: Hoboken, NJ, USA, **2010**.

(64) Li, H.; Eddaoudi, M.; O'Keeffe, M.; Yaghi, O. M. *Nature* **1999**, 402, 276.

(65) Meek, S. T.; Greathouse, J. A.; Allendorf, M. D. *Adv. Mater.* **2011**, 23, 249.

(66) Ma, S.; Meng, L. Pure Appl. Chem. **2011**, 83, 167.

(67) Noro, S.-I.; Kitagawa, S. In *The Supramolecular Chemistry of Organic-Inorganic Hybrid Materials*; Rurack, K., Martinez-Manez, R., Eds.; John Wiley & Sons, Inc.: Hoboken, New Jersey, **2009**, p 235.

(68) Campbell, J.; Jackson, D. A.; Stark, W. M.; Watson, A. A. *Dyes and Pigments* **1991**, 15, 15.

(69) Von Kameke, A.; Tom, G. M.; Taube, H. *Inorg. Chem.* **1978**, 17, 1790.

(70) Almeida Paz, F. A.; Klinowski, J.; Vilela, S. M. F.; Tome, J. P. C.; Cavaleiro, J. A. S.; Rocha, J. *Chem. Soc. Rev.* **2011**, DOI: 10.1039/c1cs15055c.

(71) Atkins, P. J.; Shriver, D. F. *Inorganic chemistry*; 3rd ed.; W.H. Freeman and CO: New York, **1999**.

(72) Yamane, R.; , H., Youichi, ; Zou, X. *US 20040082460*, **2004**

(73) Speit, B.; Karnehm, A.; Winkler-trudewig, M. *US 5173212*, **1992**

(74) Sakagami, T.; Ogihara, T.; Fujii, Y.; Katono, H. *US 5466755*, **1995**

(75) Hayasaka, H.; Takano, T.; Satake, T. *US 5723075*, **1998**.

(76) Demartin Maeder, M.; Müller, E.; Despland, C. A.; Degott, P. *US2008/0241492*, **2008**

(77) Osahisa, M.; Yoshie, A. *JP 06-10798504-258256*, **1994**.

(78) Chiang, C.-h. P.; Dawson, W. R.; Kinney, L. F.; Sherman, C. J. *US 5800861288713*, **1998**.

(79) Monk, P. M.; Mortimer, R. J. *Electrochromism: Fundamentals and Applications*; VCH: Weinheim, **1995**.

(80) Granqvist, C. G. *Handbook of inorganic electrochromic materials*; Elsevier Science, **1995**.

(81) Deb, S. K. *Sol. Energy Mater. Sol. Cells* **1995**, 39, 191.

(82) J.S.E.M., S.; Granqvist, C. G. *Pro. Soc. Photo-Opt. Instrum. Engr.* **1984**, 502, 30.

(83) J.S.E.M., S.; Granqvist, C. G. *Solar Energy Materials* **1985**, 12, 391.

(84) Griffiths, J. *Chem. Br.* **1986**, 997.

Chapter 2 Near-IR reflective silver-based materials

2.1 Introduction

Preparation methods for silver films have been studied extensively due to applications or speculative applications in IR reflection,[1-7] Microelectromechanical system (MEMS),[8,9] surface plasma resonance spectroscopy for DNA detection and other application,[9-12] nanoscale optics,[9] metal-conducting line processing, [13,14] semiconductor (i.e. OLED),[15-18] and solar cell devices.[19] All those methods can be categorized into physical vapor deposition (PVD), chemical vapor deposition (CVD), and electroless plating (EP).

PVD is a deposition process by condensation of vaporized substance onto various surfaces. Techniques involve electron or ion beam assisted, evaporative deposition and RF/DC sputtering. The deposited film by PVD is uniform, continuous and electrically conductive, even as thin as 15 nm. However, maintaining a high vacuum is usually energy-consuming and costly. The equipment is also complicated and expensive, especially for large area deposition. In the case of CVD of silver, the major problem is the availability of stable, volatile silver complex precursors.[20,21] The equipment for CVD is also complicated and expensive. EP is a process that deposits metal films onto a surface by reducing a metal salt in a solution by chemical redox reaction. This process has been widely applied in making metal coatings for many applications. Prior to plating, surface pretreatment (activation) is essential to provide the proper nucleation center. Since the process is conducted at low temperatures and feasible to large area at low cost, many surface activation methods have been

developed for electroless plating. Pd and Sn ions are traditionally used to treat surfaces for silver plating.[22] Usually the Ag-Sn alloy formed at the early stage is dark in color and is not suitable for thin films requiring transparency in the visible region.[22,23] There are other methods to activate the surface for silver plating. Tong demonstrated silver plating on silicon using silver ion as seed layer[14]. Schaefers prepared silver films using silver nanoparticles to form a seed layer.[9] As the silver nanoparticles are stabilized by polymers, the decomposition/annealing temperature for the activation layer is as high as 420°C which limits its application.

In this chapter, the two different methods for preparing high NIR reflective silver films were studied. First of all, a spray method is explored using silver nanoparticle solution. As the stabilizers of the nanoparticle are small molecules, low temperature decomposition is possible. During the course of spraying, evaporation of fine liquid droplets makes the sprayed film dense. By repeating the spray-pyrolysis procedure, a dense thin silver film could be obtained. Secondly, electroless plating was investigated. The two surface activation methods are developed. The first one involves a modification of a substrate (e.g. glass) by a fluoro-compound to form a negatively charged surface. Positively charged silver ions and particles in solution then adsorb onto the substrate via electrostatic interaction to serve as seed layer for subsequent electroless plating. The second activation method involves the use of polymer/silver nanoparticle to form an activation layer either on glass substrate or as a free standing polymer film. To characterize the NIR reflectivity and transparency of all silver films, the reflectance and transmittance were measured.

2. 2 Silver film prepared by spray-pyrolysis method

2.2.1 Experiment method

All chemicals were purchased from Sigma-Aldrich without further purification. The water used is deionized water.

Synthesis of silver nanoparticle solution (AgNPs) To a suspension of silver nitrate ($AgNO_3$, 0.85 g, 5 mmol) in toluene (50 ml), butyl amine (1 ml) was added. The mixture was warmed up to 80 °C until silver nitrate was dissolved. Then lauric acid (0.20 g, 1.0 mmol) was added into the solution. After lauric acid was dissolved, sodium borohydride (0.38 g, 10 mmol) was slowly added into the solution. The solution turned to dark brown immediately. The reaction mixture was refluxed for 2 hours and then cooled down. 20 ml of water was then slowly added into the solution. The mixture was separated and the organic layer was washed with water until no free silver ions present in aqueous layer. To test the free silver ions, sodium chloride solution was used. The UV/Vis absorption of the solution was measured by spectrometer (Perkin Elmer Lamda 900). The particle size was also measured by GIXRD after spin coating the AgNPs on glass. The concentration of the AgNPs was determined by AAS after being dissolved in nitric acid. The silver content in AgNPS was ~6.7mg/ml. The obtained silver nanoparticle solution is ready for spray coating.

Substrate preparation and film making process The substrate, plain glass, was washed with soapy water, concentrated H_2SO_4 and then rinsed with water. The substrate was put on hotplate for spraying AgNPs, and the hotplate was set at different temperatures: room temperature, 100 °C, and 200 °C. Diluted AgNPs was

sprayed onto the glass directly. After a uniform coating was formed, the glass was put over a flame for pyrolysis with an argon flow protecting the silver film. Figure 2.1 shows the sketch of spray and pyrolysis.

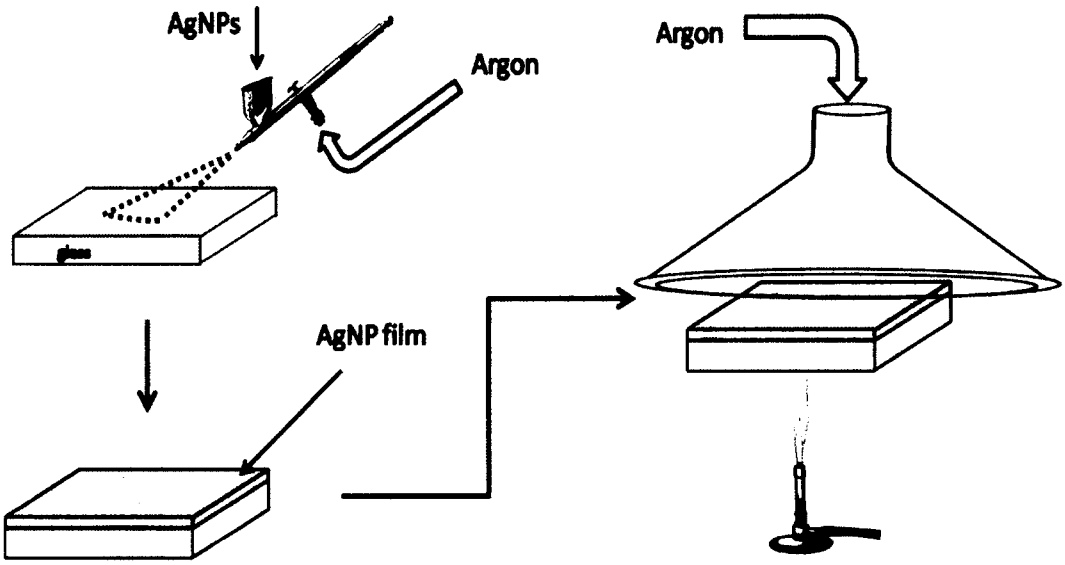

Figure 2.1. AgNPs spray-pyrolysis process

2.2.2 Results and discussion

Characterization of AgNPs In metal nanoparticles, the energy gap between the conduction band and valence band are so close that electrons move freely from each other. These free electrons give rise to a surface plasmon resonance (SPR) absorption band. As the spectral response of silver nanoparticles is a function of diameter.[24,25] UV/Vis extinction spectra can be used to determine the nanoparticle's size. Figure 2.2 shows that extinction spectrum of AgNPs peaks at 420 nm. Comparing to literature results, the particles size is deduced as less than 20 nm.[36] The particle size was also characterized by GIXRD (Figure 2.3). From the diffraction peaks, the particle size was determined to 3.5-8.3nm which agrees with UV/Vis results.

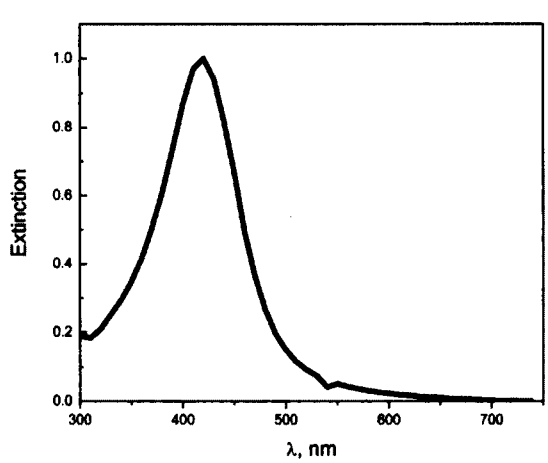

Sample #	1	2	3	4
D. F.	4	16	64	128

Figure 2.2. Left: UV/Vis absorption spectrum of AgNPs, right: diluted AgNP solution

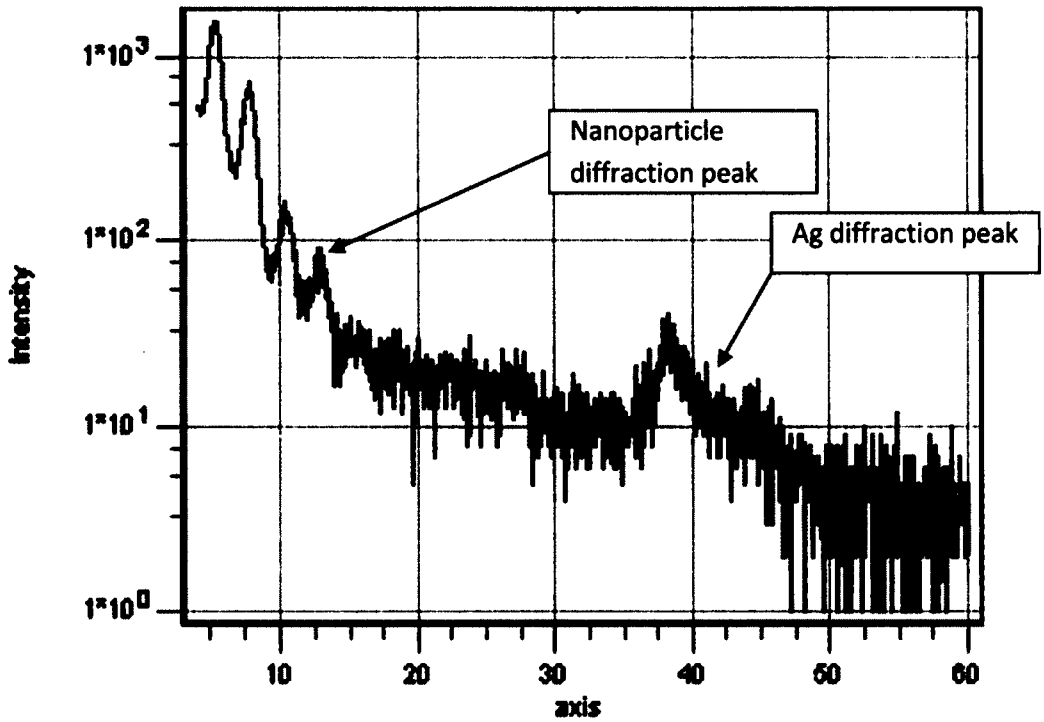

Figure 2.3.GIXRD diffraction of AgNPs

Reflectance and transmittance The specular reflection of the coating was measured using the reflection accessories shown in Figure 2.4. Aluminum mirror was used as reference with the incident angle of 45°.

Figure 2.4. Accessory to UV/Vis/NIR spectrometer (Perkin Elmer Lamda 900) for measuring specular reflectance. Light path of the beam is labeled as red arrows.

As the specular reflection of electromagnetic waves also relies on surface roughness, a smooth film is desired. On the other hand, in the case of silver film, electric conductivity would be important regarding reflection in NIR region. It is observed that a film with a high electric conductivity will show higher reflectance in NIR than that in visible region.

Figure 2.5 shows the reflectance of silver film as prepared. The reflectance increases in the region from 400 nm up to ca. 1000 nm, then it maintain fairly stable in NIR region. The slope in visible region probably comes from the surface plasma resonance (SPR) of silver particles.[33] The surface roughness of all film is similar to each other, while the electric conductivity is quite different. All five films are electrically conductive with different conductivity. The film with the highest R% of ca. 50% is the most conductive one with electric resistivity of 10 Ohm • cm (measured by multimeter); While the value for the one with lowest R% < 30% is far greater than 1000 Ohm • cm. In other words, metallic thin silver film is desired for reflection.

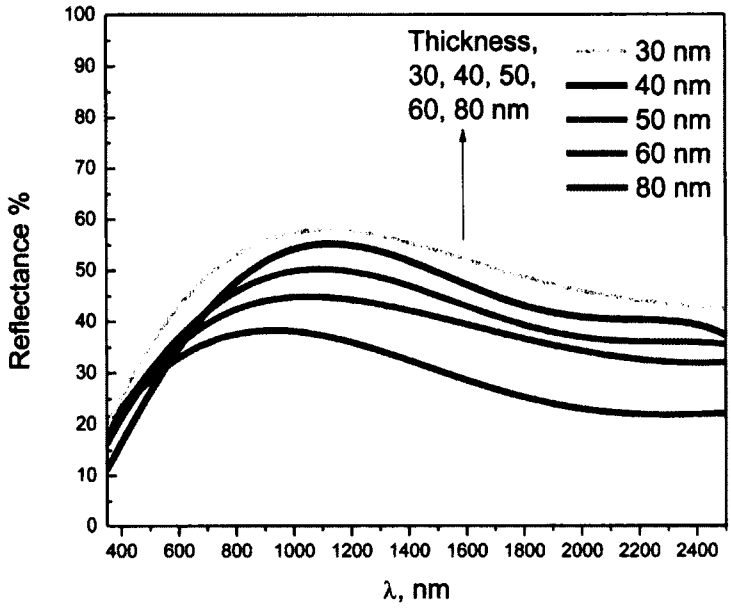

Figure 2.5. Reflectance of film after pyrolysis in flame. The thickness varies from 30 nm to 80nm.

In terms of thickness, it ranges from 30 nm to 80 nm. Generally, thickness plays an important role in reflectance. The thicker the film is, the higher reflectance the film gives. As shown in Figure 2.5, the film with 80 nm is the most reflective one. In theory, skin depth of silver in NIR region is ca. 10 nm.[26] In other words, a film with thickness of over 10 nm is, theoretically, thick enough to give as high reflectance of 90%. As a matter of fact, the thickness of film has to be at least 30 nm with a R% of ca. 30%. The density of the film accounts for the fact. With the same thickness, dense film will be more electric conductive than loose one. Thus, dense film will be more reflective. Usually, the film as prepared is porous and the porosity depends on preparation process and parameters. It is observed that the porosity can be reduced by multi-process of spray and pyrolysis.

Transmittance of films as shown in Figure 2.6 displays similar trends as reflectance. It should be pointed out that the sum of transmittance and reflectance is

less than 100, which is due to exclusion of diffuse reflection. As the setup can only measure the specular reflection, scattered light that is not refocused by the concave mirror is not detected. Generally, a thick film shows less transmittance.

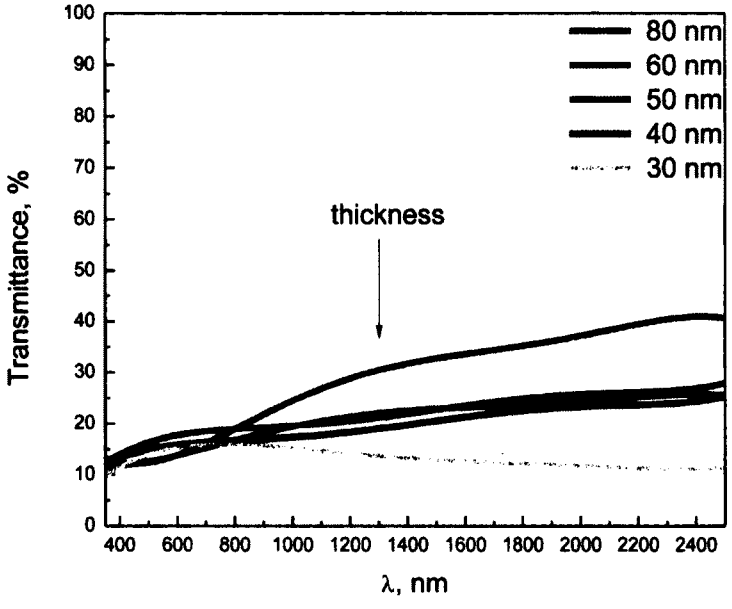

Figure 2.6. Transmittance of film after pyrolysis in flame. The thickness varies from 30 nm to 80nm.

Other parameters During the course of spray and pyrolysis, some other parameters such as substrate's temperature, dimension of droplets, concentration of nanoparticle solution, and pyrolysis time also have effect on the films quality.

The AgNPs solution was dispersed to small liquid drops by gas through spray nozzle. Since small liquid droplets promote equilibriated vapor pressure, the solvent evaporates fast during spraying.[27] A thin film will be formed instantly on the substrate surface. It is observed that small droplets contribute to uniform film. When the substrate's temperature reaches 100°C, the residue solvent in the film will evaporate immediately. In this case, silver particles coalescence and the film surface become rough due to bubbles generated. Thus, the film becomes opaque before pyrolysis.

When the temperature is over 200 °C, the ligands of the nanoparticles start to decompose. The obtained film is even worse than the one from anneal at 100 °C. To obtain a uniform film, the temperature of substrate was maintained at room temperature.

The evaporation of solvent promotes aggregation of nanoparticles during the course of spray. The thicker the solution is, the easier it will aggregate. Thus the concentration of the nanoparticle solution affects film uniformity. The original solution was diluted to one fourth of its initial concentration for spray to obtain film with smallest roughness.

Pyrolysis was carried out over natural gas flame for 5s with strong Argon flow protection. The temperature of the flame was ca.300 °C. Long-time stay in flame will result in oxidation of silver film.

Application demonstration As one of the applications of thin silver film is low emission coating, the spray-pyrolysis method was applied to fabricate low emission multilayer coatings. V_2O_5 was used as dielectric of the structure MOx/Ag/MOx. The dielectric constant of V_2O_5 is 4.2. The refractive index of V_2O_5 is 2.3. V_2O_5 layer was prepared by spincoating V_2O_5 sol which was prepared by dissolving molten V_2O_5 in water.

Figure 2.7 shows the difference of reflectance between film with and without V_2O_5 which acts as antireflection layer. Essentially, V_2O_5 layer does not affect the reflection in NIR region comparing to silver, so the R% in NIR is maintained when it decreases in the visible region. Visual transparency of the multi-layered coating is also presented in Figure 2.7.

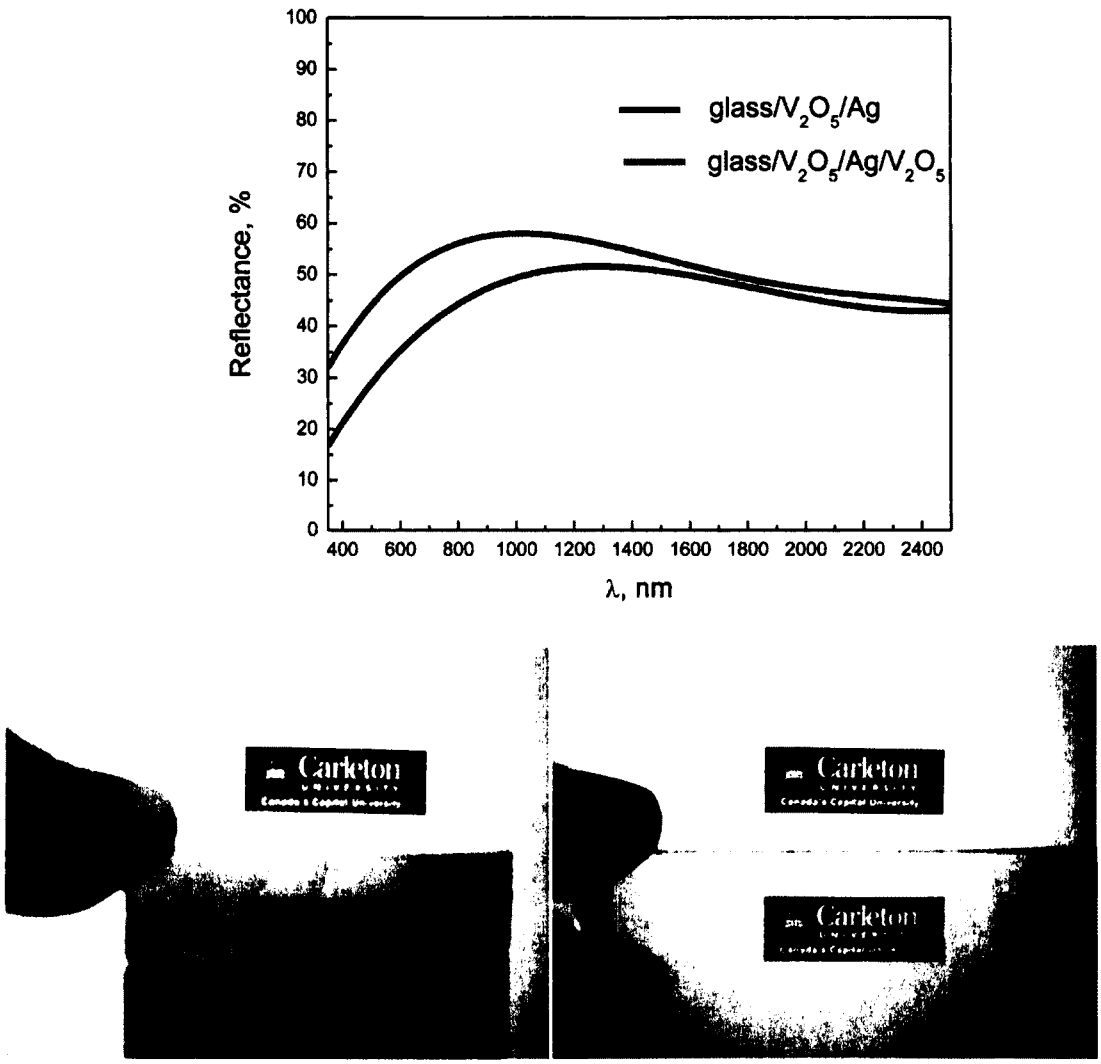

Figure 2.7. Top: reflectance of Ag film with and without antireflection layer; Bottom: Transparency comparison, lab sample (left), commercial sample (right). V_2O_5: 100 nm, Ag: 70 nm. The commercial product (Low-E glass) was from Proscience Inc.

2.3 Selective electroless plating silver film on fluorinated surface

As an alternative or supplemental technique, electroless plating method is widely utilized to fabricate micro or even nanoscale structures, due to its ease of use, simple equipments and quick plating.[28] The traditional electroless plating needs sensitization and/or activation by tin and palladium ions prior to plating. The sensitization and activation is essential to provide nucleation centers for reduction of silver ions on the surface and growth of the reduced silver particles to form a uniform coating. One of the effects from sensitization is to increase the negative charge on the surface so that the silver particles, which are positively charged, can be adsorbed onto the surface easily.[22] The mechanism of sensitization was discovered by Minjer's group.[23] During the course of plating, silver ion is first reduced by Sn^{2+} forming Ag-Sn nucleation centers. The silver particles are formed in solution by reducing reagent around the nucleation center. Due to the existence of Ag-Sn, the thin silver film is dark in color which reduces the transparency of the thin film. Besides, the Sn and Pd could be impurities for some applications. The control over the pattern (e.g. lithography) is also limited in this deposition process because the sensitization and activation is non-selective. Here a new method was developed to plate silver film on surface fluorinated glass and plastic sheets. The intrinsic property of fluorous-modified surface was investigated by Wang et al. They found the zeta potential of the fluorinated surface is negative and the negative charge increases up to -70mV at pH values of 10.0.[29] Bonn et al studied the heavy metals adsorption on fluorinated surface.[30] They confirmed that the adsorption of heavy metals on the fluorinated montmorillonite clays particles is due to the electrostatic attraction between positively

charged metals and negatively charged surface. And the negative charge of the surface does not change after the adsorption of heavy metals. Furthermore, they also found the negative charge increases with the increase of pH value of solution.

Based on these previous results, we intended to deposit silver particles on to the fluorous-modified surface by using the electrostatic interaction. First of all, the glass plate is fluorous-modified to obtain a negatively charged uniform surface. Secondly, the modified surface is immersed into silver plating solution which is alkaline with pH $\geq$ 10. Positively charged silver particles formed by reducing silver complex ions adsorb on to negatively charged surface to form a thin layer by the driving force of electrostatic interaction. To our knowledge, this is the first report of preparing thin silver film on fluorinated surface by electroless plating. The deposited thin film is IR reflective and electrically conductive. To support our hypothesis, the selective electroless plating (SEP) was also conducted on substrates modified by 1H,1H,H,2H-perfluorooctyltriethoxysilane (PFO), octyltriethoxysilane (OTES), aminopropyltriethoxysilane (APTES) and non-modified clean surface under the identical conditions. It is reported that the zeta potential of clean glass surface and of glass modified by OTES is positive.[31] As the silver particles are positively charged, there should have no silver plating on those positively charge surface. The experimental results revealed the truth of hypothesis. As the silver plating is selectively occurring on the PFO modified surface, a simple pattern is prepared by plating on substrate with PFO pattern. The demonstrated pattern could be a prospective application in printing electronic circuits. In addition, PFO has been applied onto flexible polymer surface which is subsequently plated by silver.

2.3.1 Experimental section

All chemicals were bought from Sigma-Aldrich without further purification. Toluene was freshly distilled before use. Cellulose acetate film was bought from Ted Pella, Inc.

Substrate preparation: Glass slides (1 x 1.5 in) were pretreated with fresh Piranha solution (H_2SO_4:H_2O_2 = 70/30 v/v) for 30 min at 80-100 °C. After thoroughly rinsing and being sonicated for 15 min in deionized water, slides were blown to dryness by nitrogen gas. Surface modification of clean glass was carried out immediately after cleaning. For the surface fluorination, the dried glass slides were immersed into freshly prepared solution of PFO (40 mM) for up to 4 hours at room temperature. The solution was sealed with Argon atmospheric protection. After the surface modification was complete, the slides were rinsed with toluene and dried by nitrogen gas. The same procedure was applied to surface modification with OTES (40 mM in toluene) and APTES (40 mM in toluene) respectively. To prevent competing coating of the container, a Teflon beaker was used during surface modification procedure.

To construct a PFO pattern, cellulose acetate in acetone solution was cast on glass over a mask. After the polymer pattern was dry, the glass was immersed in PFO solution for surface modification at room temperature. After immersion in PFO solution for 4 hours, the exposed area was modified by PFO. Then acetone was used to wash off the cellulose acetate film to form PFO modified pattern.

Free standing cellulose acetate film was used as a flexible substrate. Surface modification of was done in PFO at 100 °C for 1 hour.

Electroless silver plating: The plating solution was freshly prepared as follows. Ammonium hydroxide (28%) was first added to an aqueous silver nitrate solution (12.5 mM, 32 ml) to form silver complex clear solution. Then potassium hydroxide (0.1M, 15 ml) was added into the silver complex to make an alkaline solution. Additional ammonium hydroxide is needed to obtain a clear solution if the solution turns to cloudy after the addition of potassium hydroxide. At the beginning of the addition of ammonium hydroxide, the solution became cloudy and then became clear with further addition of ammonium hydroxide. The reducing solution is as aqueous glucose solution with a concentration of 32.5 mM. The slides were immersed into the prepared alkaline silver complex solution before adding the reducing reagent. With stirring, glucose solution (32.5 mM, 3 ml) was poured into the plating solution. After a certain plating time, slides were withdrawn from the plating solution followed by rinsing with plenty of water. The plated silver film was then dried by nitrogen gas. Slides modified with different chemicals were immersed in the same plating solution. The plating was conducted at room temperature.

Characterization: All AFM images were taken using the Nanowizard® II BioAFM (JPK Instruments, Berlin, Germany) mounted on an Olympus 1X81 inverted confocal microscope. Silicon nitride cantilevers (DNP-S, Veeco, CA) were used in contact mode imaging. The spring constants, typically in the range of 0.36-0.47 N/m, were determined by the thermal noise method[32] after obtaining the deflection sensitivity of the cantilever by pressing the AFM tip against a hard reference glass substrate. All AFM imaging was conducted in air at room temperature, and the scan rates were in the range of 0.8-1.6 Hz. All AFM images were plane-fit (1st order) and

the roughness values were calculated using the JPK Image Processing software (JPK Instruments, Berlin, Germany). Contact angles were measured right after preparing the samples, with an FTA 200 (Folio Instruments Inc., Kitchener, Ontario) dynamic contact angle microscope equipped with a CCD camera. Advancing contact angles were determined automatically by drop shape analysis during the growth of the droplet at a constant flow rate (1 μL/s). Contact angles were measured using ultrasonically degassed MilliQ water. Electric conductivity of the films is measured with multi-meter. Reflectance and transmittance were measured with UV/Vis/NIR instrument (PE Lamda 900) with special accessories for reflection measurement (Harrick Scientific, VRi-XXX Variable angle reflection accessory). The angle of incident light for reflectance measurement is 45°.

2.3.2 Results and discussion

The surfaces of substrate were modified with PFO, OTES and APTES in toluene solution. The silver plating was conducted on freshly prepared substrates. In the case of rigid substrates, different modified glass slides were immersed in the same plating solution.

Surface modification. During the course of plating, it was found that only PFO modified glass was plated with silver as a film. There was no visible silver deposited on OTES, APTES and non-modified clean glass. The contact angles of different modified surface were measured (Table 2.1). Both hydrophilic surface, clean glass (θ = 3 °C) and APTES (θ = 66 °C), were non-plated as shown in Figure 2.8. The two hydrophobic surfaces, OTES and PFO, show similar contact angle, but only PFO surface was silver plated. Obviously, the selective silver plating cannot be attributed to hydrophobicity. Apparently, silver is selectively plated on PFO modified surface. All other surface modifications, either hydrophobic or hydrophilic, do not activate silver electroless plating.

Figure 2.8. Samples images after silver plating. X: clean glass, non-modified; A: APTES modified; O: OTES modified; F: PFO modified. Plating time: 10min

Table 2.1. Contact angles of surfaces modified with different materials

surface	Piranha washed	APTES	OTES	PFO
Contact angle (θ, °)	3±1	66±2	90±2	93±2
Ag deposition	No	NO	NO	Yes

Surface topography of silver film. AFM images in Figure 2.8 show the growth of silver particles on PFO surface. Since there is no silver deposited on OTES, APTES and non-modified glass slide, their AFM images are not quoted. Before the plating, the glass surface is covered by PFO and the covered surface is uniform and homogeneous and smooth (Ra = 1.4nm). The AFM image of a sample in the early plating shows silver particles formed in solution adsorbed on PFO surface. The early deposited silver film was uniform but with defects resulting from the tiny defects in PFO. With the proceeding of the silver deposition, the films become thick and dense. The defects from PFO modification was partially filled by silver particles, thus the film becomes conductive and highly IR reflective. It is believed that the electric conductivity of a material relates to its reflectance in NIR region.[3] Since silver deposition does not change the surface charge, the whole plating process is selectively occurring on PFO modified substrates surface. From the general roughness of all films, the Ra value keeps at the same level indicating that the particle size maintains which is very important for preparing uniform film. The pictures under each of AFM images give an idea of the film's transparency. The film becomes dark as the plating time increases.

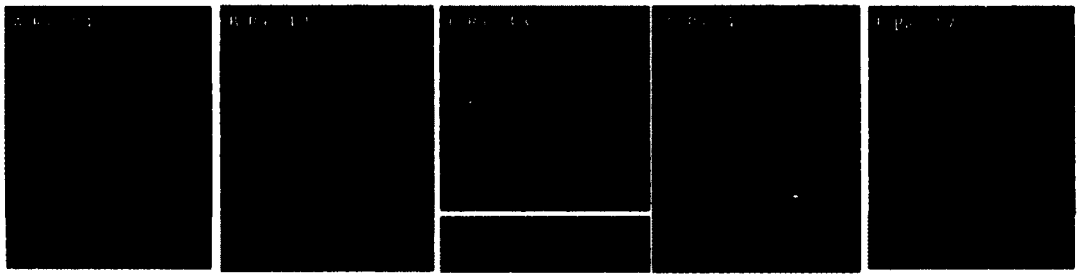

Figure 2.9. AFM height images (acquired in air) of silver films at different plating time (scan size 5 μm × 5 μm, z range is 30 nm for all images). The pictures under AFM show the visual transparency of each film. A: PFO modified surface before plating; B-E: plating for 15s, 20s, 30, 35s respectively

Reflectance and transmittance. Figure 2.10 shows the reflectance and transmittance of the silver films with different plating time. Generally, the reflectance increases along with plating time. The reflection in near-IR region increases more than that in visible region. The PFO modified slide shows exactly same reflectance as plain glass. Once the silver is plated, reflection across the visible to NIR spectral region increases. The longer the plating time is, the higher the reflectance increases. At a certain point, the reflectance shows an incredible increase, to over 85% in NIR region and 50-70% in the visible region. Afterwards, extending plating time does not further enhance reflectance because the reflection mostly occurs at the surface. The thickness of continuous silver film does not contribute to reflection any longer. It is also noted that films with high IR reflectance are also electrically conductive. It is assumed that the silver film is too thin and non-continuous in the early stage of plating. Reflectance of non-continuous film arising from those silver patches is very limited. This could address the significant increase in reflectance after certain plating time. After extending of plating time to 30 sec, the film becomes continuous and electrically conductive, thus NIR reflectance increases incredibly to 75%. Further

plating will improve the defects of the film to some extent, yielding a reflectance increase of ca. 10%.

In terms of transmittance, the PFO modified glass shows no difference in transmission from plain glass. Taking into consideration of reflection, it is clear that the PFO does not affect the propagation of either visible and NIR light. Once the silver is plated, the transmitted light is significantly reduced. In the NIR region, the light would either be reflected (specularly or diffusely) or transmitted since silver does not absorb NIR light. At the early stage of plating, the film is thin and at non-continuous patches state, the reduced transmittance is mainly caused by diffuse reflection or scattering. When the film becomes continuous and electrically conductive, the transmittance is largely reduced to less than 5% in NIR region and 10-23% in visible region. The reflection, a mainly specular one, accounts for the reduction of transmittance. The diffuse reflection explains why the sum of R% and T% is less than 100%. Moreover, the trend of transmittance is consistent with that of reflectance. The 10-23% transmission in the visible region makes these films semi-transparent.

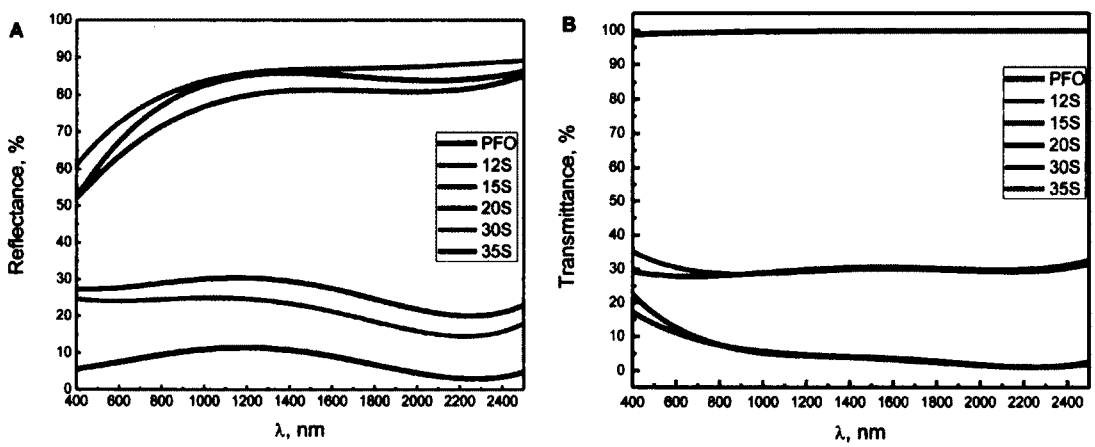

Figure 2.10. Reflectance and transmittance of silver films versus plating time. (A) Reflectance; (B) Transmittance; plating time: 12s, 15s, 20s, 30s and 35s.

Silver film pattern and plating on flexible substrate. To further demonstrate selective plating on PFO surface, silver patterns were plated. Scheme 2.1 depicts the process of plating pattern. A polymer pattern was made on glass by casting viscous cellulose acetate solution over a mask to protect the substrate from PFO modification. After immersion in PFO solution, the exposed area was modified by PFO. The cellulose acetate polymer was washed off by acetone. Then the modified glass was immersed into plating solution for silver plating. Only PFO modified area was plated with silver, E in scheme 2.1.

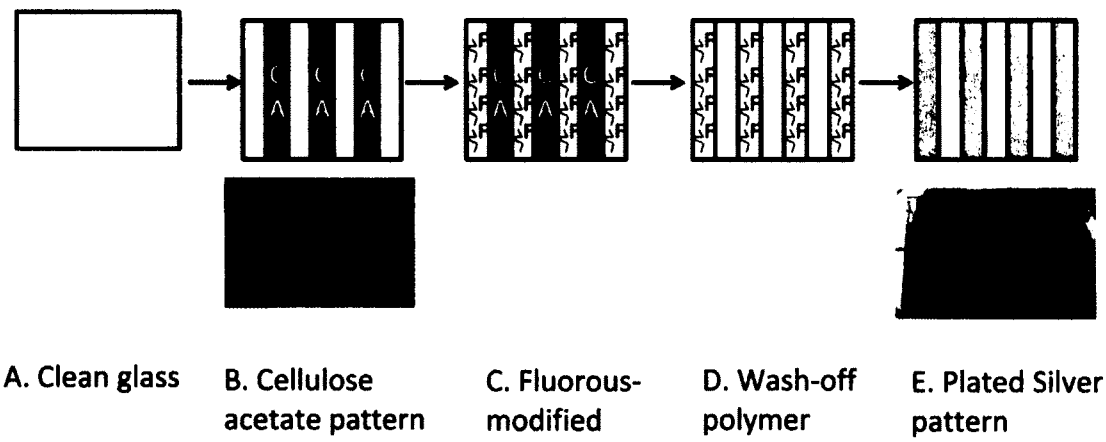

Scheme 2.1. A Process for preparation of a patterned silver coating

Flexible substrate, cellulose acetate film, was surface modified in PFO toluene at temperature of 100 °C. Then the polymer film was immersed into plating solution. The plating condition was as same as that for glass. Figure 2.11 shows images of the silver plated polymer film. The plating on cellulose acetate film makes the proposed plating method universal in prospective application.

Figure 2.11. Three pictures of silver film plated on PFO modified cellulose acetate sheets.

Mechanism of plating Scheme 2.2 depicts the process of electroless silver plating. After the surface is modified with PFO, the surface is negatively charged in alkaline solution when pH is over 10. The pH of the actual plating solution is 12. Once the substrate is immersed into plating solution, the positive silver particles and ions directionally move towards the negatively charged PFO surface by the driving force of electrostatic interaction. The adsorbed silver ions and particles on PFO surface form the first layer of plating which further catalyzes subsequent plating. The first layer on PFO surface does not change the surface charge.[30] With the proceeding plating, silver particles grow around the first layer and included silver ions will be reduced gradually by glucose. Eventually, a thin layer of silver film will be formed.

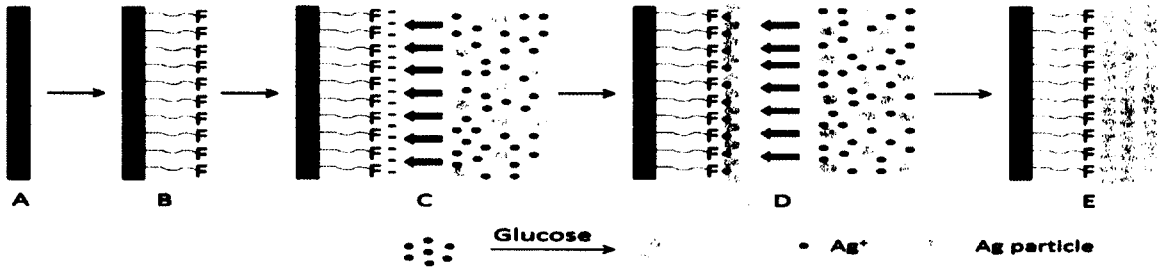

Scheme 2.2. Silver plating process on PFO modified surface. (A): Clean glass slide; (B): PFO modified; (C): Modified slide in plating solution; (D): Slver nucleation centre formed on the PFO layer; (E): Slver thin film deposited on PFO modified slide

2.4 Electroless plating of silver film on Ag nanoparticles activated surface

To make electroless silver plating more universal, a surface-activation method to promote silver plating is a key step and has been a subject of research in the field for years. Since AgNP can sinter or even melt at low temperature, it is possible to use AgNPs as seeds for electroless plating after heat treatment. Tong studied the plating on silicon substrate activated with a silver seed layer.[14] The Stanishevsky group used silver nanoparticles to form an activation layer for silver plating after thermal annealing.[9] However, the obtained films were both thick and had poor NIR reflection. The silver nanoparticles were stabilized by poly(vinyl pyrrolidone) (PVP) which requires a high temperature (420 °C) treatment prior to plating.

In this study, we first aimed to lower the annealing temperature by using small molecule stabilizers for AgNPs. The studies have shown that the annealing temperature affects the subsequent electroless plating. The directional growth of silver seeds, two/three-dimension, results in different reflectance for a given plating time. A polymer composite of PMMA and AgNPs was also used to form an activation layer for electroless plating. It was also demonstrated that free-standing polymer film plated with silver thin film can be prepared. The obtained film could be applied on another substrate, e.g. glass, to form NIR reflective surfaces.

2.4.1 Experimental section

The glass surface was washed with soapy water, Piranha solution (conc. H_2SO_4 : H_2O_2 = 70:30 v/v) and then rinsed with copious amount of water. The clean glass slides were then spin coated with AgNPs at 1000 RPM followed by heat treatment at temperatures of 90 °C, 150 °C and 210 °C for 15 to 60 min before electroless plating. AgNPs solution was prepared according to the method described in chapter 2.3.

AgNP/polymer free-standing film: AgNPs were dispersed in PMMA/$CHCl_3$ solution (20 wt %) to form AgNPs/PMMA composite. The composite was spin-coated on glass substrate at 1500 RPM followed by annealing at 200 °C. The weight percentage of silver in PMMA ranges from 1.6-7.8% (Table 2.2). A free-standing film can be obtained by soaking the film in water for a few minutes and then peeling off from the glass substrate.

Table 2.2. Silver content and thickness of PMMA/AgNP nanocomposite film

Sample #	AgNP added, ml	PMMA, ml	Weight% of silver in PMMA	Thickness, μm
1	2	0.8	7.8	1.0
2	1	1	3.2	1.3
3	0.5	2	1.6	1.4

Plating condition: Plating was conducted under identical conditions for all the samples. See chapter 2.3.

Characterization: SEM images were obtained by Tescan-Uega II XMU (Tescan, Brno, Czech Republic) at 15.00kV electron acceleration voltage operating condition. Reflection and transmission were measured as the same method and instrument described in chapter 2.3. Thickness of the film was measured using Tencor Alpha-Step 200 (Tencor, California, USA). Thermogravimetric analysis was performed on TA Instrument Hi-Res TGA2950 instrument at 10 °C/min temperature ramp.

2.4.2 Results and discussion:

Effect of annealing temperature on activation surface. The annealing temperature affects the chemical composition and morphology of activation layer. Figure 2.13 shows the SEM images of samples annealed under different conditions. At low temperature of 90 °C, the activation layer was still continuous. Since the ligand of the nanoparticles is stable at this temperature, there was no significant change in morphology with annealing time. When the transmission spectrum was investigated, however, it was found that there was surface plasma resonance (SPR) shift to longer wavelength from 420 nm to 505 nm in Figure 2.12. The reason is probably that the particles diffuse or aggregate each other to some extent resulting in bigger particles. As is confirmed by Kelly, the increasing nanoparticles size after annealing give shift to longer wavelength.[33]

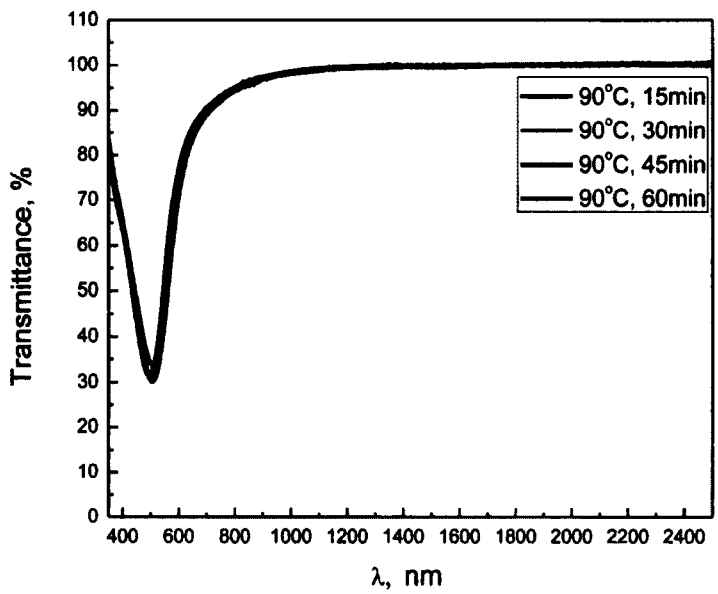

Figure 2.12. UV/Vis absorption of activation layer annealed for 15 to 60 min at 90 °C

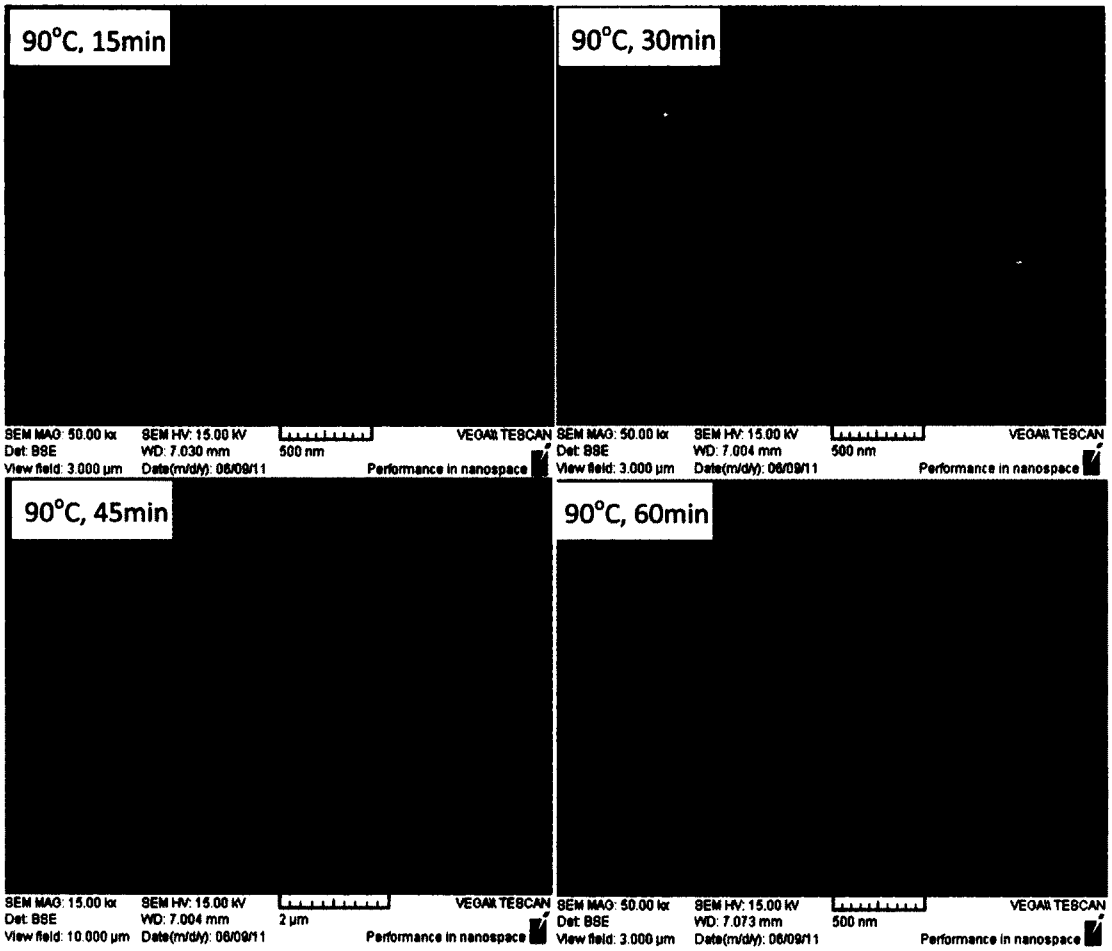

Figure 2.13. SEM images after annealed for 15 to 60 min at 90 °C

With the increase in annealing temperature to 150 °C, the ligands started to decompose. At this temperature, the particles aggregated further which is reflected by further red shift of absorption up to 597 nm in Figure 2.15, the individual particles appeared (SEM images in Figure 2.14) and silver started to become exposed to the atmosphere. With longer annealing time up to 45 min, more and more ligands decomposed and silver particles stood out. When the annealing temperature was extended to 60 min, it was found that silver particles patched.

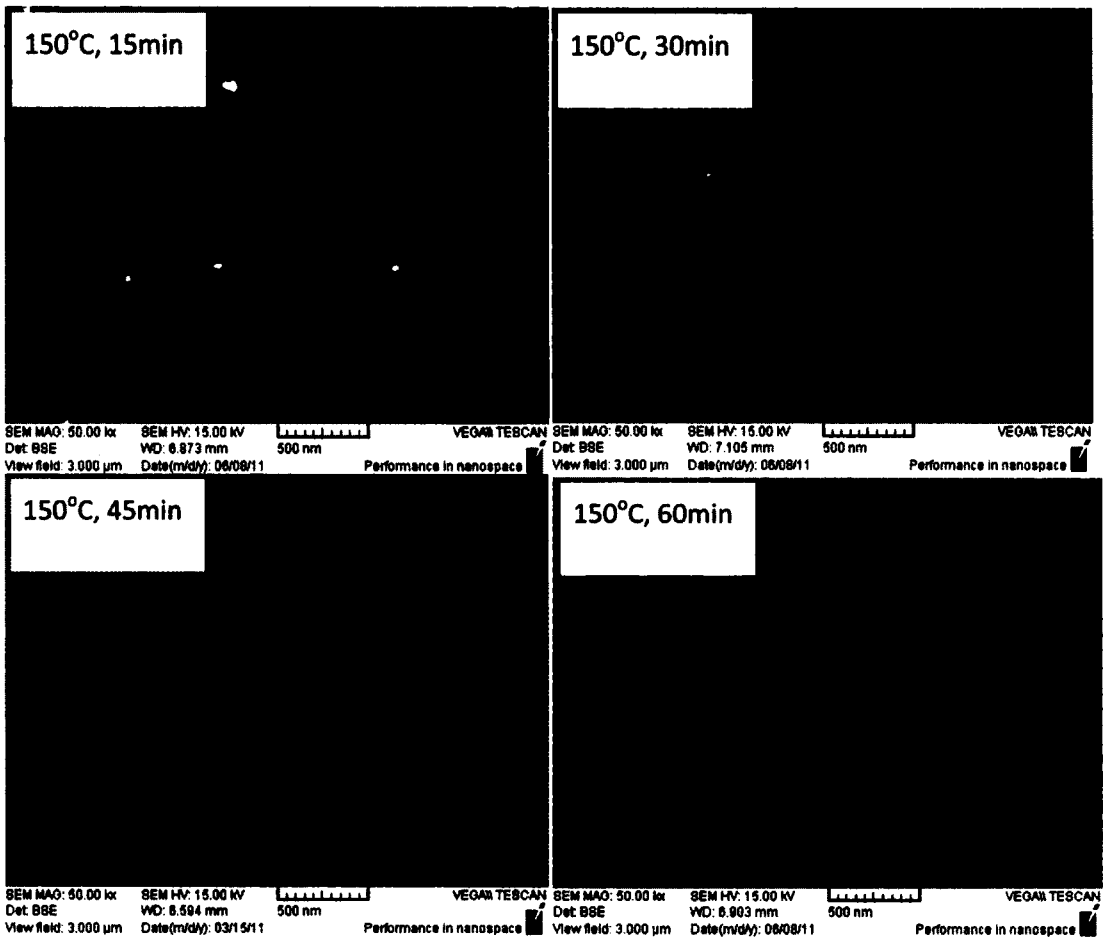

Figure 2.14. SEM images after annealed for 15 to 60 min at 150 °C

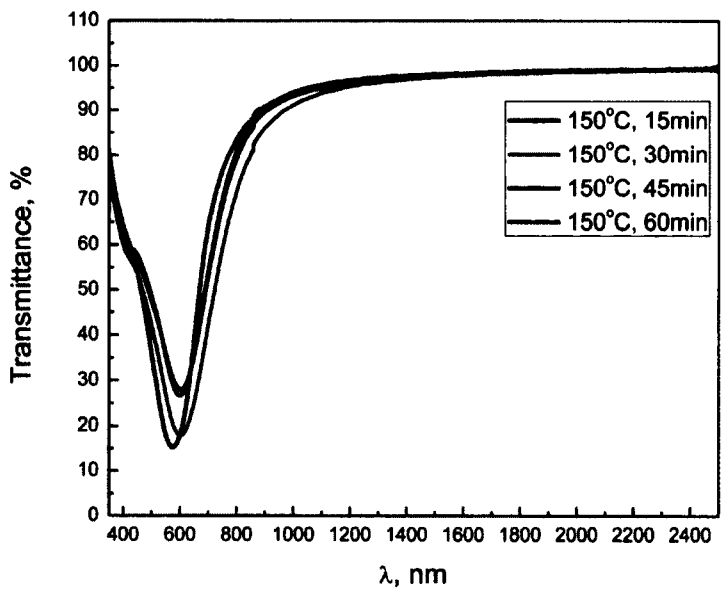

Figure 2.15. UV/Vis absorption of activation layer annealed for from15 to 60 min at 150 °C.

If the annealing temperature was increased to 210 °C, the shape of nanoparticles became round. As it is known that the melting point of silver nanoparticles could be as low as 150 °C depending on its size,[34] the nanoparticles probably started melting and became round (SEM images in Figure 2.17). It has been demonstrated by Haynes and Duyne that the annealing of small metal islands increases their diameter to height ratio (a/b) resulting blue shift of SPR up to 200 nm.[35] In the case of this sample, the absorption of the film was blue shifted to 425 nm in Figure 2.16, a 172 nm change. Meanwhile, its intensity of absorption decrease because of diffuse, agglomeration or coalescence.

EDX analysis of the films confirmed the existence of silver. Semi-qualitative analysis shows the content of silver on surface increases with annealing temperature and time (see appendix I: EDX spectrum).

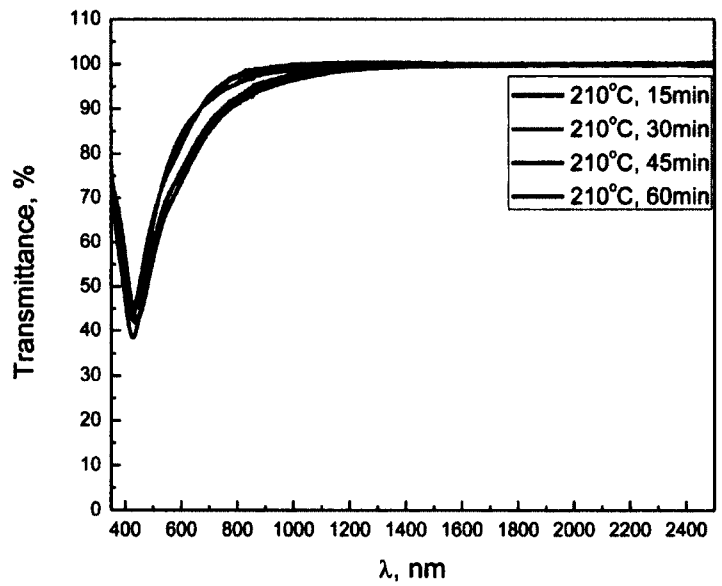

Figure 2.16. UV/Vis absorption of activation layer annealed for 15 to 60 min at 210

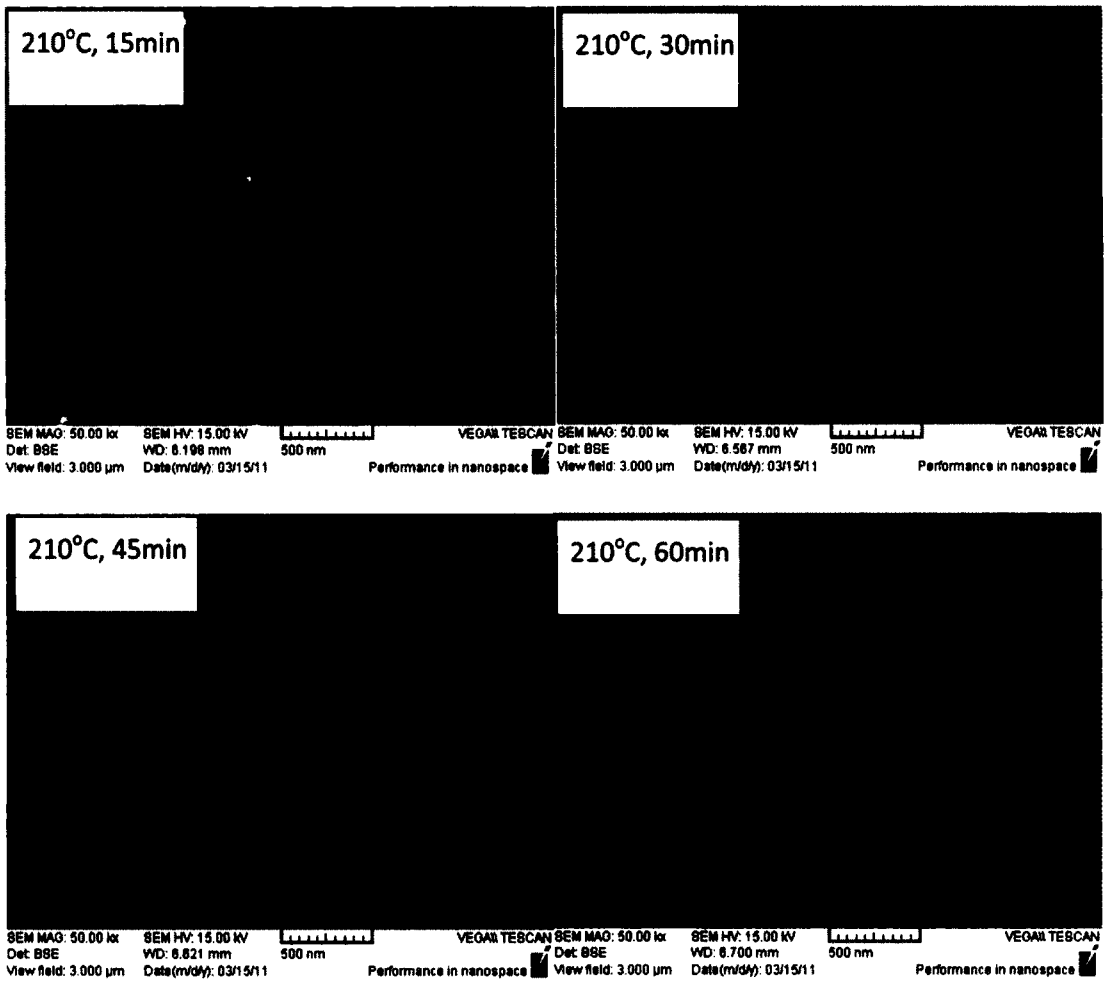

Figure 2.17. SEM images after annealed for 15to 60 min at 210 °C

To further verify the ligands decomposition temperature, thermal analysis was conducted. As shown in Figure 2.18, the decomposition temperature is 180 °C with a weight loss of 5%. The weight lost can be attributed to organic ligands. The decomposing temperature agrees with SEM images.

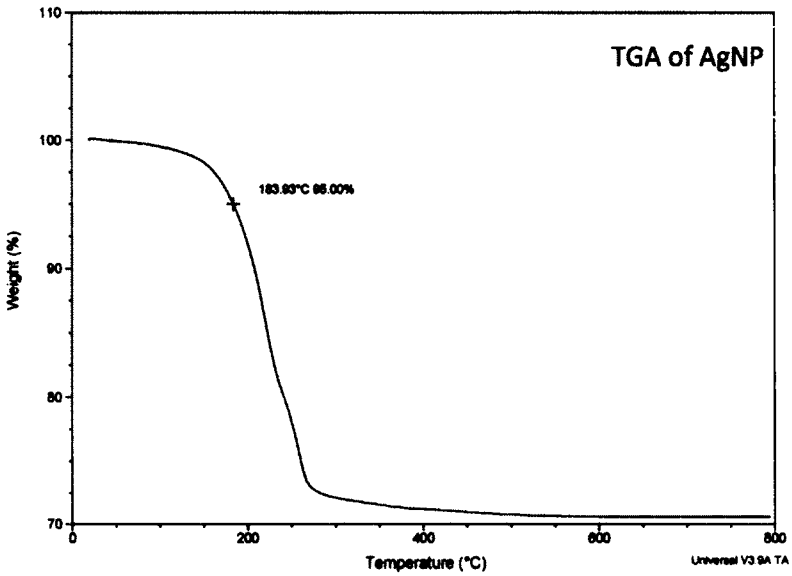

Figure 2.18. Thermal Gravity Analysis of AgNPs

Electroless silver plating on AgNP activated surface. Silver plating was conducted after AgNP activation film was formed. The reflectance of the plated film is shown in Figure 2.19~22. Generally, the longer the plating time, the higher the reflectance. The reflectance ranges from 4% up to 70% in the near-IR region. It is noticed that both annealing time and temperature of the activation or seed layer have significant effects on silver plating. Plating time varies from 1 min, 5 to 8 min, all other plating conditions, concentration and temperature, were maintained.

Effect of annealing temperature. Apparently, the annealing temperature of the activation layer plays an important role in subsequent silver plating. Figures 2.19~22 show the reflectance of plated film. With the same plating time, a low annealing temperature of 90 °C, always gives low reflectance. This probably resulted from insufficient nucleation center (exposed silver particles) because low annealing temperature cannot provide enough energy to decompose the ligands. It was also found the reflectance of films obtained from 90 °C does not change significantly with

annealing time. In other words, the density of nucleation center does not change with the annealing time. And this agrees with the SEM images of activation layer at low temperature, 90 °C.

With the increase of annealing temperature to 150 °C, the reflectance of films increases significantly with annealing time. R % reaches over 70 % in NIR region with acceptable transmittance in visible. It is understandable that silver grows around nuclei center and the film becomes dense with plating time. Thus R % increases rapidly with plating time varying from 1 to 8 min. SEM images account for nucleation center.

At an annealing temperature of 210 °C, the reflectance of plated film also increases with plating time. However, R % is lower than that from 150 °C with same plating time. Additionally, the film prefers reflecting visible light than NIR. The reason probably lies in the state of activation layer. As SEM shows agglomeration or coalescence, the distance between silver particles increased leading to patches of plated film which contribute to poor reflection. The proposed mechanism of annealing and plating in the later section of this chapter explains this phenomenon.

Effect of annealing time. Annealing time also affects silver plating. At a annealing temperature of 150 °C, if the annealing time is less than 30 min, the reflectance of plated films is quite a bit lower than those from annealing time over 45 min. As mentioned above, the ligands of nanoparticles started to decompose at ca. 150 °C, it took time to expose the naked silver nanoparticles to form nucleation. The longer annealing time is, the more nucleation centers will be formed. Therefore, the silver plating would occur easily and form thin and continuous film. While at the

annealing temperature of 210 °C, longer annealing time does promote plating. But as mentioned above, the distance between nucleation centers also increases with annealing time. Thus, the plated film is more porous resulting in much less reflection than those from annealing at 150 °C.

Transmission was measured for four films with high reflection, B60-8, B60-5 B45-8, and B45-5, because the reflectance of those four films is acceptable compared to commercial products whose reflectance ranges from 15-90% depending on application. Transmittances are shown in Figure 2.23. Therefore, both reflectance and transmittance of all four plated films are competitive with commercial products. Specifically, B60-8 shows lowest transmittance of 12-28% with the highest reflectance of over 70% along the NIR region. B45-5 is almost half transparent (29-52%) with acceptable reflectance of over 40%.

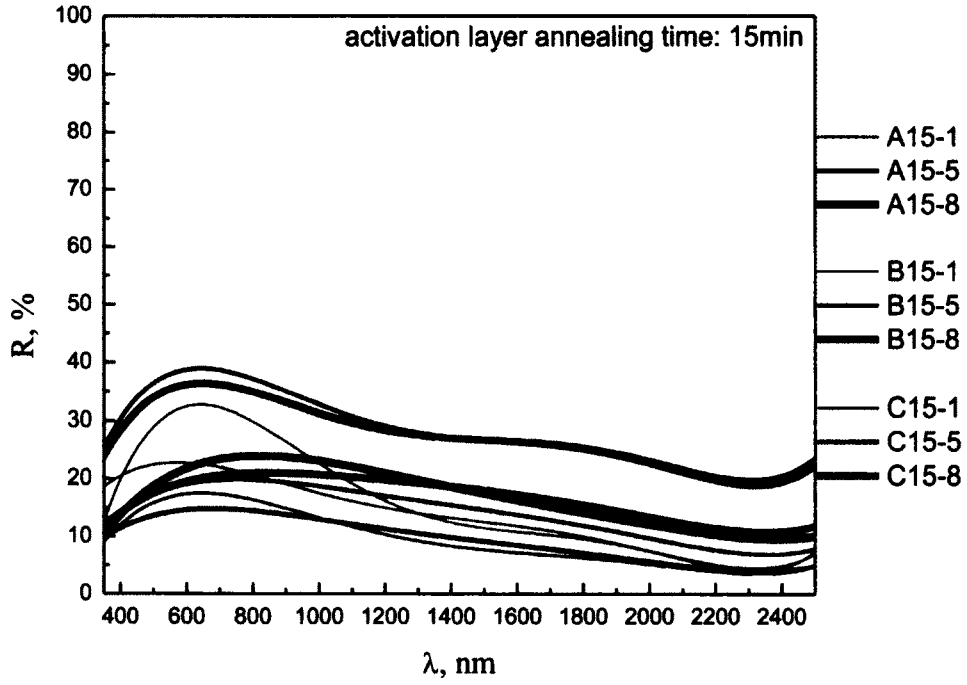

Figure 2.19. Reflectance of plated films. Annealing time: 15 minutes; Plating time: 1-8 min; Annealing temperature: A-90°C, B-150°C and C- 210°C.

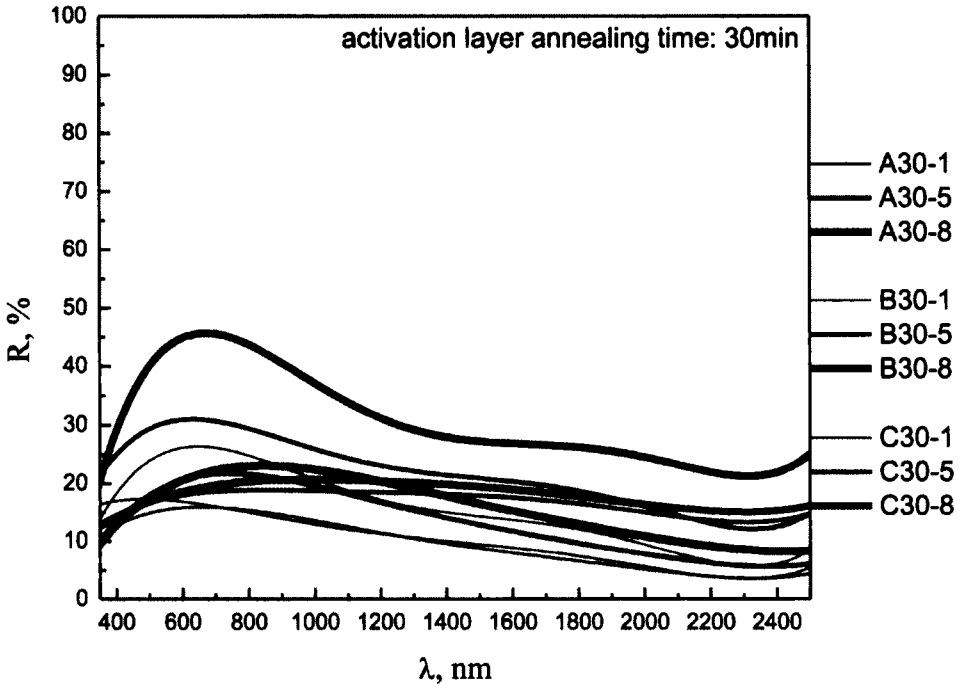

Figure 2.20. Reflectance of plated films. Annealing time: 30 minutes; Plating time: 1-8 min; Annealing temperature: A-90°C, B-150°C and C- 210°C

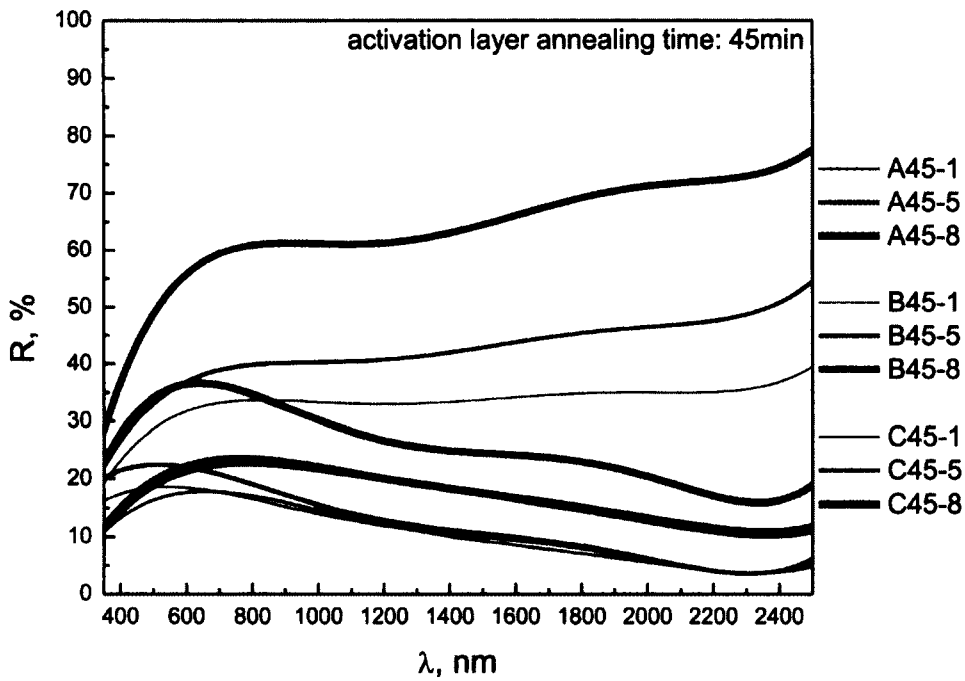

Figure 2.21. Reflectance of plated films. Annealing time: 45 minutes; Plating time: 1-8 min; Annealing temperature: A-90°C, B-150°C and C- 210°C

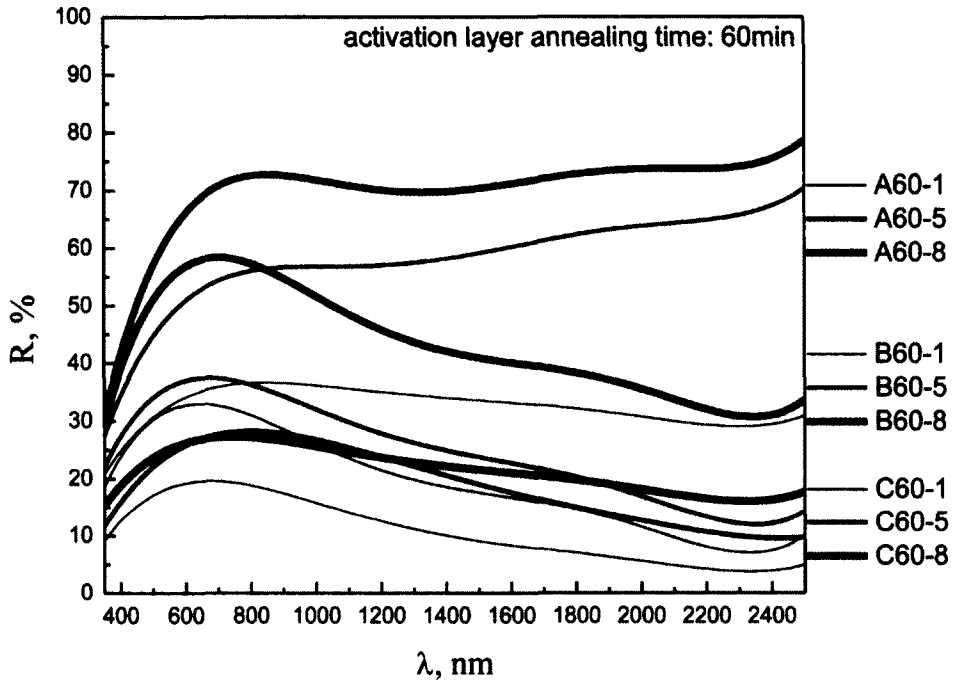

Figure 2.22. Reflectance of plated films. Annealing time: 60 minutes; Plating time: 1-8 min; Annealing temperature: A-90°C, B-150°C and C- 210°C

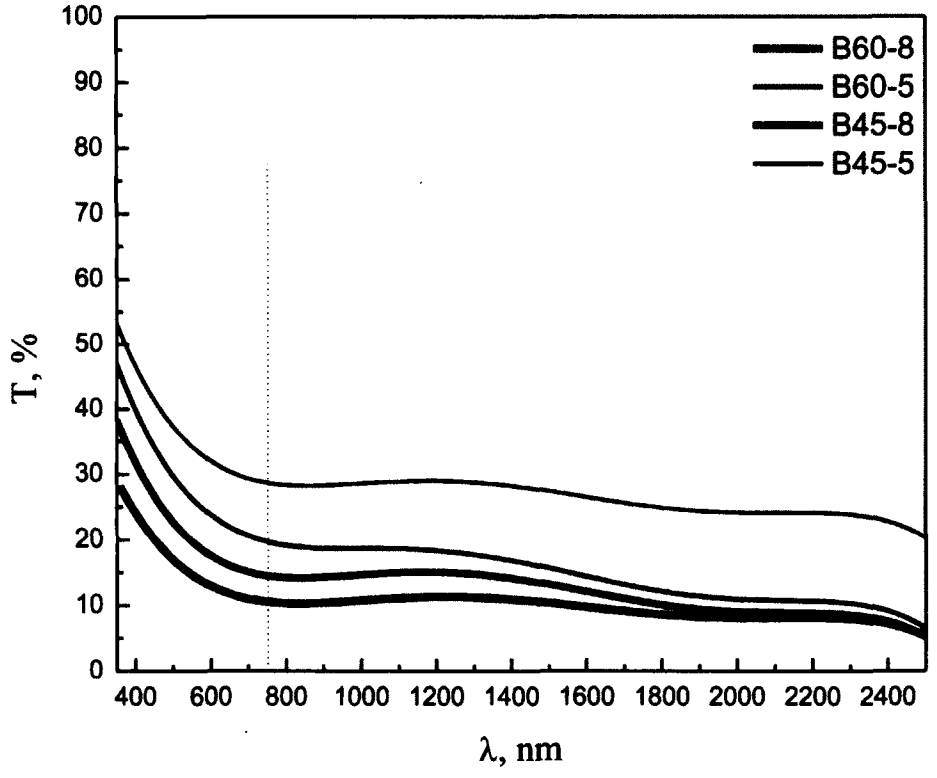

Figure 2.23. Transmittance of selected plated film with good reflectance.

Proposed mechanism Based on the above results, the mechanism of silver plating on AgNPs activated surface is proposed. Since the heat treatment of the activation layer determines the electroless plating, the mechanism of heat treatment is also very important. As depicted in Figure 2.24, AgNPs were spin-coated on a glass surface to form a uniform layer. Subsequently, the activation layer undergoes annealing at different temperature. At 90 °C, nanoparticles basically remain in their original state with only fewest ligands decomposing to form nucleation center for electroless plating. Since the temperature is so low, extending annealing time does not make a significant change in decomposition. Therefore, the electroless plating cannot occur effectively. Thus the obtained film shows poor reflectance.

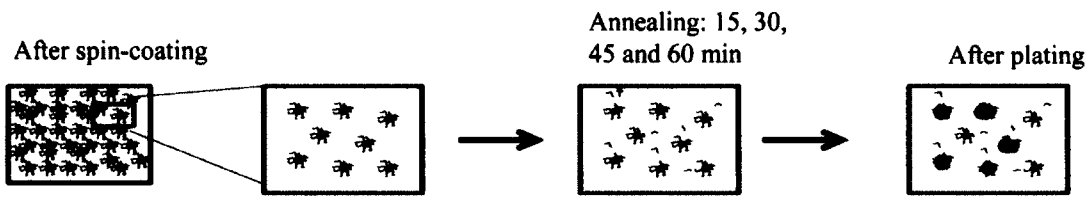

Figure 2.24. Annealing at 90°C and plating

When the annealing temperature is increased to 150 °C, silver nanoparticles start melting and some particles start decomposing. More and more nucleation centers are formed with annealing time (Figure 2.25). The activation layer contains dense nucleation center after 45 min of annealing. During the subsequent electroless plating, silver complex ions will be reduced in solution and easily deposit around nucleation centers to form a film. Additionally, silver deposition probably prefers a two-dimension growth along the surface.[13] The plated silver patches around nucleation centers meet each other forming a continuous film with plating time. The film is less porous, deduced from high electrical conductivity of the film with a thickness of 40-

50 nm. Consequently, the obtained silver film shows high reflectance, especially in NIR region.

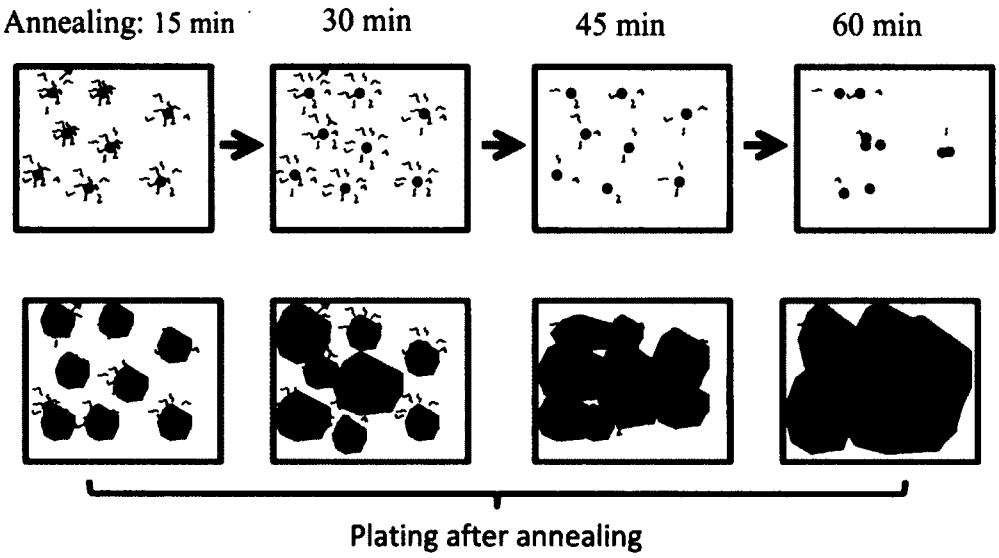

Figure 2.25. Annealing at 150°C and plating

At a higher annealing temperature of 210 °C, the ligands may decompose fast from the beginning of annealing (Figure 2.26). Then, with the proceeding of annealing, those particles start to melt resulting in round shaped particles. The SEM images show round particles with the UV/Vis absorption spectrum showing significant blue shift due to the height/diameter ratio increase. In this case, the silver deposition follows a three dimension growth. The obtained film is more porous and less electrically conductive than which from 150 °C. Even plating for 8 min, same plating time as for annealing at 150°C, the film still shows low reflectance.

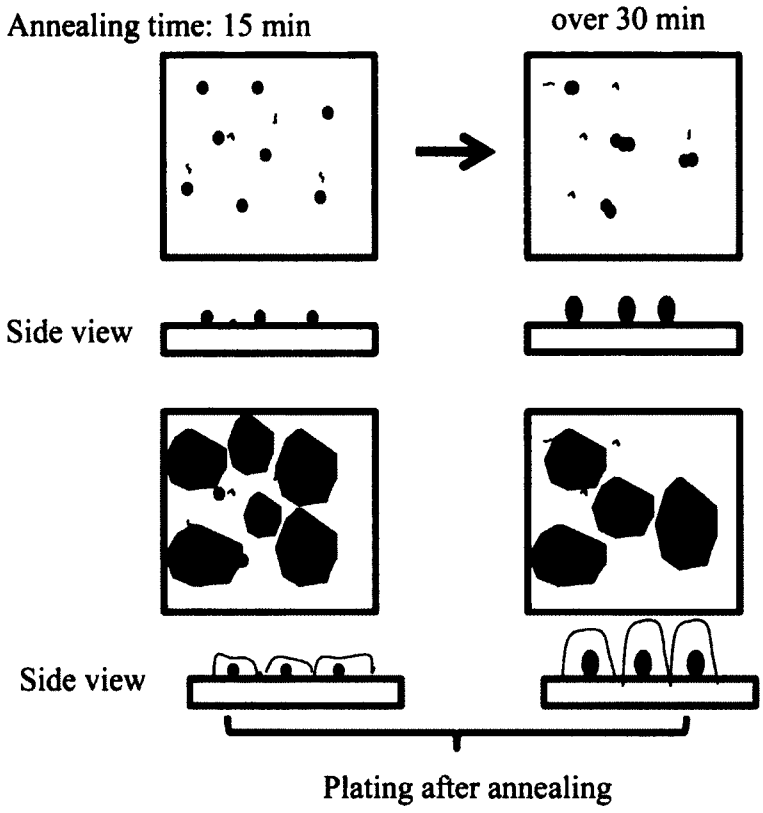

Figure 2.26. Annealing at 210 °C and plating

Electroless silver plating on PMMA-AgNP free standing film As silver nanoparticle have been proven to be able to activate the substrate surface for electroless plating, it is proposed that polymer-nanoparticle composite can be used as an activation layer as well. The reason for plating on free standing polymer film extends the application scope of silver reflective film. Once the film is prepared independently on free standing film, it is possible to apply the film on existing surfaces/glass that have no reflective coating. With minimum processing on site, the surface/glass would convert to function in reflection. In this study, PMMA was chosen as matrix because of its high transmittance and its compatibility with AgNPs.

When preparing the composite solution, AgNPs was introduced into PMMA solution with vigorous stirring. Then spincoating of the composite on glass at 1000 RPM followed by fast heat treatment at 200 °C to form a uniform film. Afterwards, electroless plating was conducted in the same plating solution as used before. To separate the film from glass, the film was immersed in water for a few minutes before it can be easily peeled off (as shown in figure 2.28). A higher annealing temperature was conducted to promote the motion of silver nanopaticles in polymer film.

Figure 2.27 shows both reflectance and transmittance of the obtained film. As the content of the silver varies, the density of nucleation center on the surface is different from each other. Generally, the higher content of silver is, the easier the plating will be. It is noticed from the spectrum that the reflectance of film increases with the silver content. On the other hand, the transmittance will decrease with the content of silver. Compromisingly, the film shows good reflectance of over 50% in NIR region with 15-20% of transmittance in visible region when the silver content reaches 3.2% by weight. It is demonstrated that the polymer silver nanoparticles composite can activate electroless silver plating to prepare free standing film which is prospectively useful in the industry of energy saving coatings.

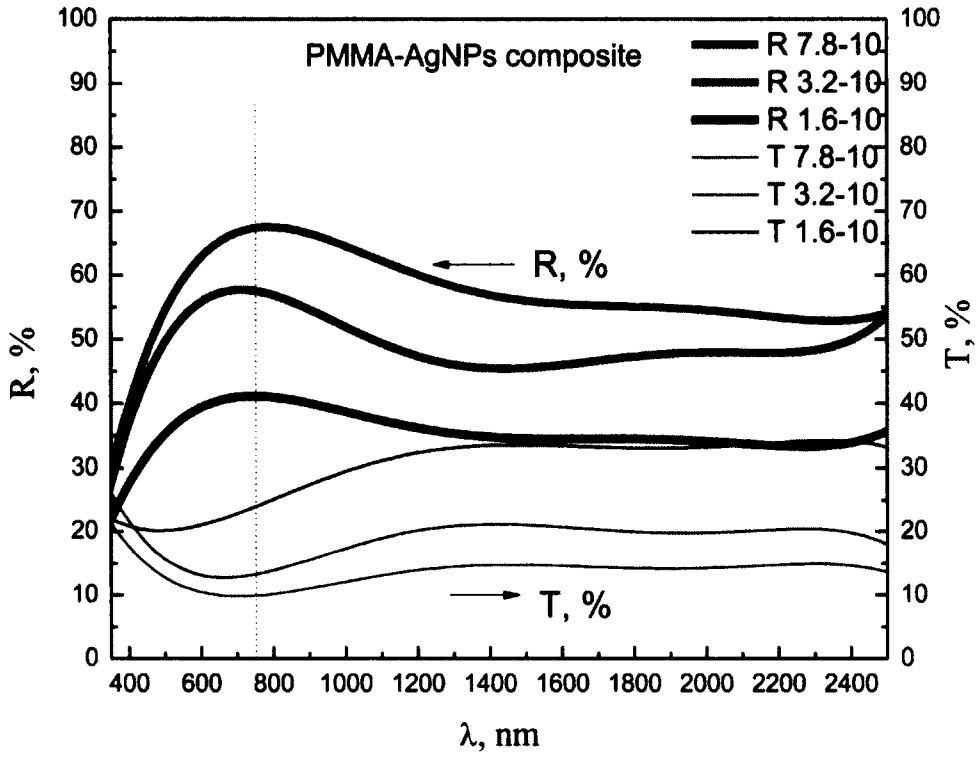

Figure 2.27. Reflectance and transmittance of silver plated free standing PMMA/AgNP film. R: reflection, T: transmission

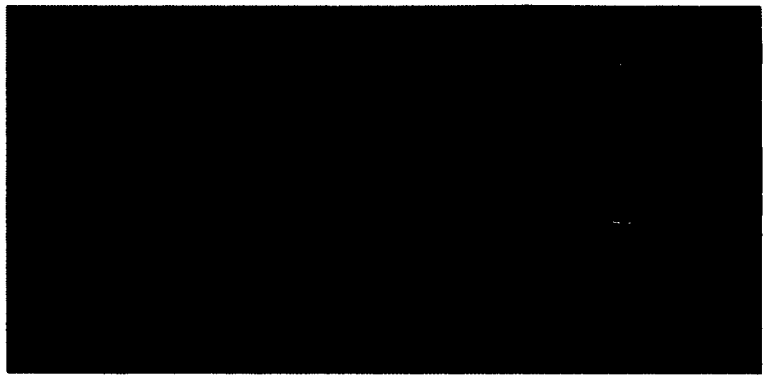

Figure 2.28. Picture of free standing PMMA/AgNP nanocomposite film.

2.5 Conclusion and future work

Two different preparation methods, spray-pyrolysis and electroless plating, of thin silver film were proposed and studied.

Spray-pyrolysis of silver nanoparticles solution is a direct method to prepare silver thin films on a substrate without surface pretreatment. The resulting film is fairly uniform with good reflectance in NIR region and transmittance in the visible region. This method can be processed to create large area surfaces with low cost.

A new method of preparing thin silver films is demonstrated by using electroless silver plating on fluorinated surface. The new electroless plating is selective and this is the first report of electroless plating on fluorinated surface. It is proposed that the mechanism of this selective plating is due to the electrostatic interaction between the negatively charged fluorinated surface and the positively charged silver particles in the alkaline solution. The deposited silver film could be semi-transparent with high NIR reflection up to about 90%. In addition, silver plated patterning was demonstrated with the proposed selective plating method. The method shows great prospective applications in the field of semi-transparent IR reflection, silver patterning, and printable electric circuit on multiple substrates.

Another electroless plating method using silver nanoparticles was investigated. Both AgNPs and and AgNPs/polymer composite were utilized as activation layer to promote electroless plating. The low annealing temperature for activation layer makes this method universal. The obtained film is highly NIR reflective. AgNPs/polymer activation layer/film makes large area plating possible.

Additionally, a silver nanoparticles solution, which is miscible with organic solvent, is synthesized. The solution is stable over six months with no significant aggregation. The decomposition temperature of ligands is as low as 180 °C.

Both electroless plating methods can be applied to conduct silver plating on flexible substrate such as polymer films.

As this thesis demonstrated three different promising thin film preparation methods on lab scale, further studies and developments are necessary to improve performances of the resulting films.

For spray-pyrolysis method: Special spray equipment is needed to promote the spray-pyrolysis method to process on a large area surface. There is also a room to improve pyrolysis process by optimizing the temperature for pyrolysis.

For electroless plating on fluorinated surface: The surface modification method by fluoro-compound needs to be further studied. More fluoro-compounds are needed to modify other flexible substrates other than cellulose.

For electroless plating on AgNPs activated surface: the AgNPs' annealing condition could be studied when AgNPs are incorporated with different polymers to make a free standing activation film. It is also possible that the ligands for AgNPs can be modified according to the polymer matrix.

2.6 References

(1) Boccas, M.; Vucina, T.; Araya, C.; Vera, E.; Ahhee, C. *Thin Solid Films* **2006**, *502*, 275.

(2) Bennett, J. M.; Ashley, E. J. *Appl. Opt.* **1965**, 4, 221.

(3) Lonke, A.; Ron, A. *Phys. Rev.* **1967**, 160, 577.

(4) Song, D.-Y.; Sprague, R. W.; Macleod, H. A.; Jacobson, M. R. *Appl. Opt.* **1985**, 24, 1164.

(5) Smith, G. B.; Niklasson, G. A.; Svensson, J. S. E. M.; Granqvist, C. G. *J. Appl. Phys.* **1986**, 59, 571.

(6) Martin-Palma, R. J., Vaquez, L., Martinez-Duart, J. M., Malats, Riera *Sol. Energy Mater. Sol. Cells* **1998**, *53*, 55.

(7) Martín-Palma, R. G.; Vinnichenko, M.; Martínez-Duart J. M. *Appl. Phys. D: Appl. Phys.* **2004**, 37, 1554.

(8) Shacham-Diamand, Y.; Inberg, A.; Sverdlov, Y.; Croitoru, N. *J. Electrochem. Soc.* **2000**, 147, 3345.

(9) Schaefers, S.; Rast, L.; Stanishevsky, A. *Mater. Lett.* **2006**, 60, 706.

(10) Roy, D.; Barber, Z. H.; Clyne, T. W. *J. Appl. Phys.* **2002**, 91, 6085.

(11) Alvarez-Puebla, R. A.; Aroca, R. F. *Anal. Chem.* **2009**, 81, 2280.

(12) Willner, I.; Shipway, A. N.; Willner, B. *ACS Symp. Ser.* **2003**, 844, 88.

(13) Koo, H.-C.; Kim, J. J. *J. Electrochem. Soc.* **2008**, 155, D176.

(14) Tong, H.; Zhu, L.; Li, M.; Wang, C. *Electrochim. Acta* **2003**, 48, 2473.

(15) Melpignano, P.; Cioarec, C.; Clergereaux, R.; Gherardi, N.; Villeneuve, C.; Datas, L. *Org. Electron.* **2010**, 11, 1111.

(16) Li, F.-J.; Roh, B.-G.; Lim, H.-T.; Kim, J.-S.; Park, J.-Y.; Yu, H.-W.; Park, S.-C.; Tak, Y.-H.; Ahn, B.-C. *Thin Solid Films* **2009**, 517, 2941.

(17) Bhatt, K.; Kalkan, A. K. *ECS Transactions* **2010**, 25, 27.

(18) Liu, C.-H.; Yu, X. *Nanoscale Research Letters* **2011**, 6, 75.

(19) Westphalen, M.; Kreibig, U.; Rostalski, J.; Lüth, H.; Meissner, D. *Sol. Energy Mater. Sol. Cells* **2000**, 61, 97.

(20) Kariniemi, M.; Niinistö, J.; Hatanpää, T.; Kemell, M.; Sajavaara, T.; Ritala, M.; Leskelä, M. *Chem. Mater.* **2011**, 23, 2901.

(21) Dryden, N. H.; Vittal, J. J.; Puddephatt, R. J. *Chem. Mater.* **1993**, 5, 765.

(22) Mallory, G. O. H.; Juan B., *Electroless plating: fundamentals and applications* Ed.; Noyes Publications/William Andrew Pub: New York **1990-2000**.

(23) Minjer*, C. H.; Boom, P. F. J. *J. Electrochem. Soc.* **1973**, 120, 1644.

(24) Chen, T.-C.; Su, W.-K.; Lin, Y.-L. *Jpn. J. Appl. Phys., Part 1* 2004, 43, L119.

(25) Mafuné, F.; Kohno, J.-y.; Takeda, Y.; Kondow, T.; Sawabe, H. *J. Phys. Chem. B* **2000**, 104, 9111.

(26) Wang, Z.; Cai, X.; Chen, Q.; Li, L. *Vacuum* 2006, 80, 438.

(27) Rodebush, W. H. *P. Natl. Acad. Sci. USA* **1954**, 40, 789.

(28) S. Schaefers, L. R., A. Stanishevsky *Mater. Lett.* **2006**, 60, 706.

(29) Wang, D.; Oleschuk, R. D.; Horton, J. H. *Langmuir* **2007**, 24, 1080.

(30) Khaldoun, A.; Wegdam, G. H.; Eiser, E.; Kerkeb, M. L.; Duran, J. D. G.; González-Caballero, F.; Bonn, D. *Colloids Surf., A* **2006**, 290, 1.

(31) Wright, D. S.; Flavel, B. S.; Quinton, J. S. *In International Conference on Nanoscience and Nanotechnology*, 2006 ICONN '06. Brisbane, Qld, Australia, **2006**.

(32) Hutter, J. L.; Bechhoefer, J. *Rev. Sci. Instrum.* 1993, 64, 1868.

(33) Kelly, K. L.; Coronado, E.; Zhao, L. L.; Schatz, G. C. *J. Phys. Chem. B* **2002**, 107, 668.

(34) Moon, K.-S.; Dong, H.; Maric, R.; Pothukuchi, S.; Hunt, A.; Li, Y.; Wong, C. *J. Electron. Mater.* **2005**, 34, 168.

(35) Haynes, C. L.; Van Duyne, R. P. *J. Phys. Chem. B* **2001**, 105, 5599.

(36) Mafune, F.; Kohno, J.; Takeda, Y.; Kondow, T. *J. Phys. Chem. B* **2000**, 104, 911

Chapter 3 Near-IR absorptive Ni coordination polymer

3.1 Introduction

In recent decades, metal coordination polymers have attracted much interest owing to their potential applications as gas storage,[1] ion-exchange,[2] catalysis,[3] and magnetic materials.[4] Specifically, the Ni(II) coordination polymers containing the bridging ligand of dianions of **1** have been prepared for potential applications in thin film transistors,[5] chloride ion-selective potentiometric sensors,[6] a catalyst for ethylene polymerization,[7] cathodes for non-aqueous electrolyte batteries,[8] and magnetic recording medium.[9] Other properties such as photochemical reactivity,[10] dielectric constant and AC conductivity[11] were also investigated. The polymer was confirmed to have one-dimensional linear structure.[12]

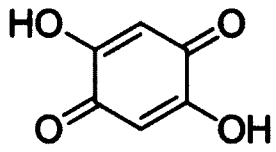

1

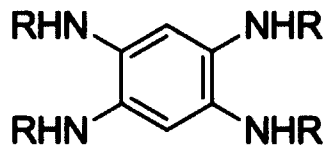

R = H, alkyl, aryl

2

Dinuclear metal complexes containing the dianion of **1** as a bridging ligand have been extensively studied owing to their specific electronic properties enabled by the quinone system.[13-17] It is believed that the electrons of deprotonated **1** are delocalized and the orbital overlap between metal and ligand is enhanced. Indeed, the delocalization of electrons and the orbital overlap stabilize the corresponding

complex and enhance the metal – ligand electron transfer, which contributes to unique optical, magnetic and electronic spectroscopic properties.[18-21]

As an analogue of **1**, the bridging ligand **2** was used to synthesize metal complexes **3** in 1998 by Kaim and co-workers.[22] Since then, this type of ligand has gained much interest, as it gives an access to a wide range of metal complexes.[23] It is expected that the scope of electronic delocalization of such complex will be increased in comparison with other nitrogen ligands such as terpyridines, Creutz-Taube species and p-benzoquinonediimine bridged ligands.

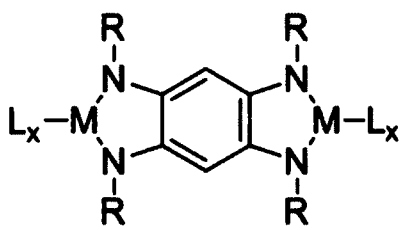

M = Ni, Pd, Pt, Cu, Ru
L_x = other ligands
R = alkyl or aryl

3

The study by Baunstein confirms the square planar geometry of Ni, Pd and Pt dinuclear complexes bridged by **2**. The strong absorptions of Ni(II) complexes in the range of 400 – 600 nm were assigned to $\pi - \pi^*$ intra-quinone charge transfer[24] and metal to ligand charge transfer MLCT transitions.[25] The weak absorption around 650 nm was linked to HOMO – LUMO allowed transition possessing a ligand to metal charge transfer (LMCT) character.[26] In the case of π – acceptor, the MLCT band was red shifted from 510 to 553 nm due to the possible participation in the π system.

Computational studies had confirmed extensively overlapping of valence d-orbitals of the metal with low-lying π^*-orbitals of the ligands and forming the covalent frontier orbitals of the complexes. As a result, the electrons are delocalized

over both metal and ligand.[16,23,27-29] Since the strong spectroscopic absorption at low energy was originated from the transition between the orbital with mainly metal characteristics to orbital with mainly ligand characteristics, the absorption was attributed to a MLCT transition.

If the bridging ligand linked to the metals forms a linear polymer chain, the electron delocalization over metal and ligand may develop further and result in a change of the band gap. The valence and conduction band development was observed in linear oligomers of ruthenium complexes in which the spectroscopic absorption was red shifted from 485 nm to 726 nm with significant increase of molar extinction coefficient by a factor of fourteen. [30]

Besides its use in preparation of dinuclear metal complexes, there is no report on metal coordination polymers containing ligands **2** to date. In this study, we intend to design and synthesize nickel coordination polymers (Figure 3.1) based on 1,2,4,5-benzenetetraamine (BTA) and N-substituted derivatives as the bridging ligands. BTA is an electron rich molecule with a planar geometry. When coordinating with nickel ions and forming a complex polymer, the resulting Ni coordination polymer would have a poor solubility in common solvents due to its rigid structure. Using N-substituted derivatives containing a long alkyl chain as bridging ligand, the polymer would be more soluble due to long alkyl side chains. When coordinating with nickel ion, which prefers a square planar geometry, the coordination polymer would have the structure of a planar one-dimensional double-chain, akin to that of a ladder (Figure 3.1). Due to strong interactions between metal and ligand within the square planar structure, a strong NIR absorption is highly anticipated.

Usually, coordination polymers are characterized by UV/Vis/NIR, IR, elemental analysis and thermal gravimetric analysis.[31] Crystal structure might be analyzed if possible. Generally one dimensional coordination polymers are highly crystalline materials, therefore, the common crystallization method, recrystallization, is not available for preparing single crystals. The designed polymers in this thesis will be characterized by UV/Vis/NIR, IR, thermal analysis and elemental analysis of metal content. In addition, NIR halochromism and stability to oxidizing chemicals will also be evaluated.

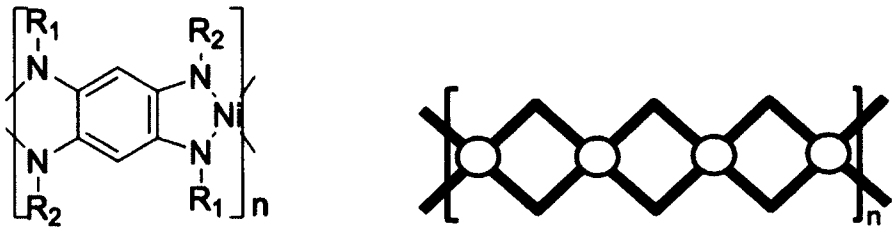

R_1, R_2 = H, aryl

4

Figure 3.1. Structure of designed coordination polymers

3.2 Choice of tetraamine as a bridging ligand

To choose the bridging ligands for coordination polymers, there are some criteria to consider such as commercial availability or easy preparation, reactivity, and effect on geometry of complex. In this study, BTA and 1,5-N,N'-bis(4-heptylphenyl)-1,2,4,5-benzenetetraamine (BHPBTA) were chosen as bridging ligands. BTA is commercially available; BHPBTA needs to be prepared through two-step synthesis. In terms of reactivity, both BTA and BHPBTA are highly reactive and are electron rich since the four amine groups are on a single aromatic ring. The *N*-substituents have a strong effect on the spatial arrangement of the resulting complexes. Wieghardt and Neese[32-34] found that bulky *N*-disubstituted *o*-phenyldiamine (N,N'-bis(3,5-di-tert-butylphenyl)-1,2-benzenediamine, BDBPBTA, **7**) would favor a pseudo-tetrahedral coordination sphere around the central Ni (II) ion instead of a planar structure $[Ni(BDBPBTA)_2]$ (**8,** structure was adopted from reference 34). There is no substitute on amine group of BTA, therefore, there is no steric hindrance problem for the geometry of complex. BHPBTA has two p-alkylphenyl substituents which would lead to steric hindrance if the coordination reaction occurs in cis-conformation. Accordingly, the anticipated complex with BHPBTA polymer would prefer trans-conformation. The alkylphenyl substituents would branch at two sides of the chain alternatively.

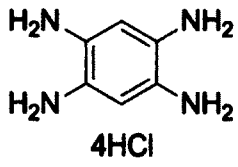

5, BTA-4HCl

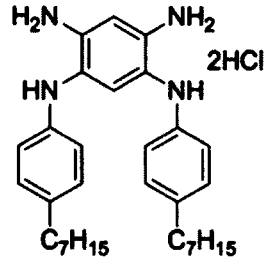

6, BHPBTA-2HCl

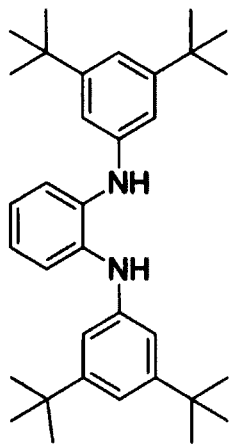

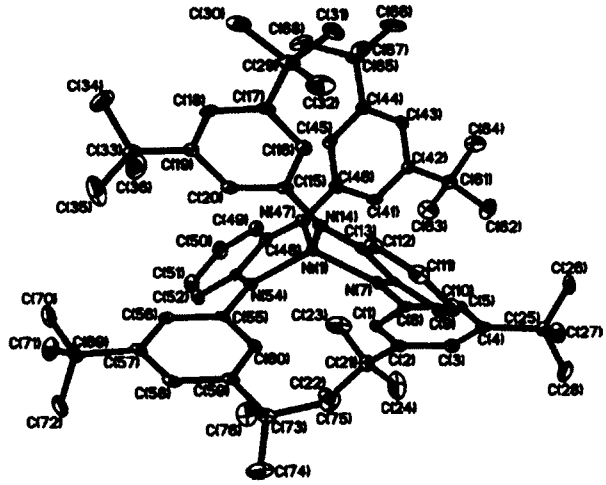

7, BDBPBTA

8, $Ni(BDBPBTA)_2$

Certainly, the π conjugating system favors a planar conformation so as to develop further. As well, the orbital overlap between metal and ligand will be affected by the geometry of complex. There is no doubt that the Ni coordination polymers with BTA have a planar geometry. Due to the trans-conformation, the coordination polymer with BHPBTA would also have a planar geometry. The *N*-substituents would branch on each side of the polymer chain and diminish steric hindrance. Thus, overlap between d-orbitals of metal and π-orbitals of ligands would readily occur.

The molecule of BTA is so electron rich that its stable form is usually hydrochloride salt. The compounds must be neutralized prior to coordination reaction. The melting point of the tetrahydrochloride salt is over 300 °C.

BHPBTA was prepared (scheme 3.1), by the nucleophilic substitution reaction of 1,5-difluoro-2,4-dinitrobenzene with 4-heptylaniline to afford N,N'-disubstituted-2,4-dinitrobenzene, followed by reduction using Pd/C and hydrazine under acidic conditions. It was isolated as hydrochloride salt. BHPBTA decomposes in air even as

a dihydrochlorice salt **6**.[35] Therefore, the salt **6** was freshly prepared prior to use and characterized by NMR.

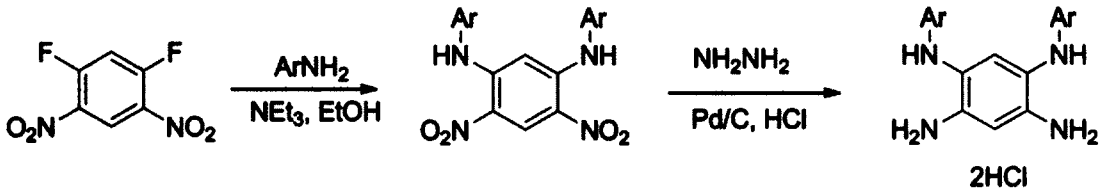

6, BHPBTA

Scheme 3.1. Synthesis of ligand 6, BHPBTA

In order to compare spectroscopic and other properties, the mononuclear complex of the same ligand was attempted to be made. However, the mononuclear complex was unstable. Since complexes **9** and **10** contained the same coordination features, they were used to compare the spectroscopic properties with the corresponding coordination polymers **4a** and **4b**, respectively.

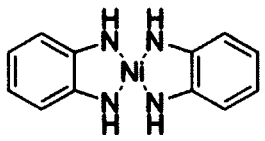

9

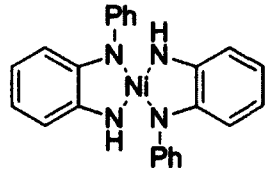

10

Table 3.1. Characterization of complexes 7 and 8

	M. P. °C	λ_{max}, nm (ε x 10^{-4} L mol^{-1} cm^{-1})	IR band of N-H ν_{N-H}, cm^{-1}	reference
9	330	780 (5.05)	3330	ref[36]
10	over 300	823(4.17)	3336	ref[32,37]

3.3 Synthesis and characterization of Ni-coordination polymer 4a

Nickel coordination polymer **4a** using BTA as a bridging ligand was synthesized according to the method depicted in scheme 3.2. BTA was neutralized and deprotonated under Argon atmosphere, followed by coordinating with nickel ions. Since the solubility of designed polymer would be very low due to its rigid planar structure, the oligomer would precipitate and coagulate and thus the polymerization may stop proceeding. Therefore, emulsion polymerization was used to prevent the polymer particles from coagulating.

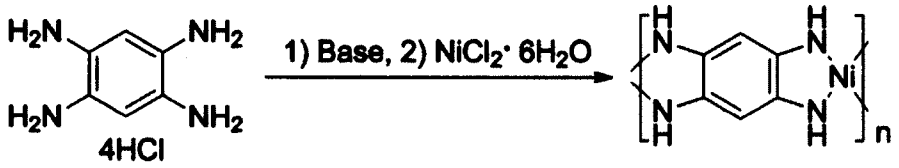

5 **4a**

Scheme 3.2. Synthesis of coordination polymer 4a

3.3.1 Polymerization methods

Method 1: Polymerization in W/O inversion emulsion.

Both bridging ligand **5** and nickel ion were dissolved and then mixed in aqueous medium. Then the aqueous solution was immediately dispersed in oil phase, dichloromethane, with vigorous agitating and emulsifying with Brij® 30 and 18-crown-6. The chain growth proceeds in individual aqueous droplets. The resulting polymer particles were well dispersed in aqueous droplet. Thus, the polymerization could possibly proceed in aqueous droplets. However, this inversion emulsion was

not stable. The aqueous droplets might diffuse to each other with time. The polymer might precipitate and stop growing. Unlike coordination reaction of small molecules, the polymerization took 3~5 days to complete.

Method 2: Emulsion polymerization using water-soluble polymer stabilizer.

Instead of using soap or surfactants as a stabilizer, emulsion polymerization could also proceed in homogeneous solution in which the particles were stabilized by a water-soluble polymer, for example, poly(vinylpyrrolidone) (PVP), serving as a stabilizer. The host polymer PVP would form a "hairy" layer around the particles and repel each other.[38] Ligands and nickel ions would diffuse into the particle through the "hairy" layer and continue the polymerization. Since the designed polymer particles were well separated by PVP, no coagulation should have occurred. The obtained coordination polymer would disperse evenly in PVP solution.

Method 3: Nano-emulsion (W/O) polymerization.

Nano-emulsion featured small droplets ranging in size from 20 – 200 nm and was transparent. In this method, ligand and metal ion were dispersed into two respective nano-emulsions, and then the two independent nano-emulsions were mixed together with vigorous agitating. Once mixed evenly, nanosized aqueous droplets would combine with each other leading to diffusion, and effectively launched polymerization. Meanwhile, the color of mixed nano-emulsion slowly turned dark indicating that a coordination reaction was occurring. Since both ligand and nickel ion were confined in nanosized droplets, the maximum particle size of obtained polymer were supposed to be less than which of liquid droplets. However, the nano-

emulsion was a kinetically stable system, it was possible that some droplets diffused into each other generating large droplets which would result in a wide distribution of polymer chain length.

3.3.2 Characterization of polymer 4a

IR analysis

It was thought that BTA would be unsuitable as a direct bridging ligand for dinuclear complexes because the benzoquinonediimine was susceptible to oxidation yielding a bridging ligand of 2,3,5,6-tetraiminocyclohexane-1,4-dione with a structure as below.[29]

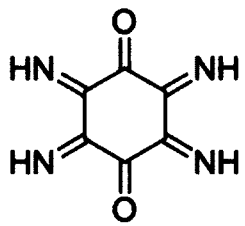

A likely explanation of oxidation was that bridging ligand BTA of dinuclear complex was only stabilized by two metal nuclei resulting in the limit conjugation and orbital overlap. During the polymerization in this study, the reaction was conducted in Argon atmosphere. The IR spectrum (Figure 3.2) of the polymer did not show any carbonyl absorption. Apparently, the ligand did not suffer oxidation during the reaction. The electrons of the bridging ligand were delocalized and stabilized by multi-metals, thus the polymer was not vulnerable to oxidation any more. The obtained dark blue powder was insoluble in common organic solvent, such as DMF, DMSO, CH_2Cl_2, dichlorobenzene, THF and toluene. Another feature of the IR spectrum was that only secondary amine absorption band presented in the IR spectrum. The ratio between secondary amine and primary amine in the dinuclear complex was 2:1, though there should be present an absorption band for primary amine if only mono- or dinuclear complex was formed. Tables 3.2 lists the ratio of

secondary amine to primary amine. When the number of metal centers in a chain was over 10, the number of primary amine would be less than one tenth of secondary amine. In this case, the IR absorption band of primary amines would be too weak to be observed. In other words, the IR spectrum also supported the coordination polymerization.

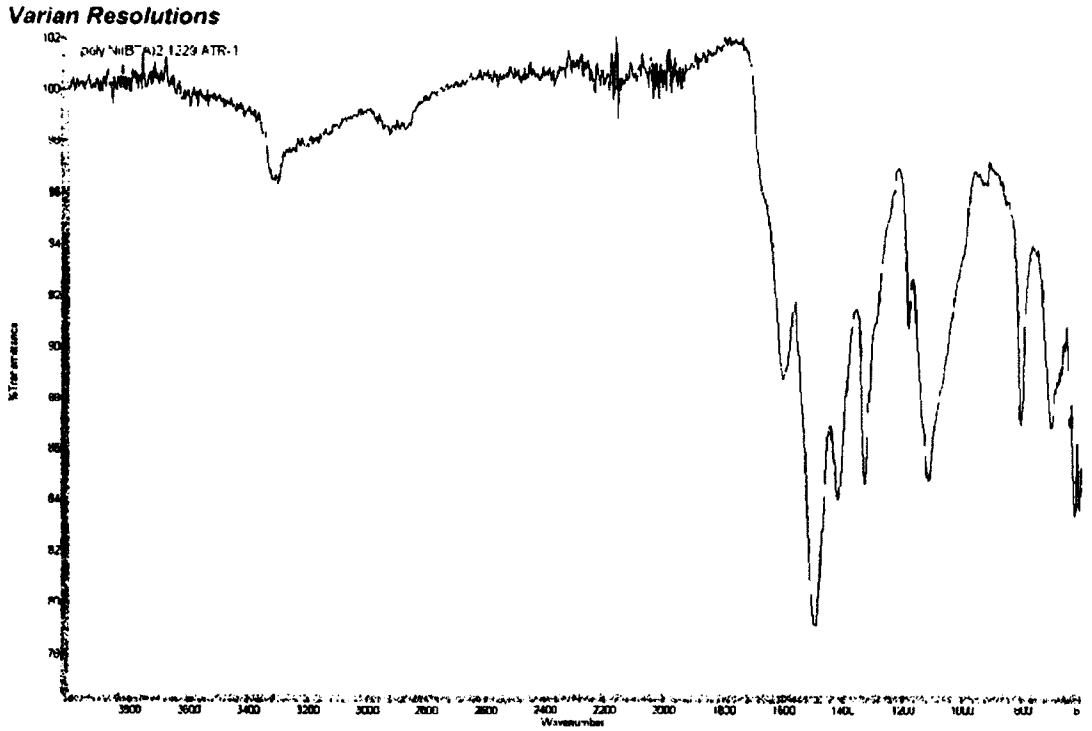

Figure 3.2. IR spectrum of polymer 4a (ATR of powder from nano-emulsion).

Table 3.2. Ratio of sec-amine to primary amine in coordination polymer 4a

# of Ni center	1	2	4	6	8	10	12
Ratio of NH to NH_2	1:1	2:1	4:1	6:1	8:1	10:1	12:1

UV-Vis-NIR absorption

The UV/Vis/NIR absorption spectra of coordination polymer **4a** obtained from different methods are shown in Figure 3.3. The broad absorption bands span from the visible region up to 1150 nm. In contrast, the absorption band of mononuclear complex **9** is narrow with a maximum at 780 nm. The NIR absorption of coordination polymer was attributed to the MLCT which was originated from the electrons delocalization and metal-ligand orbital overlap.[10,23]

Absorption of polymer **4a** from method 1: First of all, it was noticed that the absorption of **4a** obtained from this method spanned from 400 nm to 1150 nm which was broad in comparison with the absorption of mononuclear complex **9**. As designed, the electron conjugation as well as metal-ligand orbital overlap developed along the chain. As a result, the band gap was narrowed. The broad absorption also resulted from the wide distribution of chain lengths of the polymer to some extent. As aforementioned, the emulsion of W/O type was not as stable as emulsion of O/W type and some aqueous droplets in the emulsion might diffuse to each other. As a result, polymer in large droplets might precipitate due to coagulation terminating the polymerization and the chain length would be short. On the other hand, polymer in small droplets would have a long chain. As known, the development of conjugation and orbital overlap was determined by the chain length, therefore, the wide distribution of chain length led to a broad absorption band.[30]

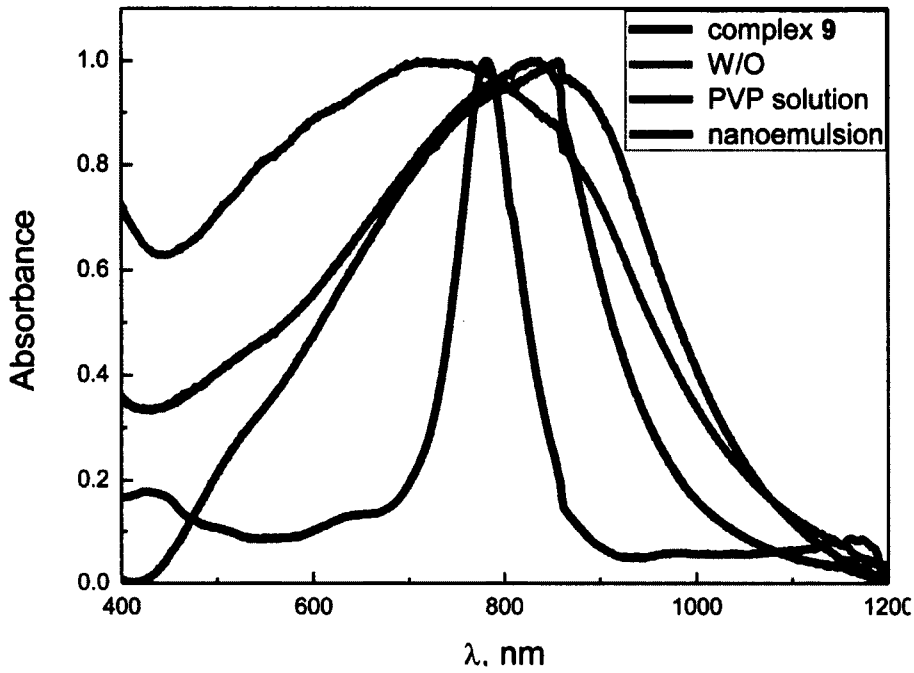

Figure 3.3. Normalized Vis/NIR spectra of polymer 4a dispersed in DMF, as prepared by different methods.

Absorption of polymer **4a** from method 2: The absorption of coordination polymer **4a** obtained by this method spanned from 420 to 1100 nm with a maximum at 835 nm. In this method, the coordination reaction was conducted in homogeneous medium. The chain of polymer **4a** grew with time but did not precipitate because the particles were well dispersed by PVP. It was believed that hydrogen bonding between PVP and polymer **4a** contributed to the stabilization to the particles. A longer chain with conjugation and metal-ligand orbital overlap was obtained compared to that from W/O emulsion polymerization. Therefore, the maximum absorption band was red shifted to 835 nm. Additionally, the solution could be directly used to make highly NIR absorptive clear films as the polymer complex was dispersed evenly in PVP solution.

Absorption of polymer **4a** from method 3: The absorption of the obtained polymer **4a** spanned from 420 nm to 1150 nm with a maximum at 860 nm. The max absorption was red shifted about 25 nm comparing to method 2. It was assumed that the polymer chain grew more effectively and did not forming solid aggregates in well dispersed nano-emulsion. Thus a longer conjugation and orbital overlap were generated comparing to method 2. The wide distribution of chain length was also believed to be one of the contributions to the broad absorption.

Stability to chemical oxidation

The mononuclear complex **9** was unstable to oxidizing chemicals, such as hydrogen peroxide. Figure 3.4 shows the change in NIR absorption of complex **9** during the oxidizing process. With the addition of H_2O_2, the absorption at 780 nm decreased and eventually disappeared. In comparison, polymer **4a** was found to be very stable to H_2O_2. The NIR absorption of **4a** persisted upon the addition of H_2O_2 indicating that the bonding between metal and ligands is fairly strong.

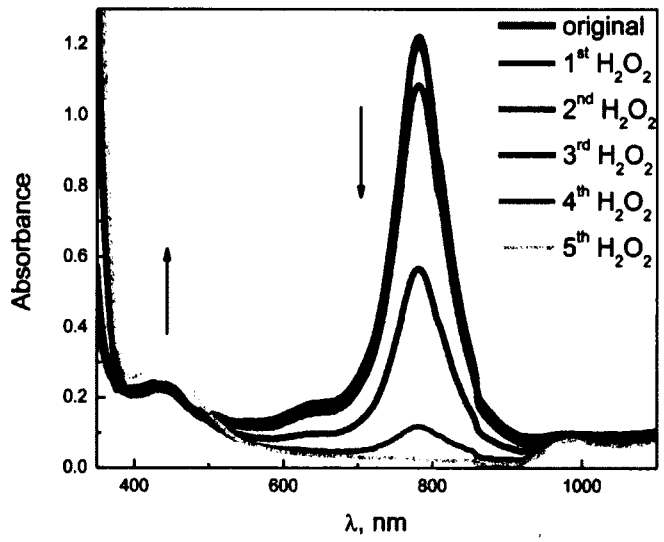

Figure 3.4. Changes in NIR absorption during the oxidation of complex **9** by H_2O_2

NIR halochromism

Halochromism means the color change which occurs on addition of acid (or base, or a salt) to a solution of a compound. In this case, the color falls in NIR region. The amino groups on bridging ligands along the polymer chain could be protonated.[23] As known, the NIR absorption of the coordination polymer was determined by the electron delocalization of ligand and orbital overlap between metal and ligand. Once the amino groups of the bridging ligand were protonated, the electron delocalization would be significantly influenced resulting in the change in NIR absorption. As a matter of fact, the NIR halochromic property of polymer **4a** was observed. Figure 3.5 shows the reversibility and the absorption evolution process of NIR halochromism. Upon the addition of HCl, NIR absorption disappeared immediately. After neutralizing with KOH, NIR absorption resumed with a blue shift of 60 nm. The blue shift was probably caused by the polarity change of the solvent by adding aqueous acid and base.

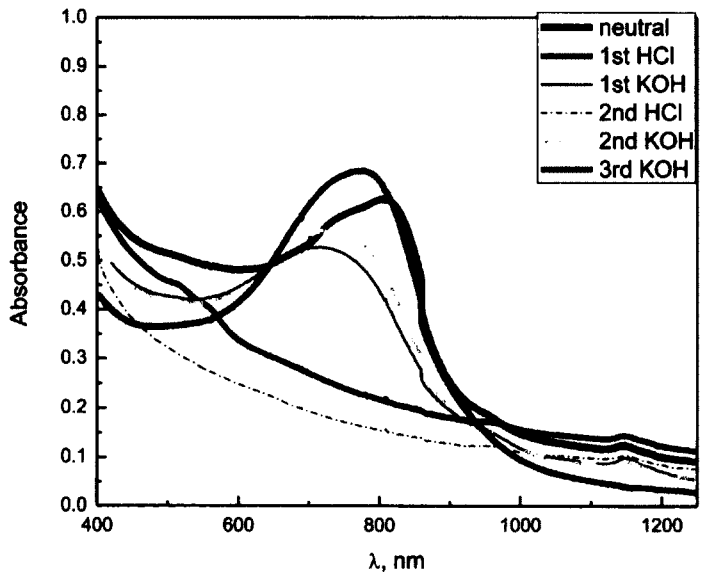

Figure 3.5. NIR halochromism of polymer 4a (obtained from dispersion polymerization in single phase)

In summary, polymer **4a** was synthesized using three different emulsion polymerization methods. The spectroscopic absorption of the polymer spanned from 400 to 1150 nm. The polymer **4a** was stable to chemical oxidation with a persisted NIR absorption comparing to the mononuclear complex **9**. The stability to H_2O_2 probably proved to be the strong bonding between metal ions and ligands and delocalization of π conjugation system. In addition, the polymer was NIR halochromic. By protonating and deprotonating the amino group on the chain, the interaction between metal ion and ligand would be weakened and rebuilt resulting in the reversible NIR halochromism. Due to rigid structure of the chain, the solubility of the polymer was so poor that it was insoluble in common organic solvents.

3.4 Synthesis and characterization of Ni-coordination polymer 4b

3.4.1 Synthesis

Freshly prepared ligand **6** was used to conduct the coordination polymerization reaction as shown in scheme 3.3. DMF was degassed by bubbling with Argon for over 2h prior to use and the reaction was maintained under Argon atmosphere. After sodium tert-butoxide was added into the solution and stirred for 30 min, the reaction mixture turned to purplish red indicating neutralization and deprotonation. Then $NiCl_2 \cdot 6H_2O$ was added into the solution and stirred for 3~5 days. The color of the reaction mixture gradually turned to blue and finally to dark blue. The ligand underwent neutralization, deprotonation and then coordinated with metal ion affording a double-chain linear polymer.

Unlike the mono- or dinuclear complex, the reaction time for polymerization lasts over days. This is probably to compensate for the decrease in solubility when the number of metal nuclei on the chain is over five.[30]

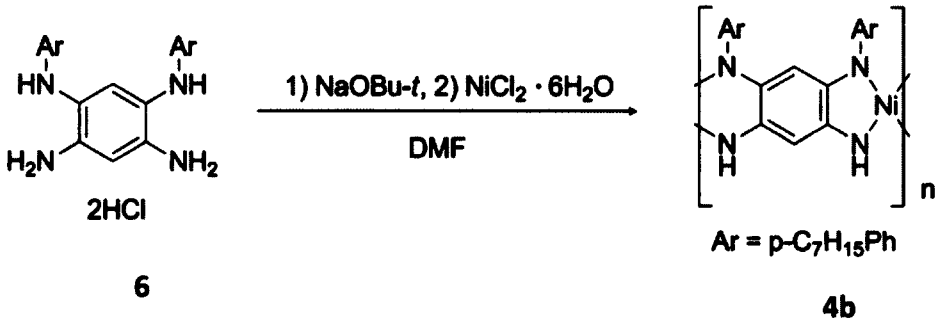

Scheme 3.3. Synthesis of coordination polymer **4b**

3.4.2 Characterization of polymer 4b

Solubility

Before isolating from the solution, the polymer **4b** was fairly soluble in DMF. The improvement of the solubility was originated from long alkyl side chains branched the polymer backbone. Once precipitated from the solution, the polymer would not dissolve in any common organic solvent that was available.

IR spectrum of polymer 4b

The IR spectrum of polymer **4b** was taken with attenuated total reflection (ATR) method (Figure 3.6). The spectrum shows a typical absorption of secondary amine (N-H) at 3348 cm^{-1} which is close to absorption band of N-H (3336 cm^{-1}) from complex **10**. Similar to polymer **4a**, the ratio of secondary to primary amine varies with the degree of polymerization (as shown in Table 3.3). The absorption of primary amines was too weak to be observed if the polymer chain contained over ten metal centers. The lack of absorption for primary amine NH_2 supported the coordination polymerization. In addition, there was no absorption band for carbonyl group on the spectrum. It meant that the ligand did not suffer any oxidation during the coordination polymerization.

Table 3.3. Ratio of sec-amine to primary amine in coordination polymer 4b

# of Ni center	1	2	4	6	8	10	12
Ratio of NH to NH_2	2:1	3:1	5:1	7:1	9:1	11:1	13:1

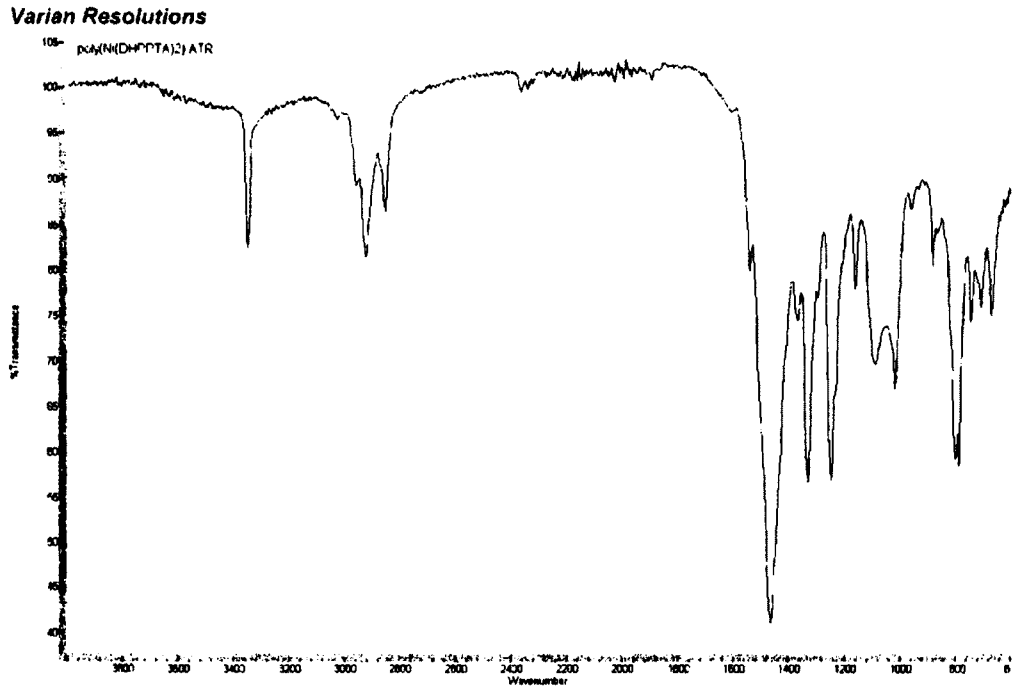

Figure 3.6. IR spectrum of polymer 4b (ATR method)

NIR absorption of polymer 4b

Figure 3.7 shows the NIR absorption spectra of polymer **4b** in DMF solution and in poly(methyl methacrylate) (PMMA) film. The broad absorption spans from 640 up to 1500 nm with a maximum at 880 nm. There are indeed three absorption bands from the polymer, peaking at 750, 880 and 995 nm. Comparing to literature data for Ni coordination polymer bridged by dianion of 2,5-dihydroxy-1,4-benzoquinone (380 nm, broad) and dinuclear Ni complexes bridged by 2,5-diamino-1,4-benzoquinondimine (550 nm, narrow), the absorption of **4b** was red shifted to 880 nm. In comparison, the absorption of the mononuclear complex **10** was narrow with maximum at 823 nm. Three absorption bands at 750, 880 and 995 nm were originated from the $\pi - \pi^*$ transition of bridging ligands,[32] MLCT[23,25,26,39] and LLCT[26]

respectively. With increasing delocalization, the LLCT transfer lost CT character but involved delocalized orbitals.[40]

The red shift of absorption was apparently due to the delocalization of the π electrons over both metal and ligand. The π conjugation system was able to develop along the polymer chain from the interaction of orbital overlap with metals. Thus the energy gap between HOMO – LUMO was reduced. Due to integration of multi-chromophores into one macromolecule, the absorption should be stronger than that of mononuclear product.

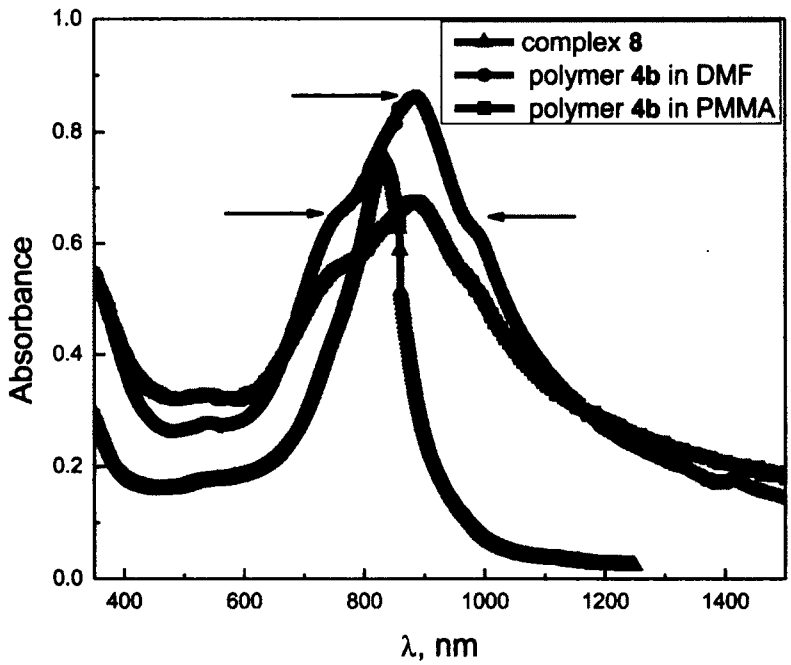

Figure 3.7. NIR absorption spectrum of polymer 4b in DMF and PMMA film

The extinction coefficient was calculated using L• mg^{-1}•cm^{-1} as unit. The calculated value was 0.089 L• mg^{-1}•cm^{-1}. The elemental analysis shows that the Ni content is ~10.63%. Based on this value, the repeat unit of the polymer would be 10~12 with molecular weight of 6700~8100 g/mol. The molar extinction coefficient

would be 5.9~7.2 x 10^5 L • mol^{-1} • cm^{-1} which is about ten times of the value of complex **10**.

When the polymer **4b** was dispersed in PMMA film, extinction coefficient was calculated as per cm of film thickness. The thickness of polymer was calculated based on its content in PMMA (Table 3.4). Figure 3.8 shows the relationship between the absorbance and thickness. The calculated extinction coefficient is $6.5x10^4$ cm^{-1}. The absorbance of the film is 0 at a certain thickness if the plot is extended. This experimental error comes from the reflection of film. The baseline of absorption shifts upward due to the reflection.

Table 3.4. Absorbance of polymer film at different thickness

	wt.% of 4b in PMMA film	thickness of PMMA Film, μm	Absorbance	Thickness equivalent to polymer **4b**, nm
1	2.1%	1.1	0.095	23
2	4.2%	1.1	0.19	46
3	4.2%	2.8	0.3	59
4	2.1%	7.7	0.98	162

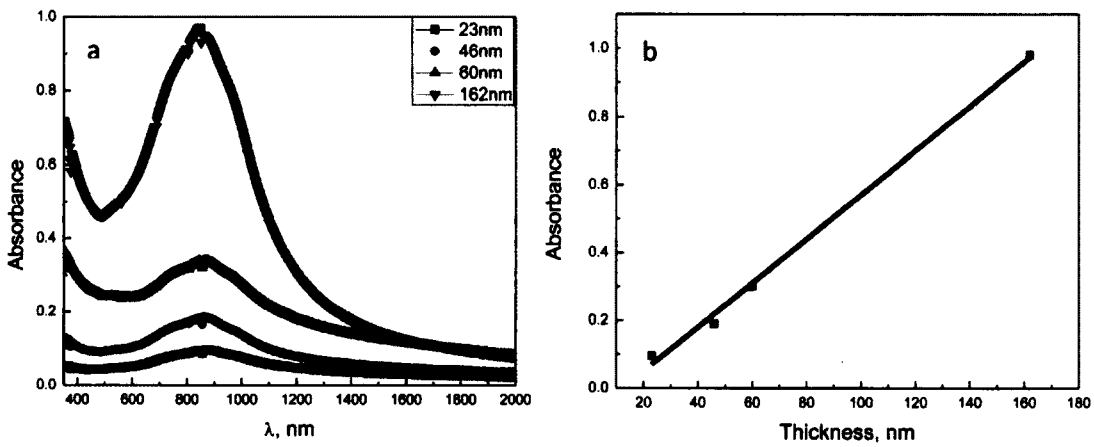

Figure 3.8. (a) Absorption spectra of polymer 4b film with different thickness (b) Plot of absorbance against thickness

Thermal stability of 4b

The melting point of polymer **4b** was over 300 °C. The polymer was dried at 110 °C overnight before thermogravimetric analysis (TGA). The polymer started to decompose at 340 °C (Figure 3.9). The decomposition temperature of **4b** is 65 °C higher than that of its analogue with bridging ligands **1**.[41] According to one of general decomposition mechanisms of polymers, the alkyl side chains were eliminated during the first stage of decomposition.[42] The resulting weight loss was 32% corresponding to theoretical calculated value of 34% when the alkyl side chain was removed. Afterwards, the polymer continued decomposing slowly with the temperature increase. The weight of residue was 18% which was higher than nickel content (10%). The discrepancy between the actual residual weight and nickel content was due to charring during thermal decomposition.

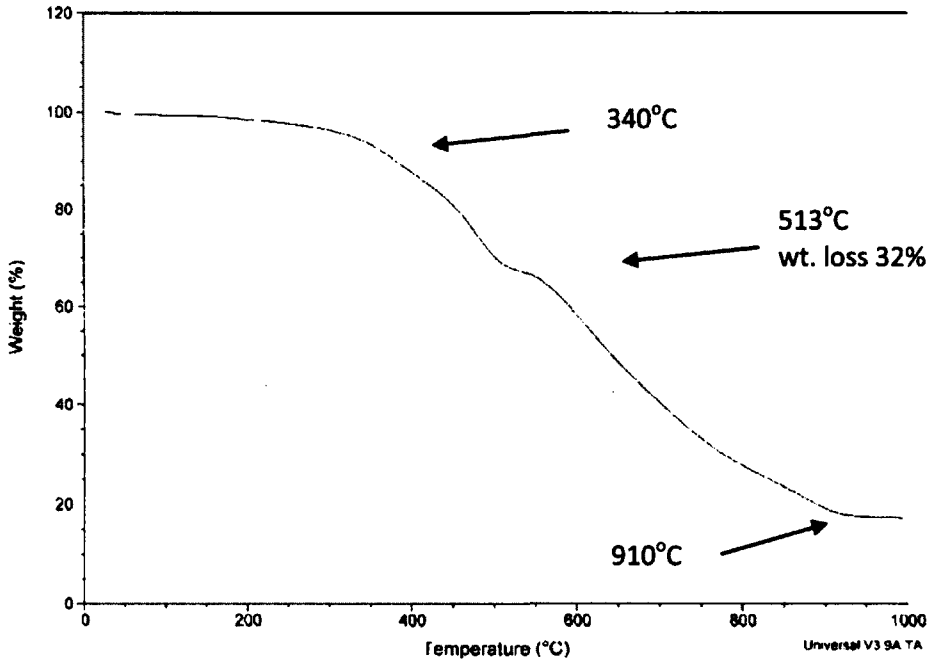

Figure 3.9. TGA traces of polymer 4b

Stability to chemical oxidation

Similar to polymer **4a**, polymer **4b** was stable to chemical oxidation comparing to mononuclear complex **10**. Figure 3.10 shows the change in NIR absorption of complex **10** during oxidizing process. The absorption at 820nm decreased and eventually disappeared with the addition of H_2O_2. However, the polymer **4b** was found to be stable to H_2O_2. The persisted NIR absorption of polymer 4b upon the addition of H_2O_2 indicates that the bonding between metal and ligands is fairly strong.

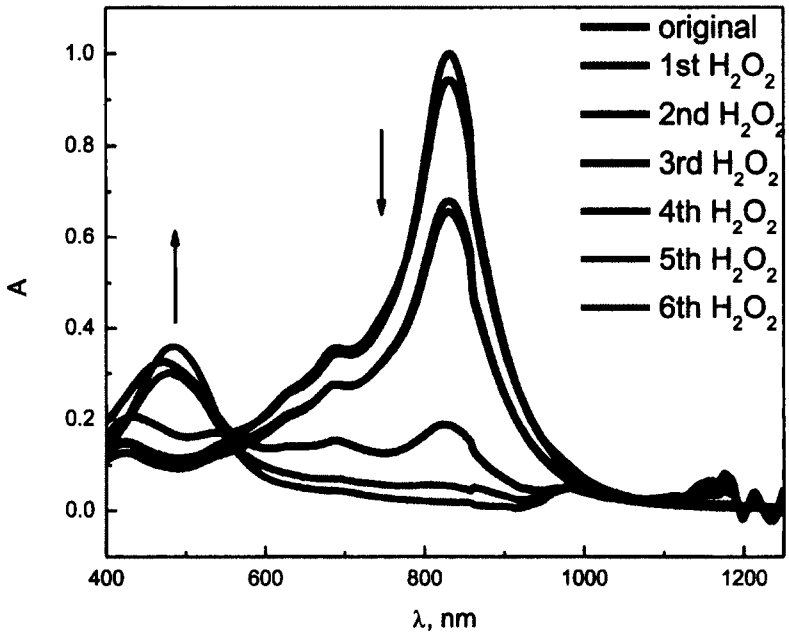

Figure 3.10. Changes in NIR absorption during the oxidation of **10** by H_2O_2

NIR halochromism

Similar to polymer **4a**, polymer **4b** also was found to be NIR halochromic. It is possible to protonate the amino groups which are already bonding with nickel ions.[24] Once the amino groups are protonated, the bonding character between amino group and metal ion will be significantly influenced. Therefore, the energy gap of the

protonated polymer will be changed comparing to the non-protonated one. Figure 3.11 shows the reversible NIR halochromism of polymer **4b** in DMF. Once protonated, the absorption at 880 nm disappeared and a new absorption band at 420 emerged indicating that the interaction between ligand and metal was changed. Furthermore, the configuration of Ni complex might be altered by water molecules, which were introduced into the solution when adding diluted hydrochloric acid, after protonation.[43] When the solution was neutralized by adding aqueous KOH, the absorption in the NIR region was resumed with a blue shift which was probably caused by polarity change of the solution. The resumed absorption indicated that the interaction between ligands and metal is strengthened. Also, the square planar structure resumed and water molecules were expelled.

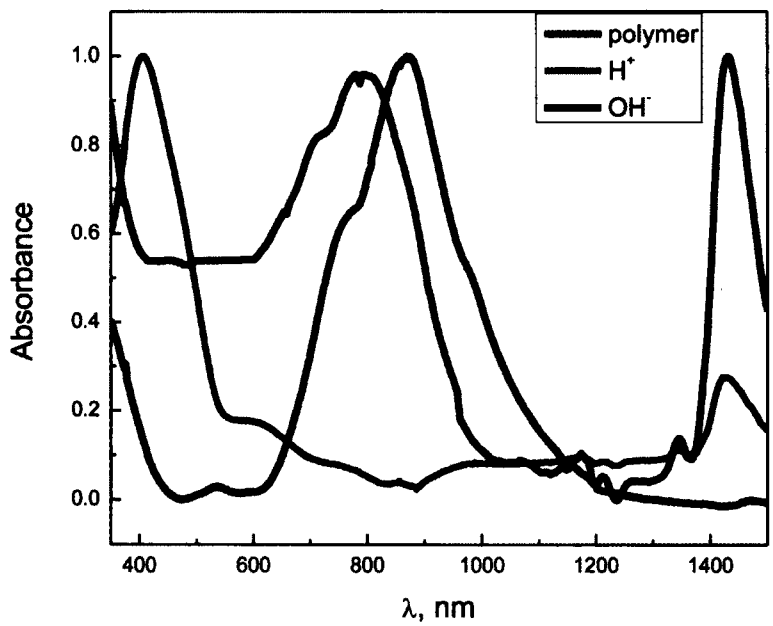

Figure 3.11. NIR halochromism of polymer 4b in DMF

When polymer **4b** was dispersed in PMMA film, it showed similar NIR halochromic properties to that in DMF dispersion, except that response time was longer, likely due to slow diffusion of acid or base through the polymer matrix.

In summary, the solubility of **4b** was improved owing to its long alkyl side chains. The spectroscopic absorption of the polymer is broad and spans from 620 to over 1400 nm. The IR spectrum supports the coordination polymerization. Polymer **4b** is also stable to chemical oxidation such as hydrogen peroxide with a persisted NIR absorption comparing to the mononuclear complex **10**. The thermal stability of **4b** was evaluated and the decomposition mechanism agreed the general mechanism, in which the side alkyl chain was first eliminated followed by decomposing of backbone. The reversible NIR halochromism of **4b** was also investigated.

3.5 Conclusion and future work

Two types of Ni coordination polymers based on bridging ligand benzene-1,2,4,5-tetraamine and 1,5- N,N'-bis(4-heptylphenyl)-1,2,4,5-benzenetetraamine were designed, synthesized and characterized. The absorption band of polymer **4a** is broad and spans from 400 to 1150 nm with a maximum at 835 nm. The absorption of polymer **4b** is also broad and spans from 640 nm to 1500 nm with a maximum at 880 nm. The absorptivity of polymer **4b** in DMF is 0.089 $L \cdot mg^{-1} \cdot cm^{-1}$. Both polymers **4a** and **4b** are stable to chemical oxidation. The polymers are also thermal stable and reversibly NIR halochromic.

Comparing to the polymer with oxygen-based bridging ligands, the coordination polymers with tetraamino ligands have lower energy gap so that the absorption is extended to the NIR region. The electronic delocalization and orbital overlap between metal and ligand explains the low energy gap. Protonation/deprotonation of the polymer can significantly influence the interaction between metal center and ligands. The reversible NIR halochromism is the result of protonation/deprotonation of the polymer. The solubility of the polymer can be improved to some extent by N-substituents which is an advantage over oxygen-based ligand. Unfortunately, the molecular weights of both polymers are low which are unsuitable for direct film-forming. As an alternative, the produced polymers can incorporate with commercial available polymers such as PMMA to make a film so as to serve as a functional film. This ground work points out the Ni coordination polymers as potential NIR absorption materials with thermostability, stability to chemical oxidation and NIR halochromism.

The future work for Ni-coordination polymer would be in three aspects. First of all, the polymerization method would be improved to make the polymer be suitable for making film with no other matrix polymer. Secondly, other properties such as magnetism and surface area would be studied. The stability to oxidizing chemicals should be investigated in acidic/basic solution. Thirdly, the application of polymer would be developed corresponding to its properties.

3.6 Experimental section

NMR characterization was conducted using a Bruker Advance 300 MHz or AMX 400 MHz spectrometer in $CDCl_3$. Mass spectra of the ligands were acquired by a Kratos Concept IIH mass spectrometer electron ionization (EI) mode and peaks are reported as m/z (% intensity relative to the base peak). UV-Vis-NIR absorption spectra were recorded using a Perkin-Elmer Lamda 900 spectrometer. Thermal stability was evaluated by AutoTGA 2950HR (TA Instruments) at ramp of 10 °C/min under argon atmosphere. Melting point was measured using Fisher Johns Melting Apparatus. IR spectra were recorded using Varian 1000 FTIR Scimitar Series. The Pike MIRacle ATR accessories were used to take ATR spectrum.

Synthesis of ligand

N,N'-di(p-heptylphenyl)-4,6-dinitrobenzene-1,3-diamine, (**5**)

To a solution of 1, 5-difluoro-2, 4-dinitrobenzene (0.204 g, 1.00 mmol) in 10 mL of ethanol were added mixture of *p*-heptylaniline (0.382 g, 2.00mmol) and triethylamine (0.28 mL, 2.0 mmol). The reaction mixture was refluxed for 48 h. After cooling to room temperature, the mixture was poured into water to precipitate the product. The solid was collected by filtration, rinsed with water, and dried under vacuum. The obtained product was yellow solid, (0.52 g, 95%). ^{1}HNMR (300 MHz, $CDCl_3$): δ 9.69 (br s, 2H), 9.34 (s, 1H), 7.13 (d, J = 8.4, 4H), 7.04 (d, J = 8.4, 4H), 6.49 (s, 1H), 2.58 (t, J = 7.5, 4H), 1.63-1.45 (m, 4H), 1.40-1.30 (m, 16H), 0.92 (t, J = 6.6, 6H).

1,5-N, N'-bis(4-heptylphenyl)- 1,2,4,5-benzenetetraamine dihydrochloride, (**6**)

Compound **5** (0.547 g, 1.00 mmol) was dissolved in ethanol (20 mL), Pd/C (10 %, 0.105 g, 0.10 mmol Pd) was added to the solution. Then $NH_2NH_2 \cdot H_2O$ (80%, 16 mmol) was added dropwise and stirred for 30 min and the solution became purple followed by dropwise addition of 1.2 N HCl (7.0 mL, 8.0 mmol), and the reaction mixture was stirred in oil bath at 80 °C for 4 h. The reaction mixture became colorless with black suspension at last. After cooling to room temperature, the reaction mixture was filtered through Celite and the filtrate was condensed under vacuum to provide corresponding tetraamines as dihydrochloride salts. H-NMR (300MHz, $CDCl_3$): δ 6.97 (d, J = 7.8, 4H), 6.87 (s, 1H), 6.56 (d, J = 8.4, 4H), 6.29 (s, 1H), 4.87 (br s, 2H), 3.78 (br s, 4H), 2.49 (t, J = 8.7, 4H), 1.62-1.45 (m, 4H), 1.35-1.20 (m, 16H), 0.89 (t, J = 6.6, 6H). EI-HRMS (m/z): 546.3219 (100%), calculated: 546.3206.

The product was collected as pale white solid with a yield of 95%. This product was stored in argon atmosphere.

Polymer (4a)

Polymer **4a** was obtained through different polymerization methods.

Method 1: Inversion emulsion polymerization in water/oil system. To 200 mL of dichloromethane, Nickel chloride hexahydrate (0.237 g, 1.00 mmol), sodium hydroxide (0.320 g, 8.00 mmol), Brij 30 (0.1 g) and 18-crown-6 (0.1 g) in 10 mL of water was added slowly with the vigorous stirring. A solution of 1,2,4,5-benzenetetramine tetrahydrochloride (0.284 g, 1.00 mmol) in 2 mL of water was added slowly (over 30 min) after emulsified for 1h followed by stirring over 3 days.

The two phases were separated by ultrasonication. The precipitate was collected by vacuum filtration.

Method 2: Emulsion polymerization stabilized by PVP. To a solution of Poly(vinyl pyrrolidone) (Mw 130k, 0.81 g) in ethanol (5 mL), 1,2,4,5-benzenetetramine tetrahydrochloride (0.284 g, 1.00 mmol) was added and stirred until dissolved. Sodium tert-butoxide (0.768 g, 8.00 mmol) was added into the mixture with argon protection and stirred for 1h. The mixture turned to orange in color. Then the solution of Nickel chloride hexahydrate (0.237 g, 1.0 mmol) in 2 mL ethanol was added and stirred at 50 °C for 3 days. The reaction mixture turned to brownish at the beginning and then dark blue.

Method 3: Nanoemulsion polymerization: both metal and ligand nanoemulsions were prepared separately and then mixed slowly with stirring. Ni nanoemulsion: a solution of nickel chloride hexahydrate (25.2 mg, 0.092 mmol) in 1mL of water was added into the mixture of cyclohexane (11.0 mL), n-hexanol(7.0 mL) and Triton X-100 (5 mL) with emulsifying (brand and model of emulsifier: IKA Ultra TURRAX T18). Ligand nanoemulsion: a solution of 1,2,4,5-benzenetetramine (27.2 mg, 0.096mmol) and sodium hydroxide (0.031 g, 0.768 mmol) in 1 mL of water was added into the mixture of cyclohexane (11.0 mL), n-hexanol (7.0 mL) and Triton X-100 (5 mL) with emulsifying under argon protection. Ni nanoemulsion was added dropwise into ligand nanoemulsion while maintaining emulsifying and argon protection. The emulsion was stirred overnight. To separate the product from emulsion, the mixture was then treated by ultrasonic, centrifugalization and filtration after the addition of 5 mL of dichloromethane. The precipitate was washed with

dichloromethane and then collected by filtration. The obtained product is dark blue with a yield of 35%. IR: 3348 cm^{-1} for N-H

Polymer (4b)

The metal coordination polymer **7** was synthesized in homogeneous phase with argon protection. To a solution of freshly prepared ligand **6** (0.560 g, 1.00 mmol) in 5mL of DMF was added sodium tert-butoxide (0.576 g, 6.00 mmol). After the solution was stirred for 1h, a solution of Nickel chloride hexahydrate (0.237 g, 1.00 mmol) in 2 mL of ethanol was added. The reaction mixture was stirred at 60 °C for 3~5days. After polymerization was complete, 5 mL of chloroform of was added into the mixture followed by extraction with water to remove salts until the washing was non-basic. The polymer suspension was concentrated by rotavaporization followed by centrifugation to afford the precipitate. The collected polymer was dark blue with a yield of 60%. Melting point: over 300 °C. IR: 3348 cm^{-1} for N-H. Anal. Calcd. For polymer with 12 repeat units: Ni, 10.08. Found: Ni, 10.06.

3.7 References

(1) Rowsell, J. L. C.; Yaghi, O. M. *J. Am. Chem. Soc.* **2006**, *128*, 1304.

(2) Maji, T. K.; Matsuda, R.; Kitagawa, S. *Nat Mater* **2007**, *6*, 142.

(3) Zou, R.-Q.; Sakurai, H.; Xu, Q. *Angew. Chem. Int. Ed.* **2006**, *45*, 2542.

(4) Hu, B.-W.; Zhao, J.-P.; Yang, Q.; Liu, F.-C.; Bu, X.-H. *J. Mater. Chem.* **2009**, *19*, 6827.

(5) Sugawara, T. *JP 2009260157*, **2009**

(6) Sundaram, R.; Hariprasad, K. S. *Indian J. Chem. Technol.* **2007**, 14, 451.

(7) Zhang, D.; Jin, G.-X. *Organometallics* **2003**, 22, 2851.

(8) Matsuki, K.; Sugawara, R.; Tanno, S. *JP1991-308599*, **1993**

(9) Suzuki, T.; Hibino, K.; Murai, M.; Fujita, T. *US 4425404*, **1982**

(10) Miyoshi, H.; Matsumoto, M.; Kanda, S. *J. Colloid Interface Sci.* **1997**, 193, 26.

(11) Rao, T. R.; Rao, P. R.; Lingaiah, P.; Deshmukh, L. S. *J. Indian Chem. Soc.* **1991**, *68*, 458.

(12) Kanda, S. *Nippon Kagaku Zasshi* **1962**, *83*.

(13) Dei, A.; Gatteschi, D.; Pardi, L. *Inorg. Chem.* **1990**, *29*, 1442.

(14) Calvo, M. A.; Manotti Lanfredi, A. M.; Oro, L. A.; Pinillos, M. T.; Tejel, C.; Tiripicchio, A.; Ugozzoli, F. *Inorg. Chem.* **1993**, *32*, 1147.

(15) Lu, K.; Earley, J. E. *Inorg. Chem.* **1993**, *32*, 189.

(16) Ward, M. D. *Inorg. Chem.* **1996**, *35*, 1712.

(17) Tinti, F.; Verdaguer, M.; Kahn, O.; Savariault, J. M. *Inorg. Chem.* **1987**, *26*, 2380.

(18) Haga, M.; Isobe, K.; Boone, S. R.; Pierpont, C. G. *Inorg. Chem.* **1990**, *29*, 3795.

(19) Lever, A. B. P.; Auburn, P. R.; Dodsworth, E. S.; Haga, M. A.; Liu, W.; Melnik, M.; Nevin, W. A. *J. Am. Chem. Soc.* **1988**, *110*, 8076.

(20) Cox, D. D.; Que, L. *J. Am. Chem. Soc.* **1988**, *110*, 8085.

(21) Benelli, C.; Dei, A.; Gatteschi, D.; Pardi, L. *J. Am. Chem. Soc.* **1988**, *110*, 6897.

(22) Rall, J.; Stange, A. F.; Hübler, K.; Kaim, W. *Angew. Chem. Int. Ed.* **1998**, *37*, 2681.

(23) Siri, O.; Braunstein, P. *Chem. Commun.* **2000**, 2223.

(24) Siri, O.; Braunstein, P.; Rohmer, M.-M.; Bénard, M.; Welter, R. *J. Am. Chem. Soc.* **2003**, *125*, 13793.

(25) Ward, M. D. *Chem. Soc. Rev.* **1995**, *24*, 121.

(26) Siri, O.; Taquet, J.-p.; Collin, J.-P.; Rohmer, M.-M.; Bénard, M.; Braunstein, P. *Chem. Eur. J.* **2005**, *11*, 7247.

(27) Masui, H.; Lever, A. B. P. *Inorg. Chem.* **1993**, *32*, 2199.

(28) Metcalfe, R. A.; Lever, A. B. P. *Inorg. Chem.* **1997**, *36*, 4762.

(29) Masui, H.; Freda, A. L.; Zerner, M. C.; Lever, A. B. P. *Inorg. Chem.* **2000**, *39*, 141.

(30) Von Kameke, A.; Tom, G. M.; Taube, H. *Inorg. Chem.* **1978**, *17*, 1790.

(31) Noro, S.-i.; Kitagawa, S.; Akutagawa, T.; Nakamura, T. *Prog. Polym. Sci.* **2009**, *34*, 240.

(32) Herebian, D.; Bothe, E.; Neese, F.; Weyhermüller, T.; Wieghardt, K. *J. Am. Chem. Soc.* **2003**, *125*, 9116.

(33) Herebian, D.; Wieghardt, K. E.; Neese, F. *J. Am. Chem. Soc.* **2003**, *125*, 10997.

(34) Chłopek, K.; Bothe, E.; Neese, F.; Weyhermüller, T.; Wieghardt, K. *Inorg. Chem.* **2006**, *45*, 6298.

(35) Boydston, A. J.; Vu, P. D.; Dykhno, O. L.; Chang, V.; Wyatt, A. R.; Stockett, A. S.; Ritschdorff, E. T.; Shear, J. B.; Bielawski, C. W. *J. Am. Chem. Soc.* **2008**, *130*, 3143.

(36) Park, S.; Jun, K. *Journal of Industrial and Engineering Chemistry (Seoul, Republic of Korea)* **2005**, *11*, 883.

(37) Cheng, H.-Y.; Lin, C.-C.; Tzeng, B.-C.; Peng, S.-M. *Journal of the cChinese Chemical Society* **1994**, *41*, 775.

(38) Odian, G. *Principles of Polymerization*; 4th ed.; Wiley: Hoboken, NJ, USA, **2004**.

(39) Braun-Sand, S. B.; Wiest, O. *J. Phys. Chem. A* **2003**, *107*, 285.

(40) Vogler, A.; Kunkely, H. *Comments Inorg. Chem.* **1990**, *9*, 201.

(41) Bottei, R. S.; Fangman, J. T. *J. Inorg. Nucl. Chem.* **1966**, *28*, 1259.

(42) Beyler, C. L.; Hirschler, M. M. In *SFPE Handbook of Fire Protection Engineering*; 3rd ed.; DiNenno, P. J., Ed.; Quincy, Mass: National Fire Protection Association: **2002**.

(43) Wrobleski, J. T.; Brown, D. B. *Inorg. Chem.* **1979**, *18*, 498.

Appendix 1: EDX spectrum of AgNP Film

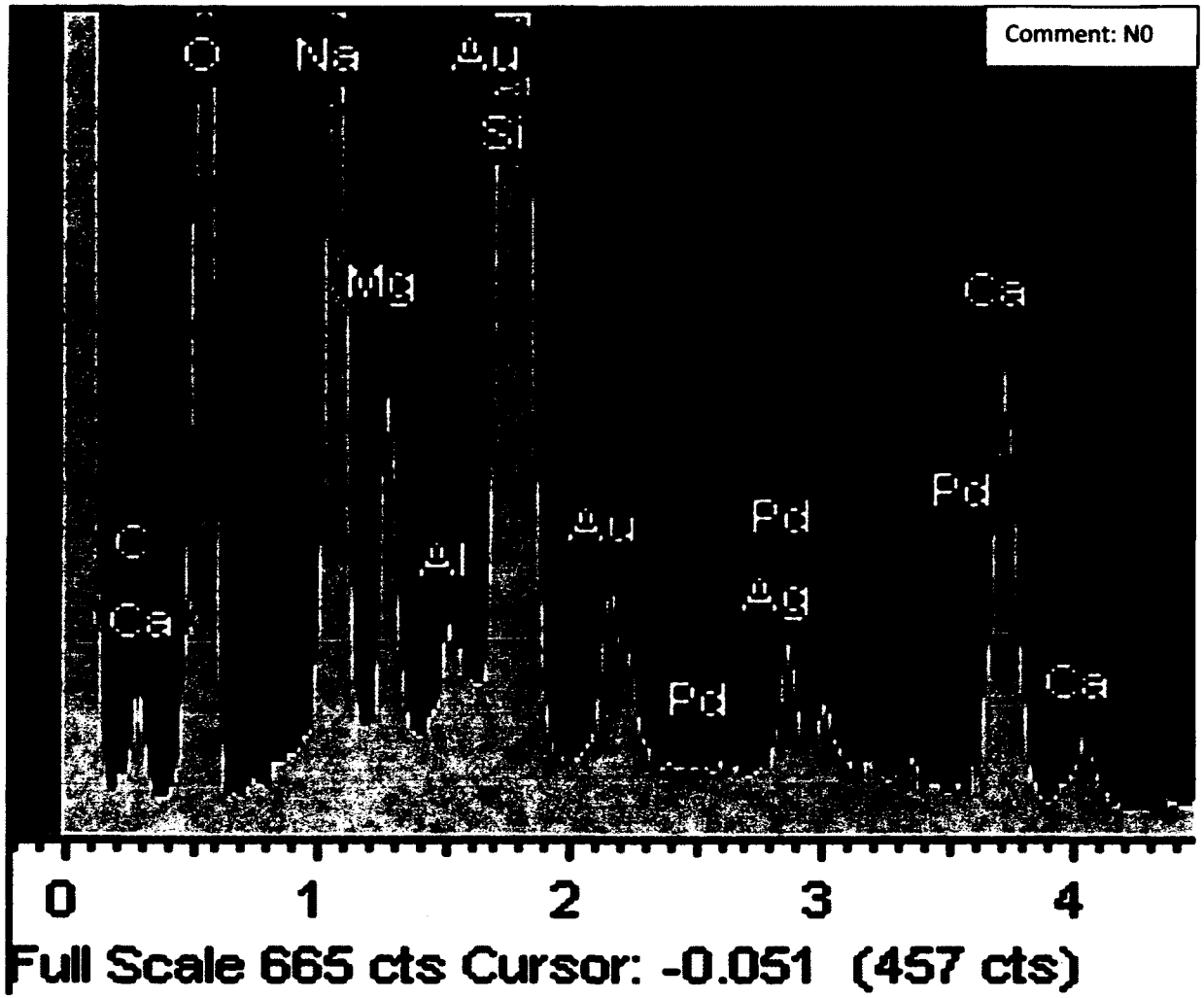

Element	Weight %	Atomic %
C K	13.97	23.27
O K	36.21	45.28
Na K	6.68	5.81
Mg K	1.78	1.47
Al K	0.36	0.27
Si K	28.71	20.44
Ca K	4.82	2.41
Pd L	3.01	0.57
Ag L	0.51	0.10
Au M	3.94	0.40
Totals	100.00	

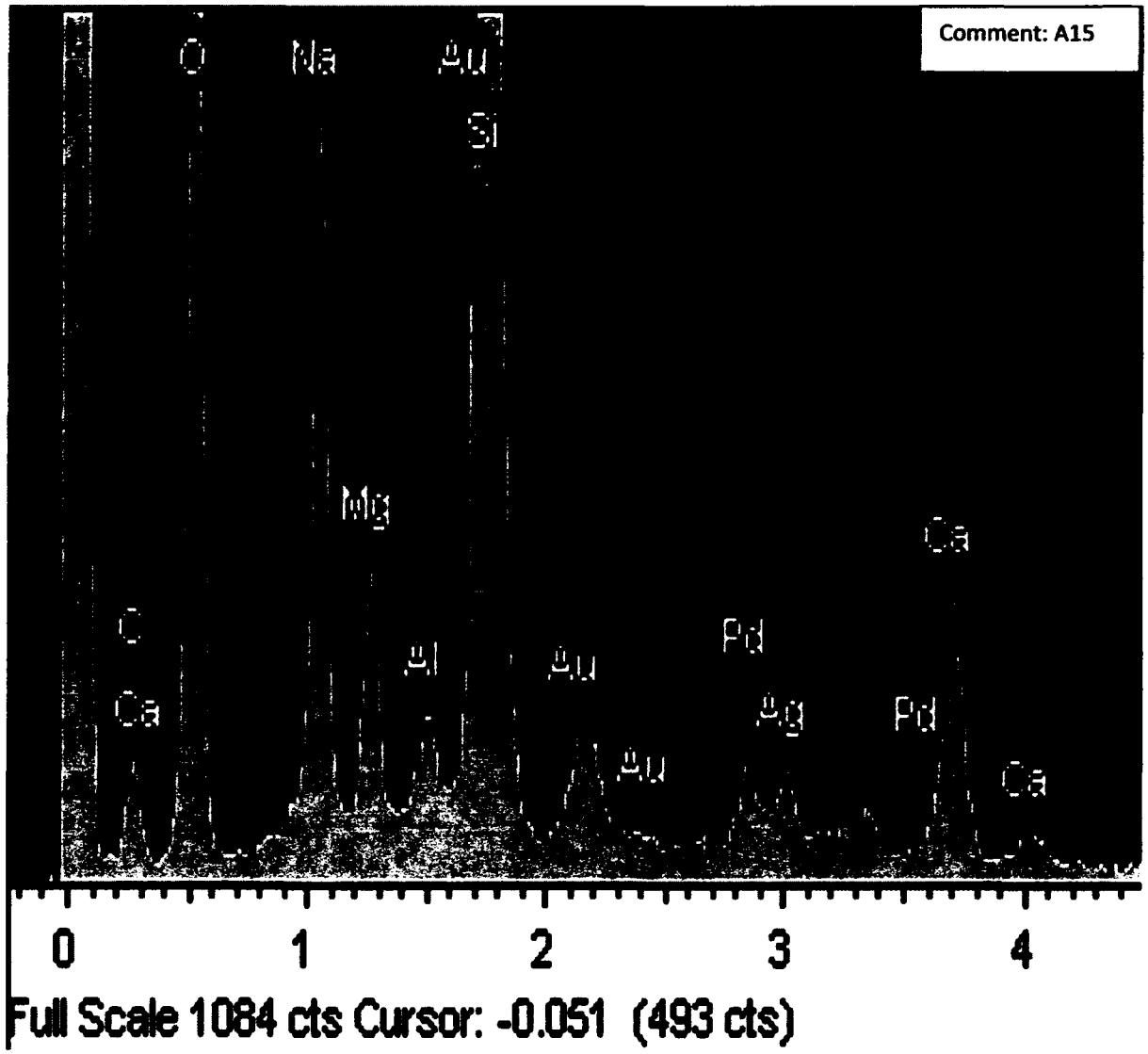

Element	Weight %	Atomi c%
C K	16.54	27.40
O K	33.46	41.61
Na K	6.13	5.30
Mg K	1.91	1.57
Al K	0.56	0.41
Si K	28.76	20.37
Ca K	4.31	2.14
Pd L	2.79	0.52
Ag L	1.54	0.28
Au M	4.00	0.40
Totals	100.00	

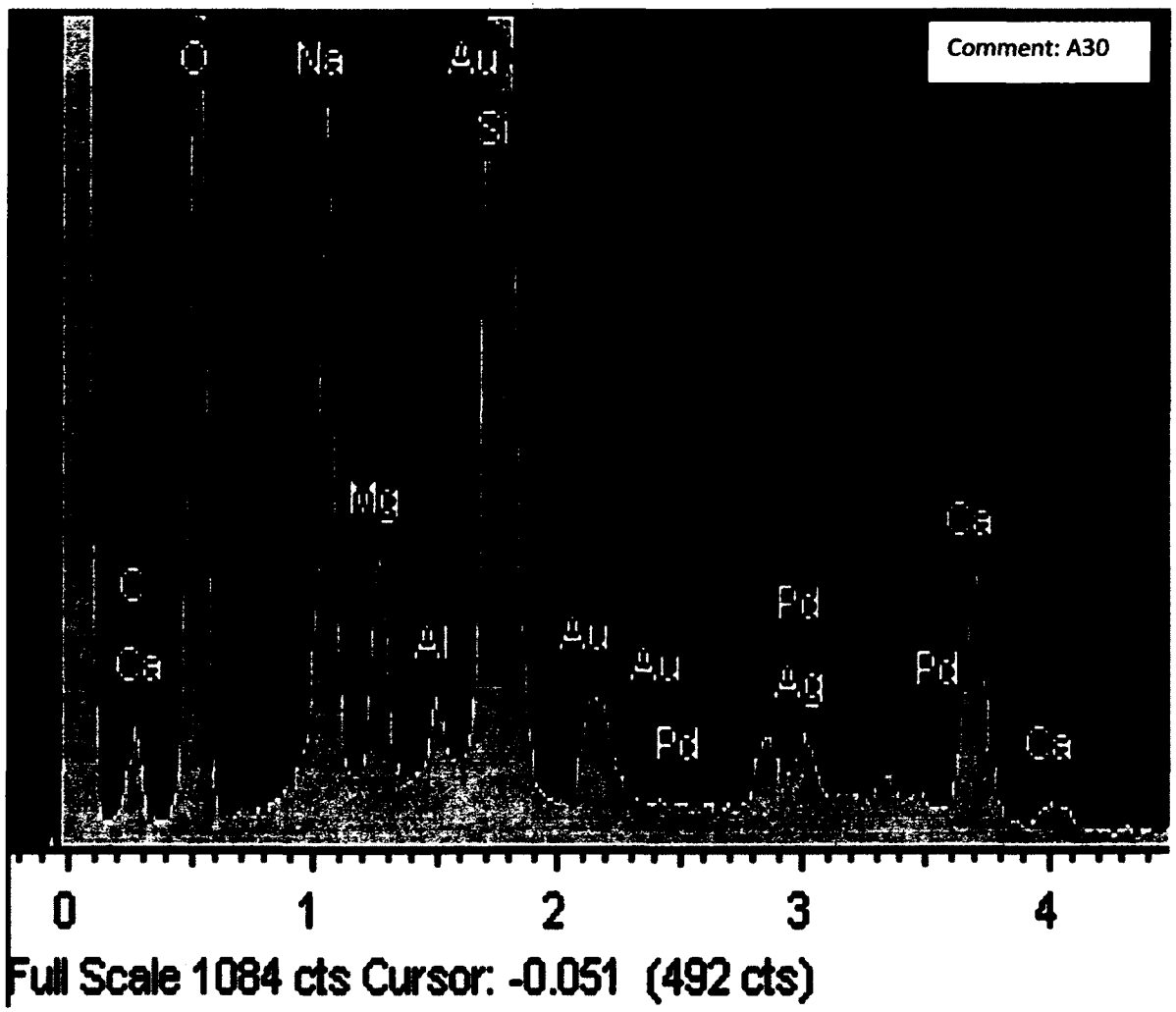

Element	Weight %	Atomic %
C K	14.05	23.67
O K	35.03	44.30
Na K	6.35	5.59
Mg K	1.99	1.66
Al K	0.56	0.42
Si K	28.91	20.82
Ca K	4.56	2.30
Pd L	2.81	0.53
Ag L	1.40	0.26
Au M	4.35	0.45
Totals	100.00	

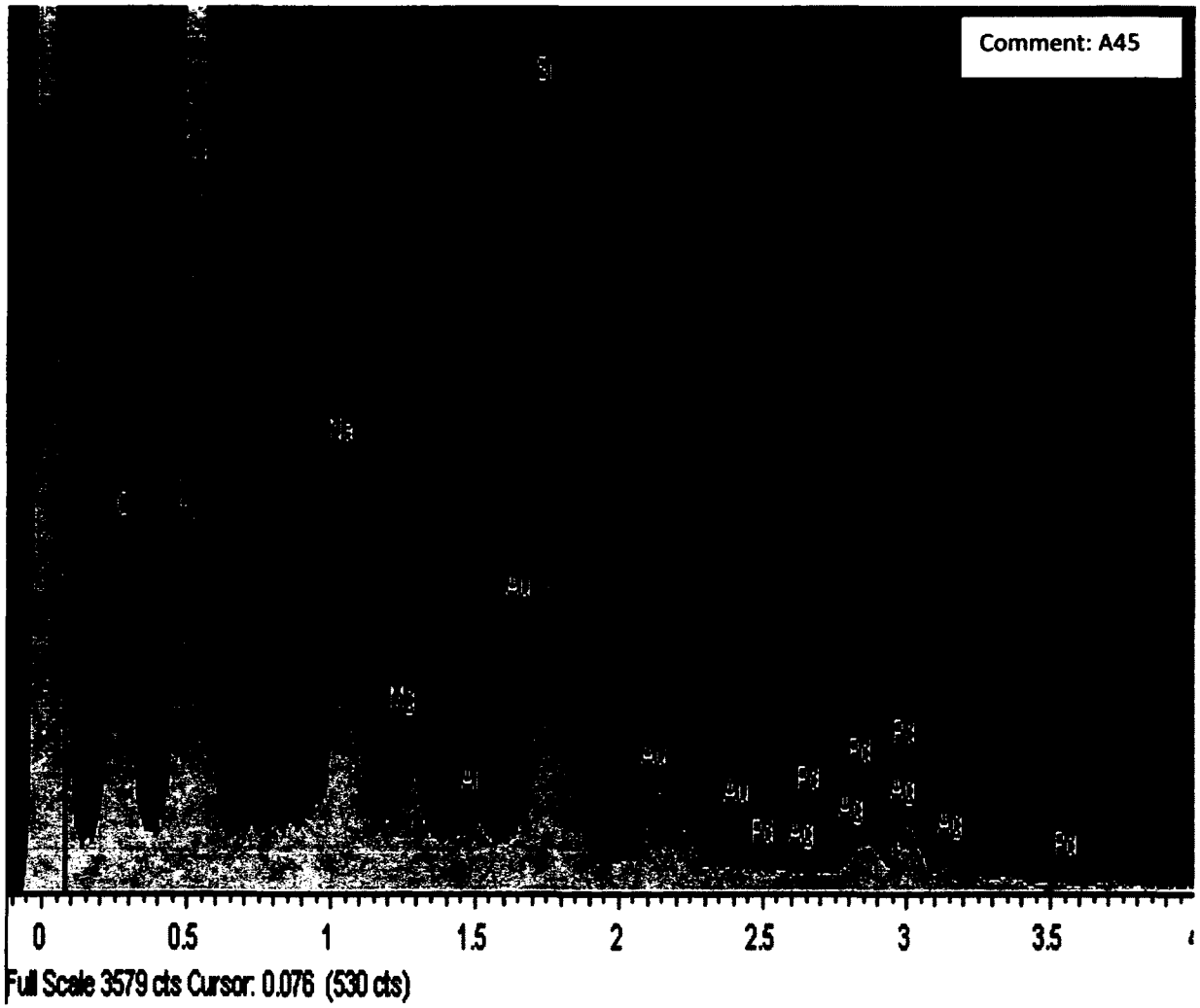

Element	Weight %	Atomic %
C K	7.90	14.11
O K	39.36	52.76
Na K	5.54	5.17
Mg K	1.89	1.66
Al K	0.56	0.45
Si K	23.27	17.77
Pd L	13.17	2.66
Ag L	19.69	3.92
Au M	13.79	1.50
Totals	125.18	

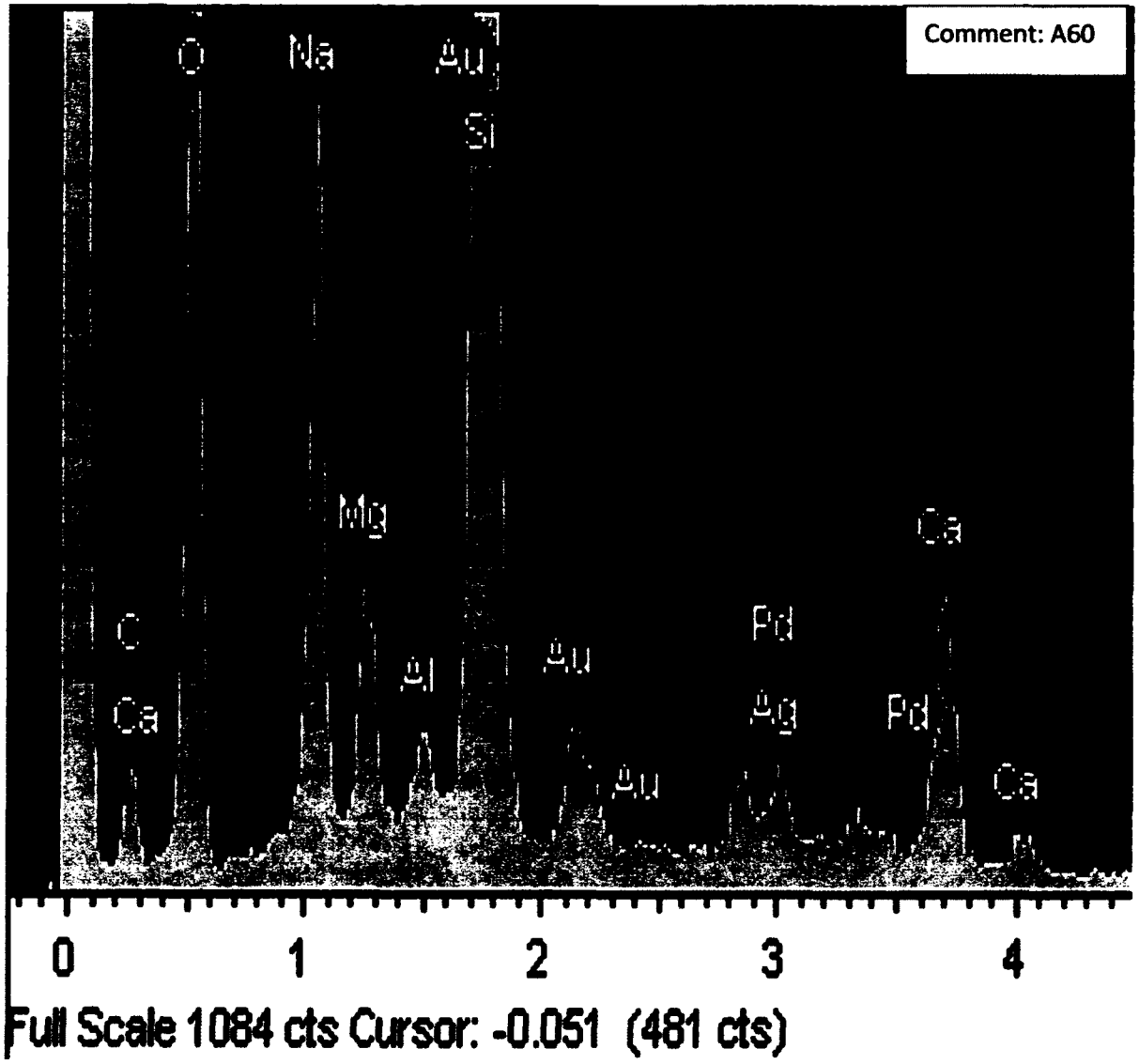

Element	Weight %	Atomic %
C K	13.73	23.25
O K	34.96	44.45
Na K	6.33	5.60
Mg K	1.93	1.61
Al K	0.57	0.43
Si K	28.87	20.91
Ca K	4.90	2.49
Pd L	2.71	0.52
Ag L	1.53	0.29
Au M	4.48	0.46
Totals	100.00	

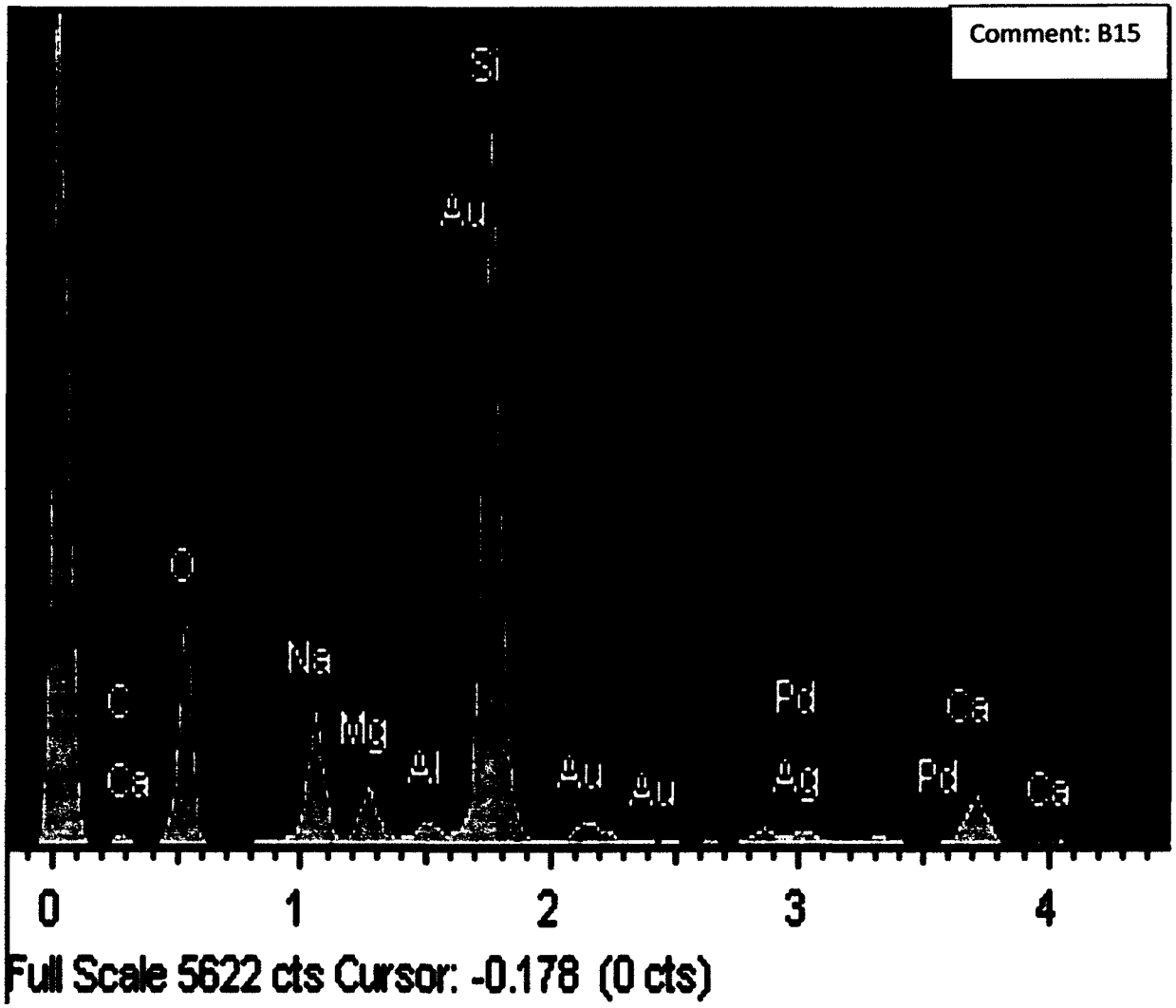

Element	Weight %	Atomic %
C K	14.88	24.68
O K	35.54	44.27
Na K	6.10	5.29
Mg K	2.08	1.70
Al K	0.56	0.42
Si K	28.64	20.33
Ca K	4.42	2.20
Pd L	2.60	0.49
Ag L	1.23	0.23
Au M	3.95	0.40
Totals	100.00	

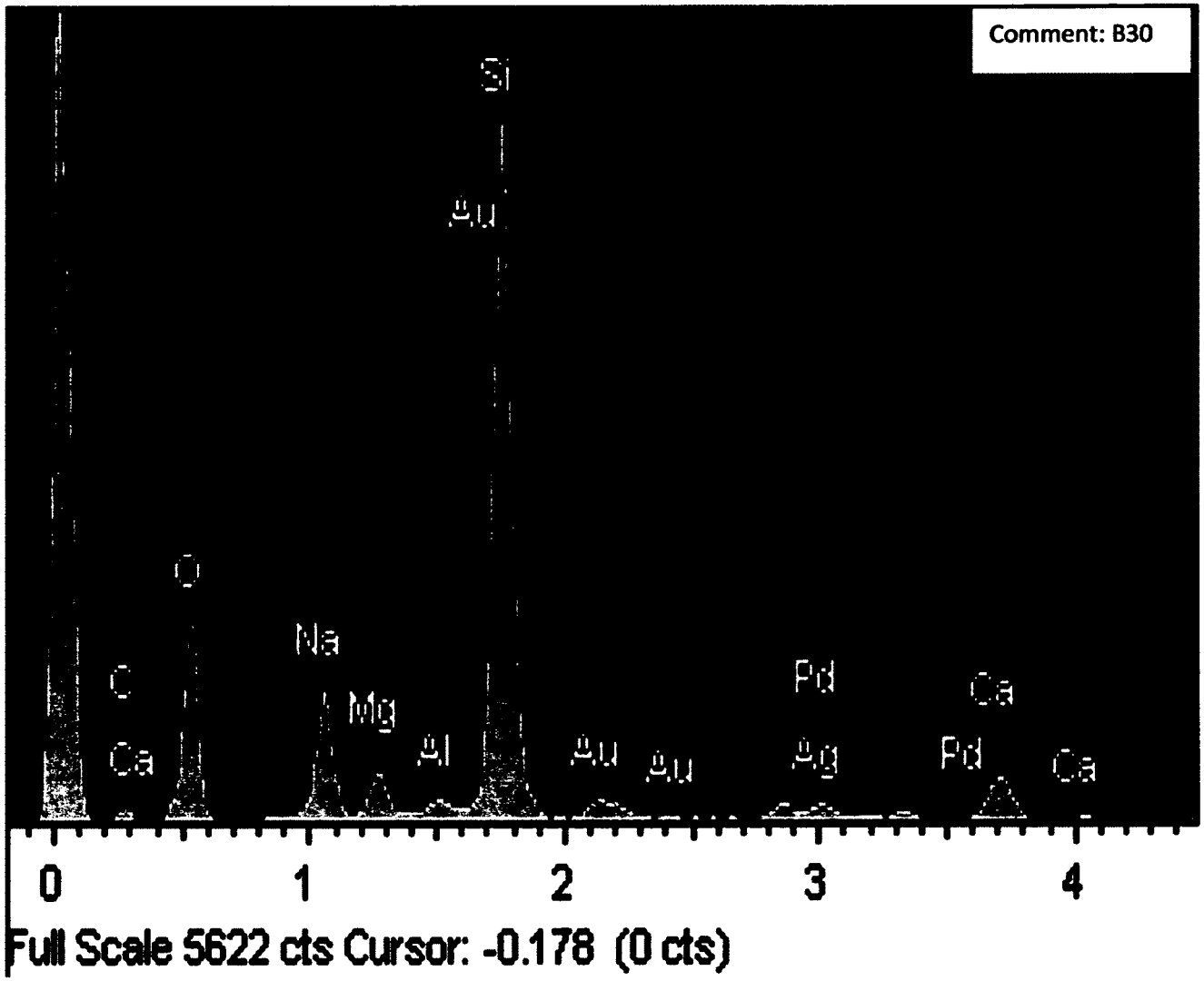

Element	Weight %	Atomic %
C K	15.37	25.64
O K	34.27	42.91
Na K	6.14	5.35
Mg K	1.89	1.56
Al K	0.42	0.32
Si K	29.09	20.75
Ca K	4.49	2.25
Pd L	2.97	0.56
Ag L	1.54	0.29
Au M	3.81	0.39
Totals	100.00	

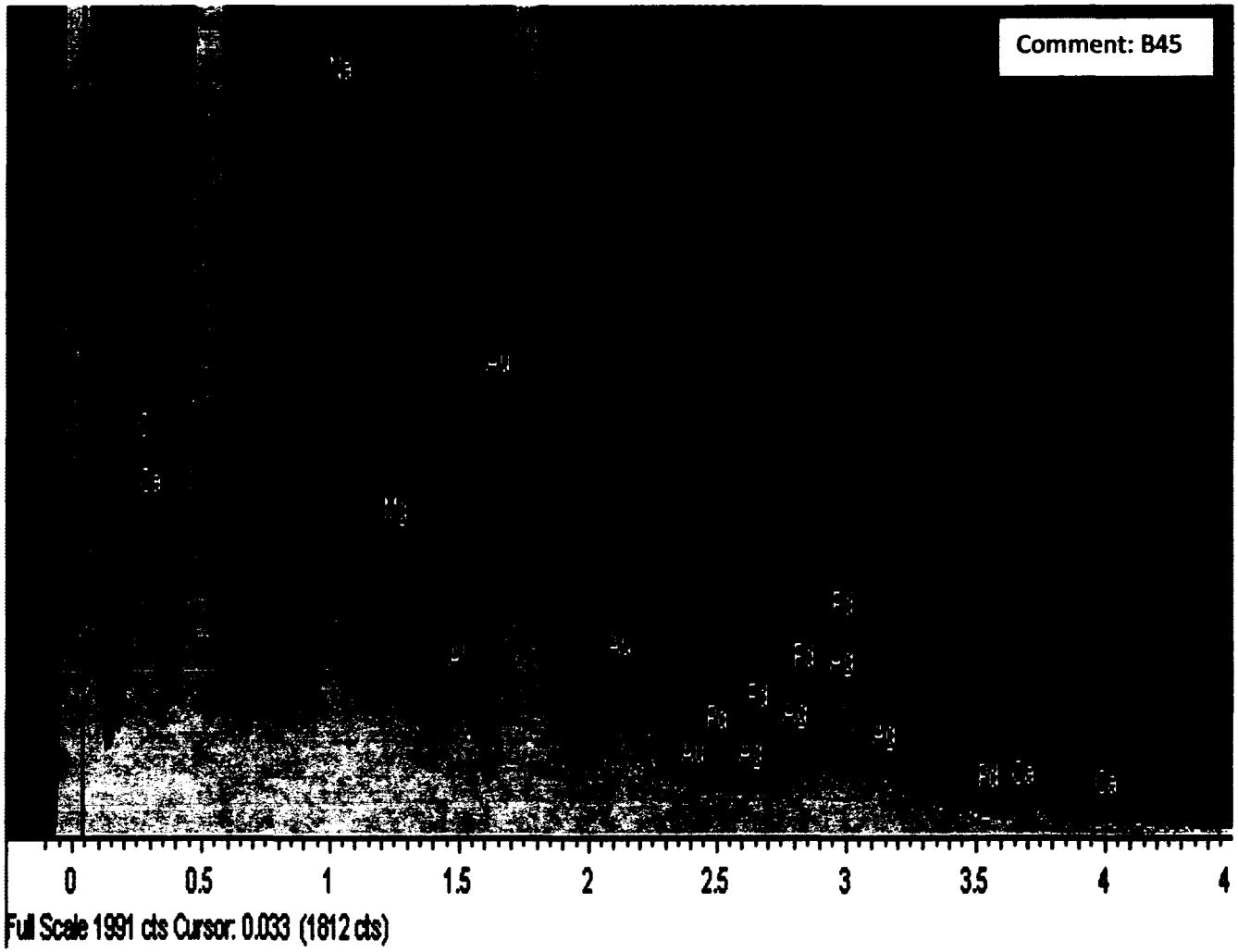

Element	Weight%	Atomic %
C K	2.58	4.76
O K	41.46	57.47
Na K	5.96	5.75
Mg K	1.86	1.70
Al K	0.48	0.39
Si K	25.21	19.91
Ca K	3.47	1.92
Pd L	9.87	2.06
Ag L	24.09	4.95
Au M	9.63	1.08
Totals	124.61	

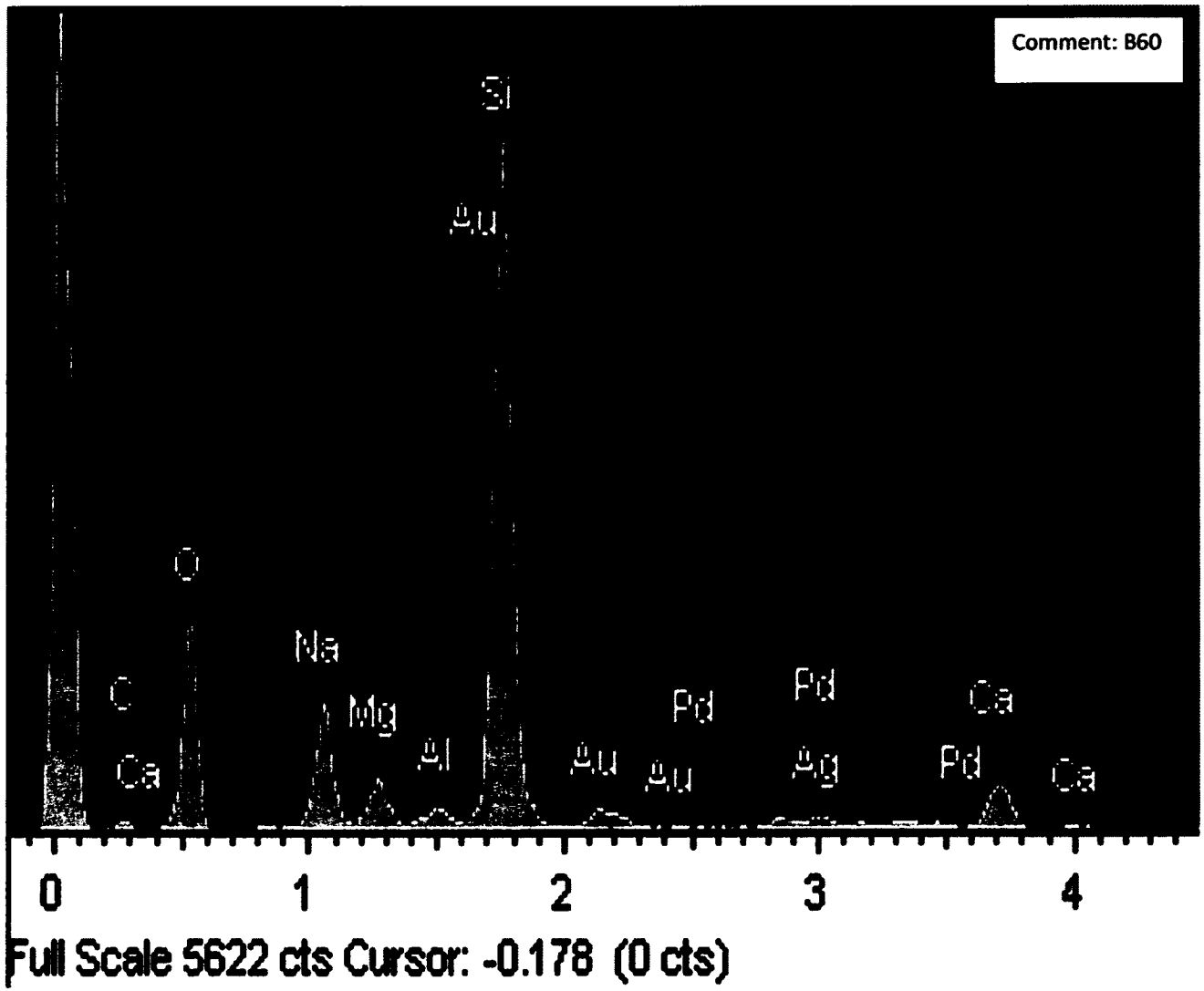

Element	Weight %	Atomic %
C K	12.37	21.06
O K	35.53	45.38
Na K	6.41	5.70
Mg K	2.09	1.75
Al K	0.57	0.43
Si K	30.15	21.94
Ca K	4.95	2.52
Pd L	2.46	0.47
Ag L	1.96	0.37
Au M	3.51	0.36
Totals	100.00	

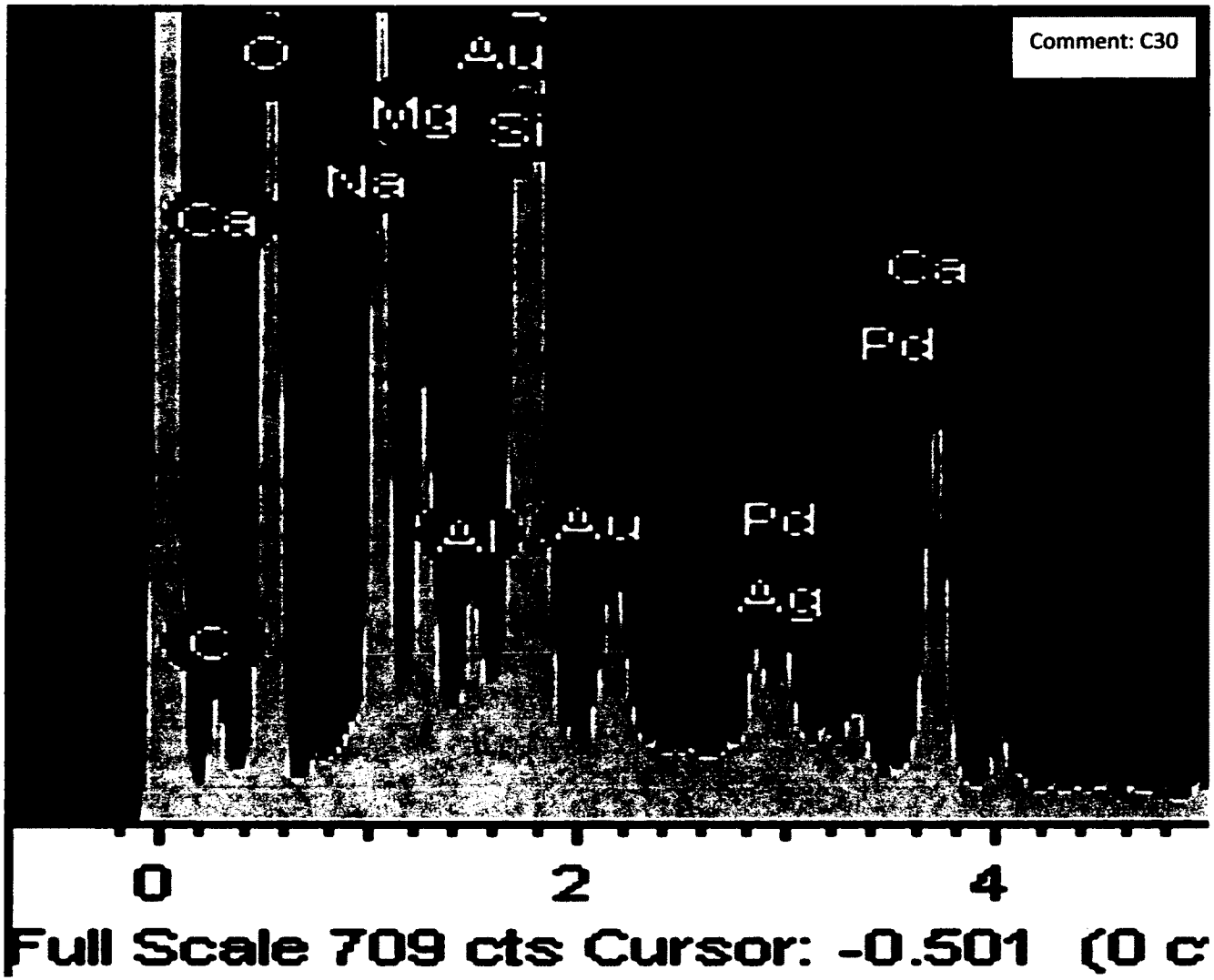

Element	Weight %	Atomic %
C K	14.46	24.23
O K	35.12	44.19
Na K	6.25	5.47
Mg K	1.83	1.52
Al K	0.60	0.44
Si K	28.85	20.68
Ca K	4.44	2.23
Pd L	2.69	0.51
Ag L	1.65	0.31
Au M	4.11	0.42
Totals	100.00	

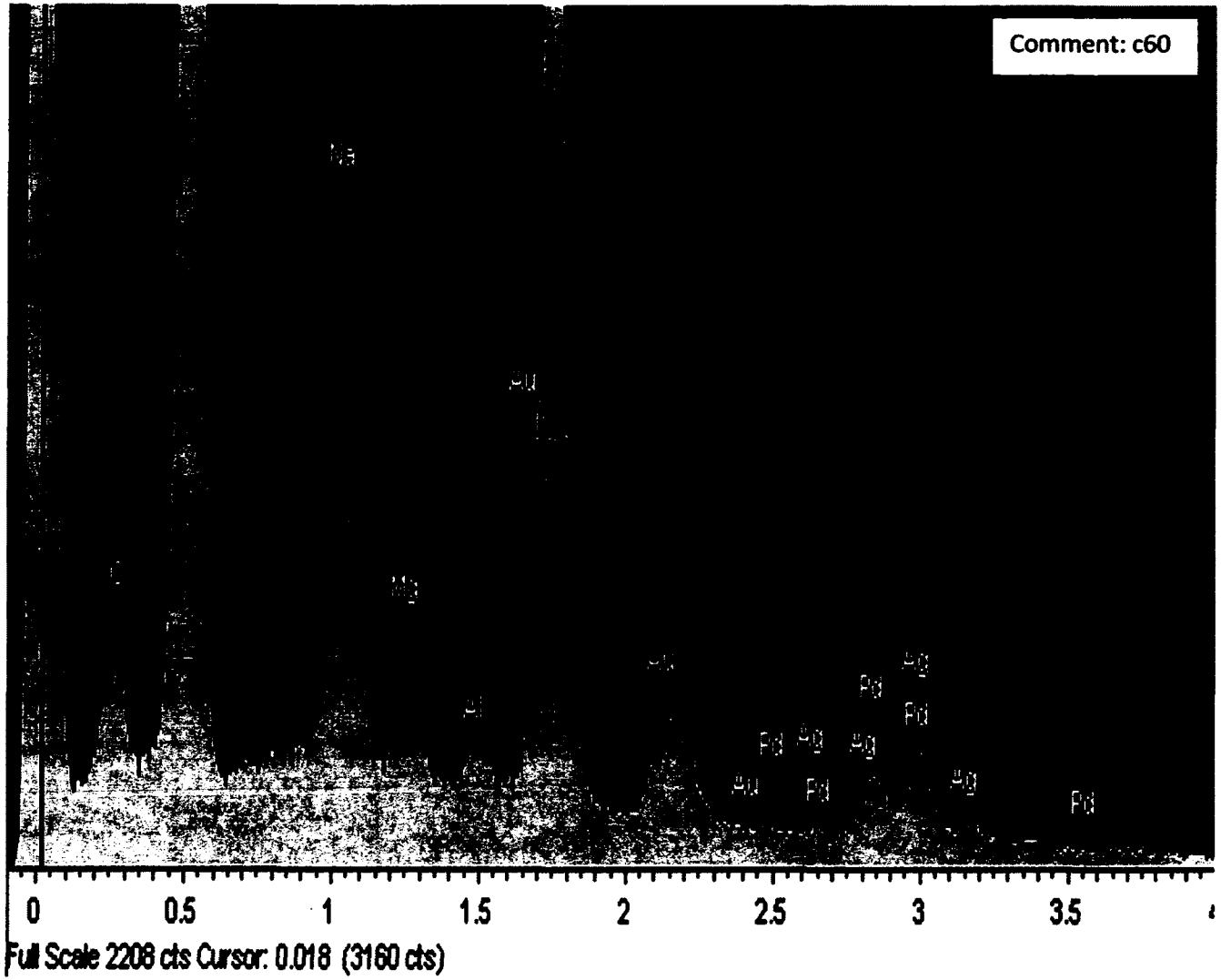

Element	Weight %	Atomic %
C K	3.10	5.86
O K	40.48	57.46
Na K	5.86	5.79
Mg K	1.82	1.70
Al K	0.44	0.37
Si K	24.37	19.71
Pd L	16.23	3.46
Ag L	19.78	4.16
Au M	12.99	1.50
Totals	125.07	

Appendix 2: NMR spectra of ligands

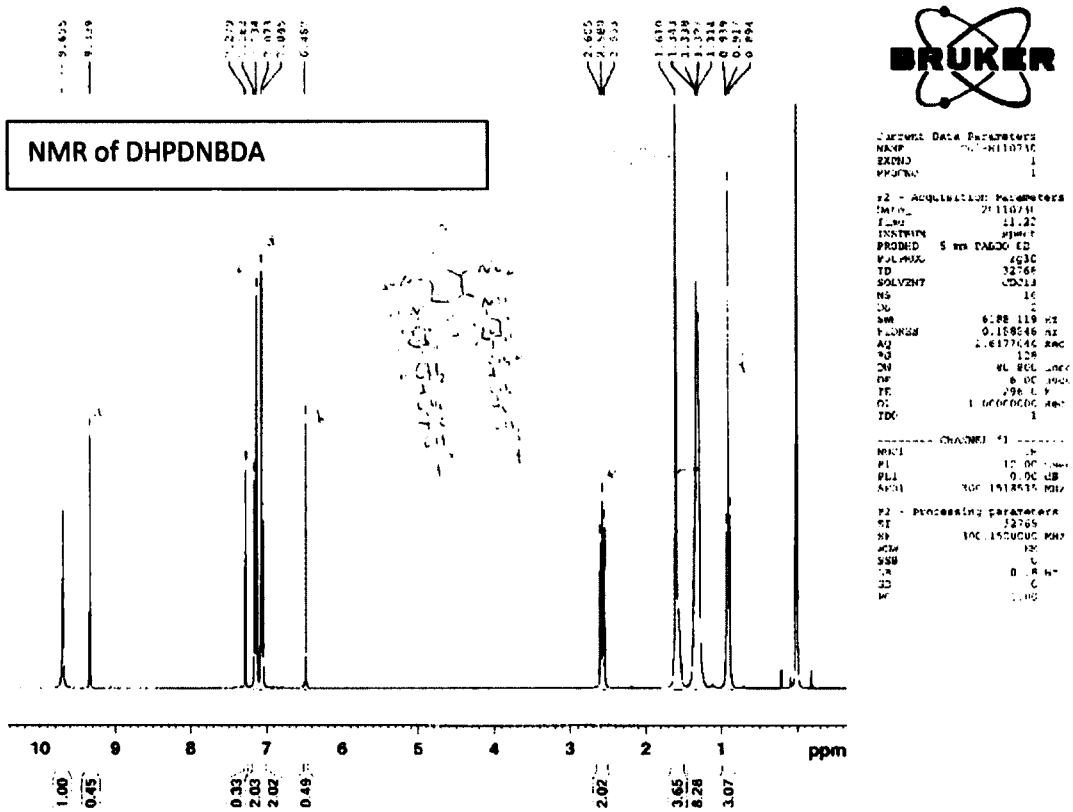
NMR of DHPDNBDA
BRUKER
ppm

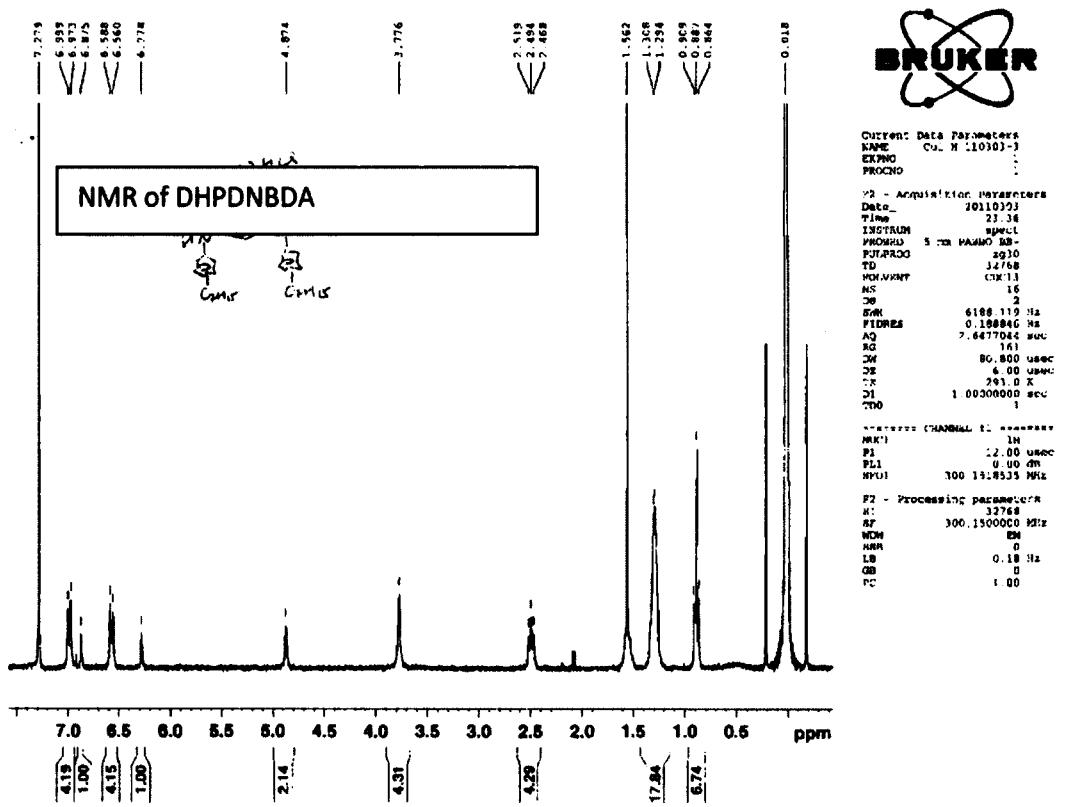
NMR of DHPDNBDA
BRUKER
ppm